ALMA MATER STUDIORUM - UNIVERSITÀ DI BOLOGNA

Dottorato di Ricerca in
Scienze Biochimiche e Biotecnologiche
ciclo XXIX

Settore concorsuale di afferenza: 05/E1

Settore scientifico-disciplinare: BIO/10

THE FUNCTION OF CYCLIN D1 IN DNA REPAIR: A NEW POSSIBLE APPROACH TO INCREASE SENSITIVITY OF OVARIAN CANCER CELLS TO IRRADIATION

Presentata da
Laura Verardi

Coordinatore Dottorato:
Chiar.mo Prof.
Santi Mario Spampinato

Relatore:
Chiar.ma Prof.ssa
Natalia Calonghi

Esame finale anno 2017

TABLE OF CONTENTS

ABSTRACT

Cyclin D1 has been recently investigated as an important protein in DNA damage repair mechanisms, especially in homologous recombination-directed repair (HDR). Cyclin D1 is recruited to damaged foci by BRCA2 and it enhances RAD51 binding to BRCA2 because cyclin D1 prevents BRCA2 inhibitory phosphorylation on serine 3291. Furthermore, cyclin D1 is essential for *RAD51* gene up-regulation in case of double-stranded break (DSB). Meanwhile molecule 3l, an E-3-(2-chloro-3-indolylmethylene)1,3-dihydroindol-2one, has been showed to reduce cyclin D1 transcript and protein levels and, for this reason, 3l treatment could be used to study cyclin D1 role in DNA damage repair, especially in ovarian cancer, that has not been well addressed yet.

Scope of this thesis is to find a new possible combined approach to increase sensitivity of ovarian cancer IGROV1 cells to irradiation: 3l treatment for 24 hours in order to deplete cyclin D1 expression, with a further UV irradiation to induce DNA damages. In this case, the repair of induced DSBs are analyzed in cells with a small amount of cyclin D1.

Time and duration of UV treatment have been set up using the well studied breast cancer cell line MCF7 as a template: 15 minutes of UV irradiation result optimal to induce DNA damage; the time point of 4 hours after irradiation results optimal for DNA repair pathway analysis. *CCND1* siRNA silencing has been also assessed: 10 nM siRNA treatment for 48 hours results as the maximum silencing pick of cyclin D1 protein. In IGROV1 cells, UV irradiation induces histone H2AX hyperphosphorylation on serine 139, marker of DSBs, and down-regulation of cyclin D1 in all the samples. UV-irradiated cells show up-regulation of *RAD51* gene and formation of repair complex BRCA2-cyclin D1-RAD51 on damaged foci. 3l-treated cells show a depletion of cyclin D1 protein levels and irradiation of these 3l-treated cells induces DNA damage as normal. However, 3l-treated and then UV-irradiated cells do not present up-regulation of *RAD51* gene and repair proteins colocalization. Anti-*CCND1* siRNA silenced cells show comparable results to 3l-treated cells, while scramble siRNA silenced cells present comparable results to control cells.

This thesis confirms the important role of protein cyclin D1 in the repair pathway of DSBs: cyclin D1 participates in and it is essential for repair complex formation on damaged foci; cyclin D1 is also necessary for *RAD51* gene up-regulation in case of DSB. The combined treatment of a drug leading to a depletion of cyclin D1 and a DNA damage inducer, such as irradiation, could be a potent potential therapy to target cancers with an elevated rate of DNA repair pathways, especially in case of chemo- and radio-resistant tumours.

CHAPTER 1
INTRODUCTION

The combined effects of DNA damage, DNA repair defects, and a failure to stall the cell cycle, lead to genomic instability, the most pervasive characteristic of cancer.[1]

DNA damage can arise from many sources: endogenous (chemicals or radicals produced by the normal cellular metabolism) or exogenous (environmental such as radiations or pharmaceutical). All these genotoxic sources can manage to a variety of DNA damages as simple base modifications, base mismatches, bulky DNA adducts, inter-strand and intra-strand crosslinks, protein-DNA crosslinks, single-strand breaks (SSBs) or double-strand breaks (DSBs).[2]

Given the potentially devastating effects of these varied and frequent DNA lesions, cells have evolved an intricate and complex series of mechanisms that counteract these threats to genomic integrity. Collectively, these mechanisms are known as DNA damage response (DDR) pathways.[1]

DDR mechanisms are activated only for those cell types where repairing the damage is advantageous; otherwise apoptosis occurs.[3] Cell death following DNA damage is a well regulated process during which the cell decides its outcome, determined by a threshold of pro-survival factors versus pro-death factors.[2]

Of all these DNA damages, SSBs are the most common ones (roughly 10,000/day), they are mainly caused by endogenous reactive oxygen species (ROS) produced by cellular metabolism. SSBs are primarily repaired by the base excision repair (BER) mechanism: this pathway is extremely robust and it protects cells from both endogenous and exogenous stress (pollution, smoke, radiation). When they are not repaired, especially in proliferating cells, SSBs can lead to collapsed DNA replication forks and DSBs. However DSBs, the most lethal of all DNA lesions, are also normal events that occur during meiosis and somatic recombination. DSBs are repaired by endogenous mechanisms such as homologous recombination (HR) and non-homologous end joining (NHEJ). HR is error-free, while NHEJ is an error-prone mechanism. Interestingly, DSBs repair is dependent on the phase of the cell cycle: NHEJ is active during G0, G1, and early S cell cycle phases, whereas HR is most predominant during late S and G2 phases, when DNA is already duplicated.[4]

In *Figure 1.1* all the possible DNA lesions are described in correspondence to DDR mechanisms, DDR involved proteins and tumour types induced in case of DDR dysfunction.
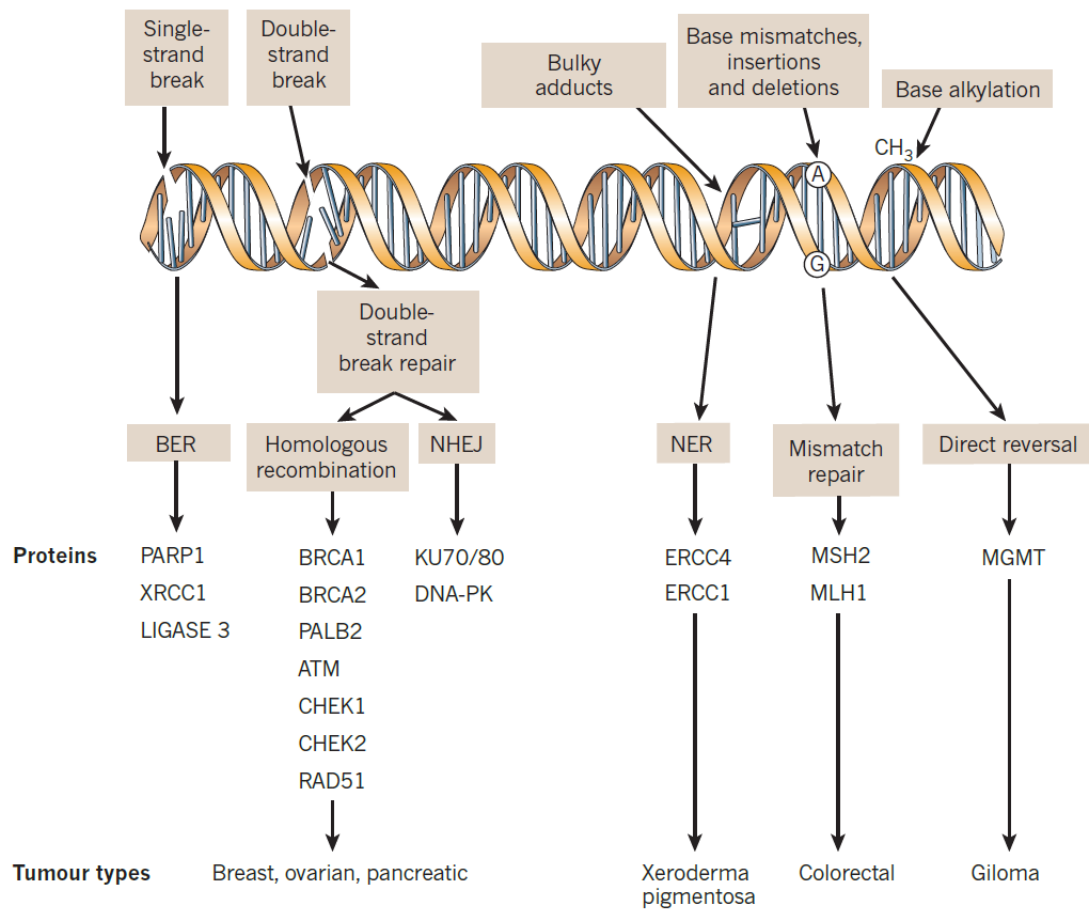
Figure 1.1: *DNA lesions in relation to DNA damage repair mechanisms.*
Figure adapted from Lord, C *Nature* (2012)[1]

The nucleotide excision repair (NER) is specific for repair of bulky adduct on DNA, while the mismatch repair (MMR) pathway is capable of repairing single base mismatches and a variety of small insertions and deletions in the genome. The repair of DNA inter-strand adducts are particularly problematic and employ the Fanconi anemia (FA) pathway, in collaboration with HDR.[3]

DNA damage and the associated DDR pathways play a crucial role in carcinogenesis, as most oncogenic alterations such as mutations, translocations, amplifications, deletions, and epigenetic modifications are caused by the inefficient repair of damaged DNA.[4] There are several examples in which there is an indisputable link between a particular DDR pathway dysfunction and a neoplastic phenotype. For example, the analysis of a wide number of high-grade serous ovarian adenocarcinoma samples has estimated that nearly 50% of them is probably defective in the homologous recombination mechanism. These homologous recombination defects are mostly driven by DNA mutations or

epigenetic silencing of genes such as *BRCA1* and *BRCA2*. Furthermore, sometimes the neoplastic condition exists because of a mutation in a gene that modulates the response to DSBs. This type of diseases include for example ataxia telangiectasia (ATM), Bloom's syndrome and FA, all of which cause extreme radiosensitivity, a characteristic of the inability to process DSBs. It is thought that critical DSB signal transduction and cell cycle checkpoint proteins, such as ATM, ATM and Rad3-related (ATR), and the master gatekeeper protein p53 become inactivated to induce precancerous lesions to progress into mature tumours.[1]

Historically, DDR defects have already been exploited therapeutically in the treatment of cancer with radiation therapies or genotoxic chemotherapies. For example, in patients with advanced ovarian cancer, platinum salts (carboplatin or cisplatin) are frequently used in combination with the taxane paclitaxel. Platinum salts cause DNA inter- and intra-strand crosslinks, lesions that are commonly repaired by NER and HR. These agents may be effective in patients with ovarian cancer because these tumours commonly harbour defects in HR, especially high-grade serous ovarian cancers.

More recently, protein components of the DDR pathways have been identified as promising targets for cancer therapeutics. For instance, topoisomerase inhibitors, such as irinotecan (TopI inhibitor) and etoposide (TopII inhibitor), leave DNA breaks across the genome and have been used effectively in some cancers.[1,5]

Furthermore, upregulated DDR mechanisms can cause resistance to DNA damaging chemotherapy and radiotherapy and so specific inhibitors of these pathways have the potential to sensitize cells to these therapies. For example, the high frequency of HR defects in tumours may provide a rationale for the use of inhibitors of HR to sensitize tumours with functional HR to conventional chemotherapy. There are few HR inhibitors: mirin is an inhibitor of MRE11 endonuclease activity, but its effects may not be specific to HR because it is involved in NHEJ, too. The activation of RAD51 by phosphorylation is an important step in HR and this step is dependent on the proto-oncogene ABL1; for this reason the BCR-ABL1 inhibitor imatinib sensitizes cells to DNA crosslinking agents and IR. Other putative RAD51 inhibitors have been identified but the most common way to target HR remains the inhibition of the ATM–CHK2 or ATR–CHK1 pathways.[6]

1.1 DNA damage repair mechanisms

1.1.1 Direct reversal

Besides DDR pathways, nature has also evolved single enzyme mechanisms in which the damage is directly reversed by a single repair protein without the incision of DNA backbone. Although such direct repair processes mediate the reversal of a relatively small set of DNA lesions, they are relatively simple and essentially error-free.[7]

There are two main types of direct DNA damage reversal:

- repair of base alkylation by alkyltransferases and dioxygenases;
- repair of UV-induced photolesions by photolyases.[8]

In addition to BER pathway that corrects many N-alkylated lesions, other two direct pathways exist: O^6-alkylguanine-DNA alkyltransferases (AGTs) reverse O^6-alkylated guanines and AlkB family dioxygenases reverse mainly N-alkylated lesions blocking Watson-Crick pairings.[7]

UV radiation produces mainly two types of DNA damages: the cyclobutane pyrimidine dimer (CPD) and the pyrimidine pyrimidones 6-4 photoproduct (6-4 PP). Photolyases are specific to either CPD or 6-4 PP lesion and they use blue and near-UV light to reverse UV-induced lesions. The study of these enzymes let Aziz Sancar get the Nobel Prize in 2015.[9]

1.1.2 Base excision repair

In 1974, Tomas Lindahl (Nobel Prize in 2015) identified a uracil DNA N-glycosylase (UNG), that excises uracil residues from DNA by cleaving the bond between uracil and deoxyribose. This was the starting point for the identification of the base excision repair (BER) pathway.[10]

BER pathway evolved with the high level of spontaneous decay products that are formed in DNA, as well as those damages created upon reactions with natural endogenous chemicals, especially ROS. BER corrects small base lesions that do not significantly bulk the DNA double helix structure, such as deamination, oxidation, alkylation or methylation.[11,12]

The repair pathway could be divided into these five following steps:

- recognition and removal of the damaged base by a DNA glycosylase and creation of an abasic site;

- incision of the abasic site by an apurinic/apyrimidinic (AP) endonuclease or by an AP lyase;
- removal of the remaining sugar fragment by a lyase or by a phosphodiesterase;
- gap filling by a DNA polymerase;
- sealing of the nick by a DNA ligase.[13]

In humans BER is initiated by one of eleven damage-specific DNA glycosylases which display substrate specificity for particular types of damaged DNA bases: four devoted to the removal of mispaired uracil and thymine, six to the repair of oxidative damage, and one to the removal of alkylated bases. There are two different types of DNA glycosylases: monofunctional glycosylases (that recognize uracil, thymine, and alkylated bases) or bifunctional glycosylases (DNA glycosylase plus DNA strand cleavage activities).[14] Monofunctional glycosylases employ a base-flipping mechanism to break the N-glycosidic bond between the damaged base and the phosphodiester DNA backbone, creating an AP site. The resulting abasic site is recognized by an AP endonuclease (APE1), which cleaves the abasic site leaving a sugar attached to the 5' side of the nick. The resulting 3' hydroxyl is a substrate for the repair polymerase, DNA polymerase β (Pol β), which also has a lyase activity that removes the sugar attached to the 5' phosphate. A complex consisting of DNA ligase III α (Lig IIIα) and X-ray cross-complementing protein 1 (XRCC1) finally seals the remaining nick in the DNA backbone. Conversely, bifunctional glycosylases that recognize oxidative lesions excise the damaged base but also cleave the DNA backbone, leaving either an α, β unsaturated aldehyde or a phosphate attached to the 3' side of the nick. The sugar is removed by the phosphodiesterase activity of APE1 and the phosphate group by the polynucleotide kinase phosphatase (PNKP). This is the predominant process mode of BER and is commonly referred to as short-patch BER. In some circumstances the process can be redirected to a long-patch BER, often because the sugar is inefficiently removed from the 5' end of the nick; in these cases different DNA polymerases can take over, including the replicative polymerases δ or ε (Pol δ/ε). Pol δ/ε act by adding several nucleotides into the gap, generating a 5' flap structure which is excised by the flap endonuclease-1 (FEN-1) in a proliferating cell nuclear antigen (PCNA)-dependent process. Finally DNA ligase I (Lig I), always in concert with PCNA, seals the remaining nick in the DNA backbone (*Figure 1.2*).[11,15]
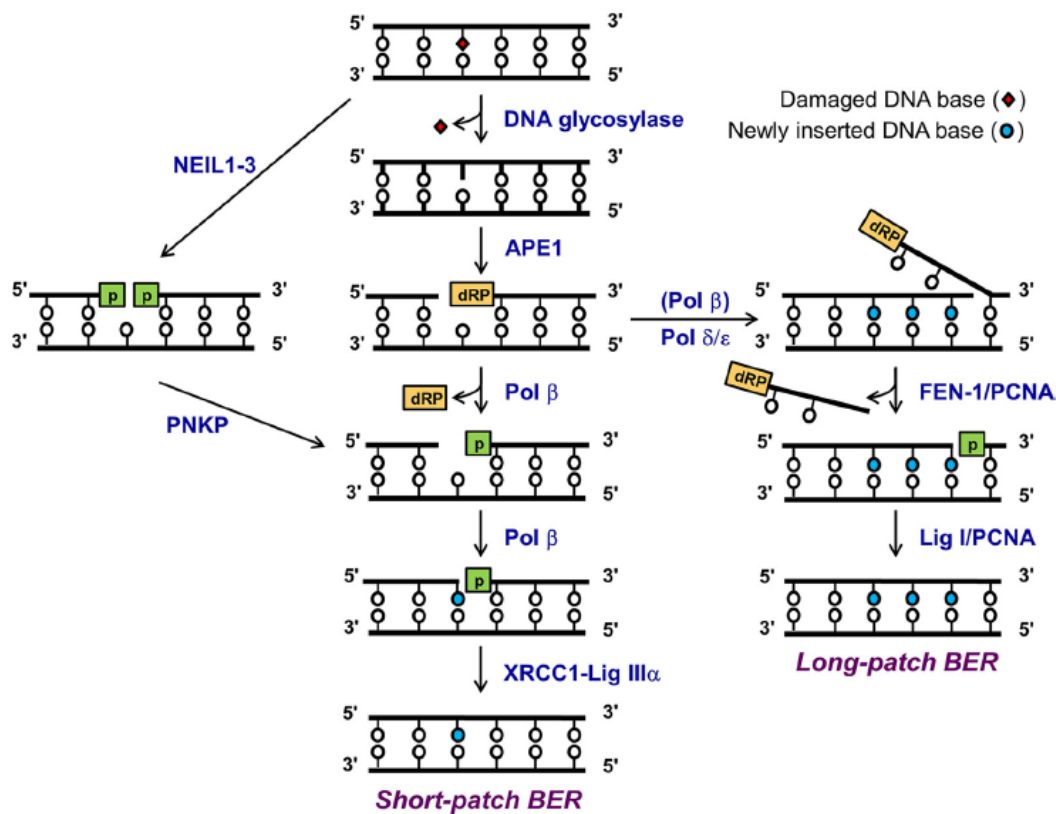
Figure 1.2: *Base excision repair pathway.*

Figure from Carter, R J *Mol. Cell. Biol.* (2016)[11]

1.1.3 Nucleotide excision repair

Nucleotide excision repair (NER) is the main pathway responsible for the removal of bulky lesions in the DNA. NER can be subdivided into two pathways:

- global genome NER (GG-NER) can occur anywhere in the genome;
- transcription-coupled NER (TC-NER) is responsible for the accelerated repair of lesions in the transcribed strand of active genes.[16]

GG-NER is initiated by the recognition of the bulky lesion by the specific factor XPC complexed with RAD23B and centrin 2 (CETN2), in some cases with the help of UV-DDB (UV-damaged DNA-binding protein). The XPC-RAD23B-CETN2 complex melts the DNA around the lesion and recruits the multiprotein complex TFIIH. A stalled RNA polymerase (RNA Pol II) constitutes the first step of TC-NER. The blocked complex recruits CSB, a transcription elongation factor, and other specific factors as CSA and XAB2, that translocate along template DNA with RNA Pol II. The UVSSA protein and its partner USP7 are transiently associated with elongating RNA Pol II but, in case of

transcription arrest, they bind more strongly and stabilize CSB. Both subpathways converge when TFIIH (transcription initiation factor II H) is recruited to the repair site (**Figure 1.3**).[17]
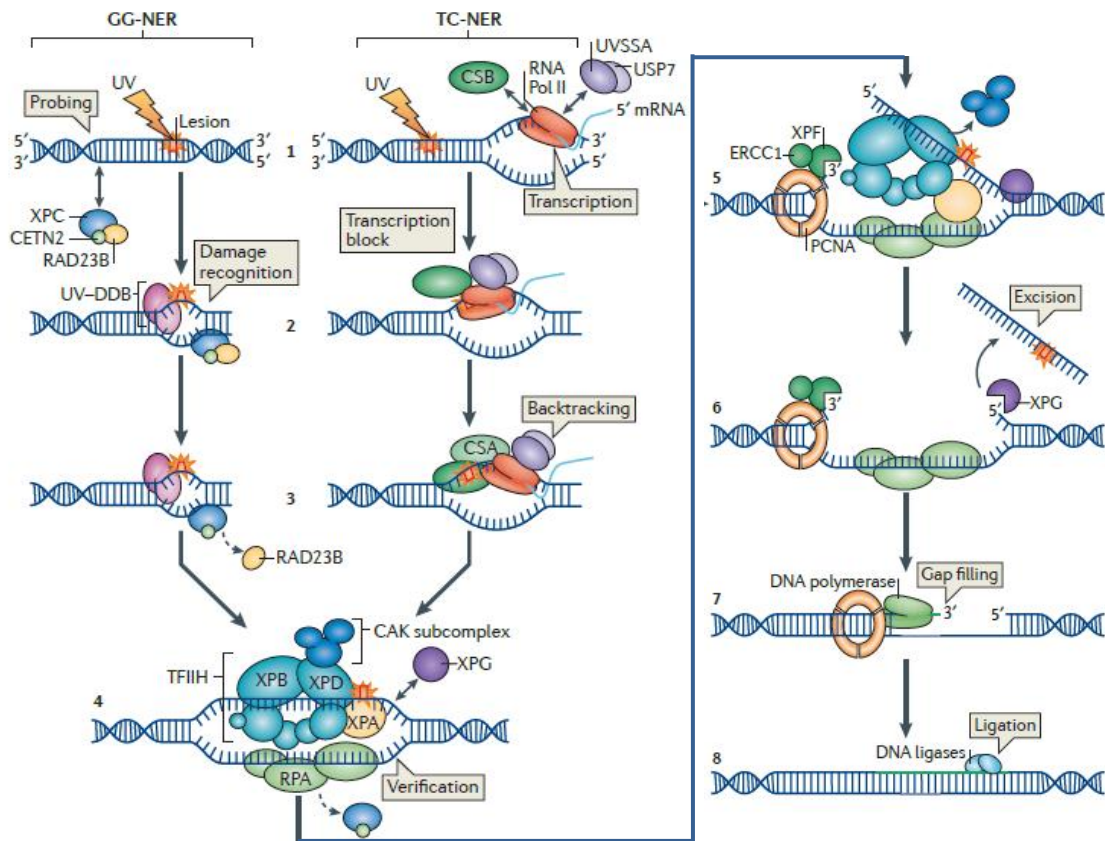
Figure 1.3: *Nucleotide excision repair pathway.*
Figure adapted from Marteijn, J A *Nat. Rev. Mol. Cell. Biol.* (2014)[18]

Then, the XPG structure-specific endonuclease binds to the pre-incision NER complex and the CAK (CDK-activating kinase) subcomplex dissociates from the core TFIIH complex. TFIIH comprises ten proteins, one of them is the ATPase helicase XPB: the helicase activity of TFIIH further opens the double helix around the lesion, creating a 20-30 nucleotide bubble. Another ATPase helicase complex protein, XPD, detects and verifies the existence of lesions. Once the pre-incision complex is assembled, XPA, RPA, and XPG are recruited. XPA binds to the altered single-stranded DNA; RPA (replication protein A) coats the ssDNA opposite the lesion, protecting it from degradation and helping to coordinate excision and repair events. XPA recruits the heterodimer structure-specific endonuclease ERCC1-XPF, which is directed to the 5'

end of the bubble. XPG is then activated and cuts the damaged strand 3' to the lesion and it excises the lesion within a 22-30 nucleotide-long strand. The proliferating cell nuclear antigen (PCNA) ring, which is directly loaded after the 5' incision by ERCC1-XPF, recruits DNA Pol δ, Pol κ or Pol ε for the filling of the created gap. Pol ε is active in replicating cells, while Pol δ/κ are the main NER polymerases in non-replicating cells. NER pathway is completed through sealing of the final nick by DNA ligase I (in replicating cells) or XRCC1-ligase III (in quiescent cells).[17,18]

1.1.4 Mismatch repair

DNA mismatch repair (MMR) is a highly conserved biological pathway that plays a key role in maintaining genomic stability, in fact inactivation of this repair system confers a large increase in spontaneous mutations and a strong predisposition to tumour development. MMR research conferred to Paul Modrich the Nobel Prize in 2015.[19]

The specificity of MMR is primarily for base-base mismatches and insertion/deletion mispairs generated during DNA replication and recombination. MMR also ensures the fidelity of genetic recombination, and participates in the earliest steps of damage signaling in eukaryotic cells.[20]

MMR repair is a strand-specific process. During DNA synthesis, if the newly synthesised strand includes errors, this repair machinery can distinguish the new strand from the methylated template (in prokaryotes). In eukaryotes, the newly synthesized lagging-strand DNA transiently contains nicks, before being sealed by DNA ligase, and for this reason it provides a signal that directs mismatch proofreading systems to the appropriate strand.[21]

These nicks are sites for the RFC-dependent loading of the replication sliding clamp PCNA, in an orientation-specific manner. Oriented PCNA then directs the action of the endonucleases MutS, MutH and MutL, forming the MutSHL complex, which remove the wrong nucleotides. The removal process involves more than just the mismatched nucleotide itself: a few or up to thousands of base pairs of the newly synthesized DNA strand can be removed.[22]

The entire process ends when the single-strand gap created is repaired by DNA Pol III that uses the other strand as a template, with the help of the single-strand DNA-binding protein SSB. Finally, the nick is sealed by a DNA ligase.[23]

1.1.5 Repair of DNA double-strand breaks

DNA double-strand breaks (DSBs) are cytotoxic lesions generated when the phospho-sugar backbones of both strands of DNA are broken at the same position. Among DNA damages, DSBs are considered to be lethal within the cells because failure to repair a DSB has deleterious consequences, including chromosomal rearrangements, such as translocations and deletions, and resulting in oncogenic transformation or cell death. In contrast to DNA single-strand breaks (SSBs), in which the genetic information is retained on the complementary strand, repair of DSBs can be problematic. Obviously, DSB repair must restore both the physical integrity of the chromosome and its genetic information.[24]

DSBs can be generated by physiological processes as recombination or exogenous agents as radiations or chemicals. These include base alkylating agents such as methyl methane sulfonate (MMS), as well as intra- or inter-crosslinking agents, including mitomycin C, platinum derivatives and nitrogen mustards. Drugs that generate DSBs are widely used in cancer treatment since tumor cells are often more sensitive to DSBs than normal cells. DNA topoisomerase inhibitors induce the formation of SSBs or DSBs by trapping topoisomerase-DNA intermediates during isomerization reactions. For example, camptothecin, irinotecan and topotecan inhibit type I topoisomerases, generating DSBs primarily during DNA replication. Meanwhile, etoposide, mitoxantrone, teniposide and doxorubicin inhibit type II topoisomerases, generating DSBs throughout the cell cycle. Ionizing radiations (IR) and ultraviolet radiation (UV, especially UV-B) are generators of DSBs, furthermore radiations produce DSBs because they induce reactive oxygen species (ROS). ROS are also generated during normal cellular metabolism, they can oxidize bases and induce both single- and double-strand breaks. Physiological sources of endogenous DSBs include DNA replication and meiotic recombination, that are the major causes of DSBs in proliferating cells because of fragile and breakable DNA intermediates. Clearly, breaks can occur following replication stalling forks, which leads to the generation of persistent single-strand DNA intermediates.[25,26]

The repair of DSBs involves two major possible mechanisms: non-homologous end joining (NHEJ) and homologous recombination (HR). In NHEJ the DSB is repaired by blunt end ligation in a sequence homology-independent way. In contrast, HR requires

extensive homology for the repair of DSBs, in fact HR plays a major role during the S and G2 phases of the cell cycle, when the template homologous sister chromatids are available.[27,28]

1.1.5.1 Non-homologous end joining

While the template-independent nature of non-homologous end joining (NHEJ) suggests its error-prone characteristic, it is a highly faithful mechanism, with an error rate of about 10^{-3} per joining event between fully compatible DSB ends.[29]

NHEJ repair pathways are subdivided into the canonical non-homologous end joining pathway (c-NHEJ), which is dependent on Ku proteins and DNA ligase IV, and a group of less well elucidated alternative pathways (alt-NHEJ), dependent on DNA ligase I/III (*Figure 1.4*).
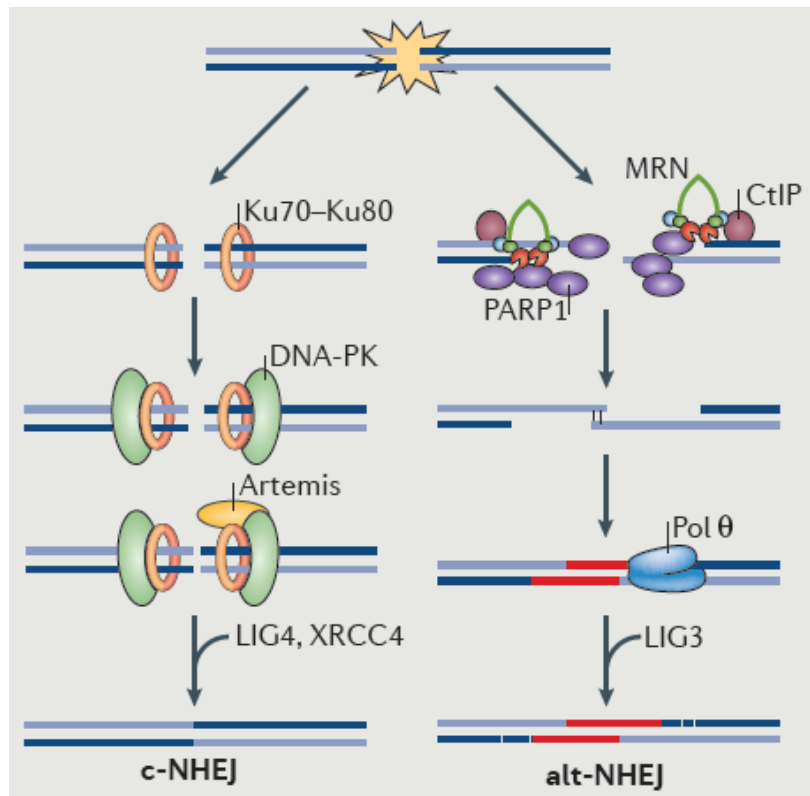
Figure 1.4: Non-homologous end joining repair pathway.
Figure from Lazzerini-Denchi, E *Nat. Rev. Mol. Cell. Biol.* (2016)[30]

C-NHEJ begins when the Ku70-Ku80 heterodimer binds to DNA ends with high affinity. Ku dimer then recruits the Ser/Thr kinase DNA-dependent protein kinase catalytic subunit (DNA-PKcs) to phosphorylate a number of downstream targets,

including the terminal end-processing enzyme Artemis. Artemis cleaves single-stranded overhangs and the complex XRCC4-LIG4 (DNA ligase IV) seals DNA ends.[31]

Alt-NHEJ is dependent on poly(ADP-ribose) polymerase 1 (PARP1) signaling and it depends on DNA 5'-3' resection by the MRN complex (constituted of MRE11-RAD50-NBS1) and CtIP (CtBP-interacting protein). Base pairing at the resected ends drives their annealing to promote synapsis of opposite ends of the DSB. The low-fidelity DNA polymerase θ (Pol θ) fills the annealed ends, and finally LIG1/3 (DNA ligase I/III) seals them. Alt-NHEJ is a more error-prone pathway in comparison to c-NHEJ: it introduces deletions caused by extended nucleolytic processing and insertions caused by the activity of Pol θ.[32]

1.1.5.2 Homologous recombination

The homology-directed repair (HDR) is a mechanism highly evolutionarily conserved from prokaryotes to humans (***Figure 1.5***). It operates on the same principles of homologous recombination (HR): the ends of a DSB are recognized and processed to generate 3' single-stranded DNA overhangs, through a process termed DNA end resection. It provides an important mechanism to repair both accidental and programmed DSBs during mitosis and meiosis, especially in S/G2 phases of the cell cycle, where it promotes an error-free repair thanks to the template sister chromatid.[33]

HDR is accompanied by histone modifications, like γH2AX, and chromatin remodeling. Phosphorylation on serine 139 of histone H2AX (γH2AX) is one of the most important markers of DSBs and it is involved in the induction of repair signaling.[34,35]

The central reaction in HR and in HDR is the pairing and exchange of strands between two homologous DNA molecules. First of all, DNA ends are processed to yield 3' single-stranded DNA tails. In humans, this 5'-3' end resection occurs thanks to MRE11-RAD50-NBS1 (MRN) complex and CtIP which clip 5' ends of DNA and thanks to EXO1 or BLM-TopoIIIα-RMI1 and DNA2 which process the early intermediate to form extensive regions of single-stranded DNA. In accordance, the replication protein A (RPA) binds the single-stranded DNA tails until RAD51 is recruited by BRCA2-PALB2 and forms a helical nucleoprotein filament around the single-stranded DNA. Once formed, the complex RAD51-ssDNA searches for a homologous sequence and then promotes invasion of the single-stranded DNA into donor double-stranded DNA to form a joint molecule with a displaced strand, called D-loop.[36,37]
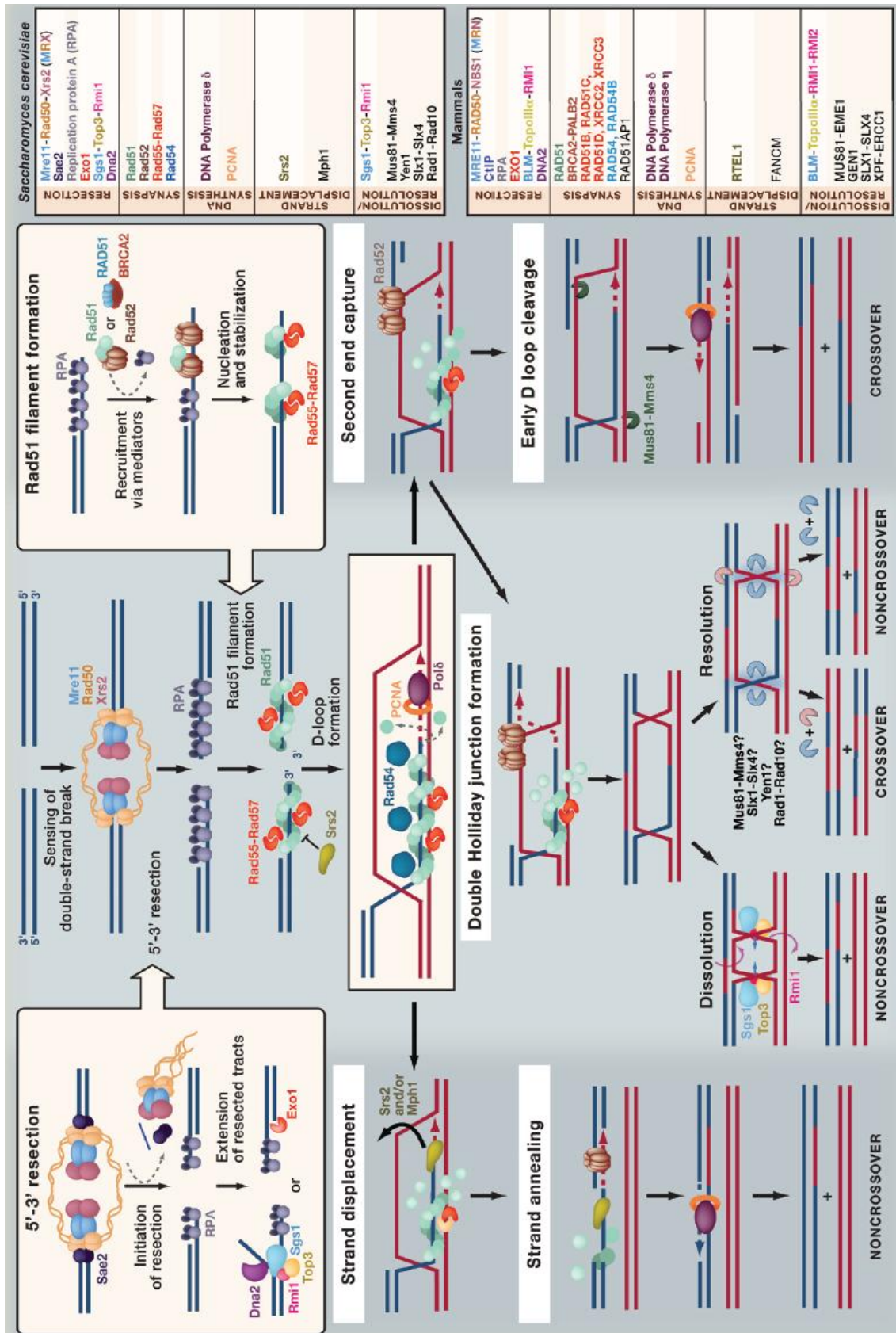
Figure 1.5: *Homologous recombination pathway in DNA double-strand break repair.*

Figure from Mazón, G *Cell* (2010)[38]

RAD54, a member of the Swi2/Snf2 family of chromatin remodeling proteins or ATPases, stimulates homologous pairing and DNA polymerase δ/η extends the 3' end from the broken chromosome using the donor strand as a template and replacing nucleotides lost by end resection. Here, the D-loop can be resolved by different paths.[39]

In the (SDSA) path, the invading strand that has been extended by DNA synthesis is displaced (strand displacement) and it anneals to complementary sequences exposed by 5'-3' resection of the other side of the break (strand annealing). The RTEL1 helicase can dissociate D-loop intermediates to facilitate SDSA. The synthesis-dependent strand annealing forms exclusively noncrossover products.[40]

In the canonical repair path (double-strand break repair, DSBR), the other end of the break interacts with the displaced strand of the D-loop (second end capture) and the 3' end primes DNA synthesis, forming a double Holliday junction (dHJ) intermediate (double Holliday junction formation). Then, the dHJ intermediate can be dissolved or resolved to give two intact double-stranded DNA molecules. Dissolution requires the activity of the BLM-TopoIIIα-RMI1 helicase complex, which drives migration of the constrained dHJ and decatenates the interlinked strands between the two Holliday junctions, yielding noncrossover products. Otherwise, resolution through nucleolytic cleavage of the dHJ can give both crossover or noncrossover products: crossovers form from the cut of the inner strands of one Holliday junction and of the outer strands of the other Holliday junction; while noncrossovers are produced by cutting both junctions in the same plane. Following cleavage of dHJ, the ends are ligated to complete the reaction. In humans, resolvases implicated in this resolution are MUS81-EME1, GEN1, SLX1-SLX4, XPF-ERCC1.[41]

In the last possible path, the extended D-loop structure could be cleaved prior to formation of a mature dHJ intermediate (early D-loop cleavage). MUS81-EME1 nuclease could promote crossover formation by cleaving the strand invasion intermediate directly.[42]

1.1.6 Fanconi anemia

The Fanconi anemia (FA) repair pathway is required for genome protection against inter-strand crosslinks (ICLs). This type of lesions are considered ones of the most deleterious DNA lesions, because two Watson and Crick strands of DNA are covalently bound together, obstructing both replication and transcription. ICLs can be generated by

naturally occurring compounds, chemotherapeutic agents or during normal cellular metabolism. ICLs left unrepaired can lead to mutations, chromosome breakage, chromosome missegregation and mitotic catastrophe. The FA family of proteins includes 19 distinct functional complementation groups whose gene products suppress ICL sensitivity. Mutations in most FA genes in normal cells lead to a chromosomal instability disorder characterized by multiple developmental abnormalities, progressive bone marrow failure and cancer predisposition, which underlie the pathologies associated with Fanconi anemia.[43,44]

When two convergent replication forks collide and stall at an ICL site, BRCA1 acts to dismantle the replisome and RAD51 binds to the single-stranded DNA to protect the fork. Subsequent FANCM-FAAP24-MHF1/2 complex binding activates ATR signaling pathway and promotes recruitment of the FA core complex. The FA core complex in turn ubiquitinates the FANCI–FANCD2 heterodimer, which acts as a platform to recruit multiple nucleases like XPF-ERCC1, SLX1-SLX4, MUS81-EME1, FAN1, SNM1A, and SNM1B. Nucleolytic incisions unhook the ICL and facilitate translesion synthesis-dependent lesion bypass, mediated by REV1 or Pol ζ polymerase. Finally, the generated double-strand break is repaired by homologous recombination.[45,46]

1.2 Cyclin D1

The D-type cyclin family is composed of three proteins (cyclin D1, cyclin D2 and cyclin D3) that are expressed in proliferating cells. They are closely related: the human cyclin D2 and D3 proteins are 62% and 51%, respectively, identical to human cyclin D1, and 62% identical to each other. Alternative splicing can arise to another cyclin D1 isoform, cyclin D1b: it diverges from the canonical full-length cyclin D1 protein at the carboxy-terminal because it lacks some key interaction domains (*Figure 1.6*).[47]
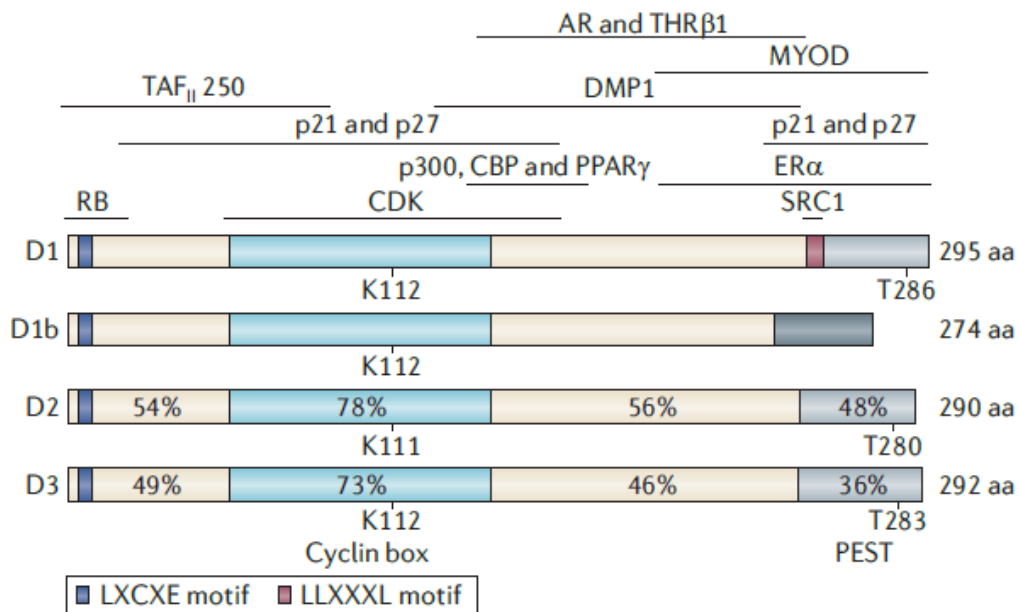
Figure 1.6: *Domain structure of D-type cyclins family.*
Figure from Musgrove, E *Nat. Rev. Cancer* (2011)[47]

The greatest homology in the D-type family of cyclins occurs in the cyclin box that mediates cyclin-dependent kinase (CDK) binding and is important for the interaction with CIP/KIP family of CDK inhibitors as p21, p27 and p57. Retinoblastoma (RB) protein-binding domain (characterized by the LXCXE motif) is always present at the extreme amino-terminal. At the carboxy-terminal there is a highly conserved PEST domain that is rich in proline, glutamate, serine and threonine and that is characteristic of proteins that are rapidly turned over. If threonine 286 in cyclin D is phosphorylated, the protein is sent to ubiquitin-mediated degradation; this phosphorylation also promotes cyclin D1 nuclear export. Mutations within these highly conserved regions have been widely used to probe cyclin D1 functions. The region between the cyclin box

and the carboxy-terminal is relatively poorly conserved and it contains domains that are responsible for transcription factor-cyclin D1 interactions. In cyclin D1, the leucine-rich motif LLXXXL at the carboxy-terminal is designated to the binding of the steroid receptor co-activators SRC1 and AIB1.[47]

The earliest known and best understood function of cyclin D1 is to promote cell proliferation as a regulatory partner for CDK4 or CDK6 but, recently, there is growing evidence that cyclin D1 plays cell cycle-independent roles that are also independent of CDKs substrate phosphorylation (***Figure 1.7***).
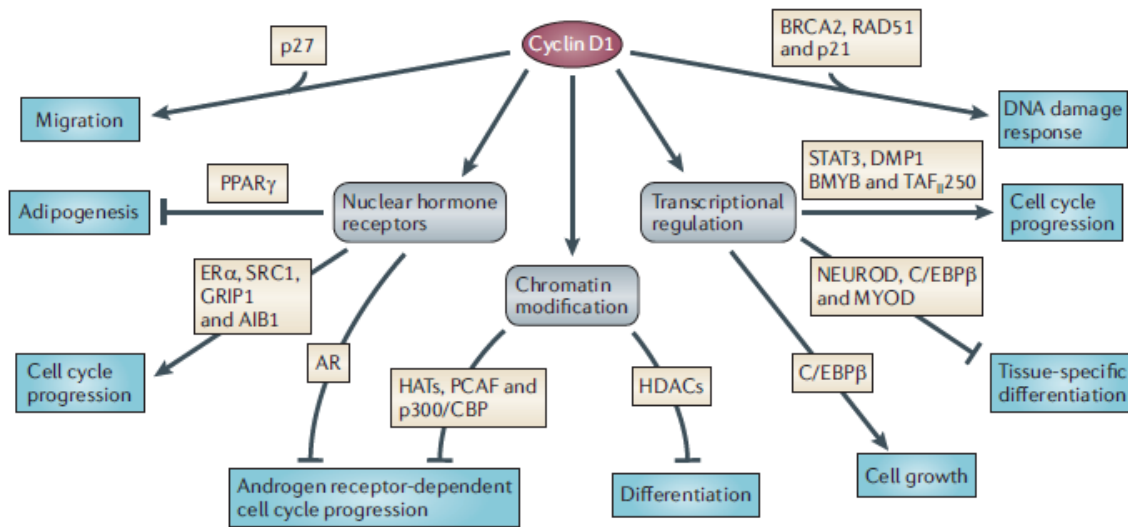
Figure 1.7: *CDK-independent functions of cyclin D1.*
Figure from Musgrove, E *Nat. Rev. Cancer* (2011)[47]

Extracellular signals, such as growth factors and integrin-derived adhesion signaling, influence cyclin D1 transcription, translation and degradation, integrating mitogenic, differentiation and adhesion signaling with the cell cycle regulatory machinery. The deregulation of cyclin expression or CDK activation can directly lead to cancer by causing proliferation or by overriding checkpoints that ensure genomic integrity and stability. Furthermore, the gene encoding cyclin D1 (*CCND1*) represents the second most frequently amplified locus in the human cancer genome. The oncogenicity and multiplicity of cyclin D1 effects on cancer cell biology, and evidence for its CDK-independent actions on end points such as cell migration and the DNA damage response, provide an impetus for targeting cyclin D1 rather than, or in addition to, CDK4/CDK6 activity.[48,49]

1.2.1 Cyclin D1 in cell cycle regulation

The cell cycle is a complex process that controls cell growth and proliferation; it is also involved in development, regulation of DNA damage and diseases such as cancer. The cell cycle is divided into phases. The first phase, G1 gap, is the preparation of the cell for DNA synthesis that occurs in the second phase, the S one. The third phase is the G2 gap in which the cell prepares for mitosis, that occurs in the fourth phase, the M one. There is also an additional G0 gap that is the phase in which cells are not cycling. Regulatory proteins can direct the cell through a specific sequence of events that go towards mitosis: these important proteins are cyclin-dependent kinases (CDKs) and cyclins. In general, the cell can go through cell cycle phases only if the specific cyclin binds and activates the specific phase CDK. CDKs are serine-threonine kinases that are regulated by phosphorylation on threonine and tyrosine residues. Cyclins have a cyclic expression because they are regulated by ubiquitination-mediated proteolysis: for this reason CDKs can be activated only at specific times during the cell cycle. The cell can enter in the next phase only if the appropriate cyclin of the previous phase is degraded and the cyclin of the next phase is synthesized. Cyclins target CDKs to the nucleus because they contain nuclear localization signals. In the nucleus, CDKs phosphorylate a variety of substrates that are necessary for cell proliferation. Cell cycle checkpoints are essential for the cell to monitor and regulate its progress through the cycle. They prevent cell cycle progression at specific points, allowing verification of necessary phase processes and repair of DNA if it is damaged. The cell proceeds to the next phase only if checkpoint requirements have been met. Several checkpoints are designed to ensure that damaged or incomplete DNA is not passed on to daughter cells. Three main checkpoints exist, but D-type cyclins control only G1/S transition, also known as restriction point.[50]

The restriction point is controlled by CDK4/CDK6 proteins that have to bind to cyclin D proteins. This active complex can phosphorylate the target protein retinoblastoma (RB) on multiple residues. RB normally binds to the transcription eukaryotic factor 2 (E2F), making it unavailable for transcription. When RB protein is phosphorylated by the specific CDK, E2F is free to act as a transcription factor for the expression of genes required for nucleotides biosynthesis, DNA synthesis, mitotic progression and DNA damage repair (*Figure 1.8*).[51]
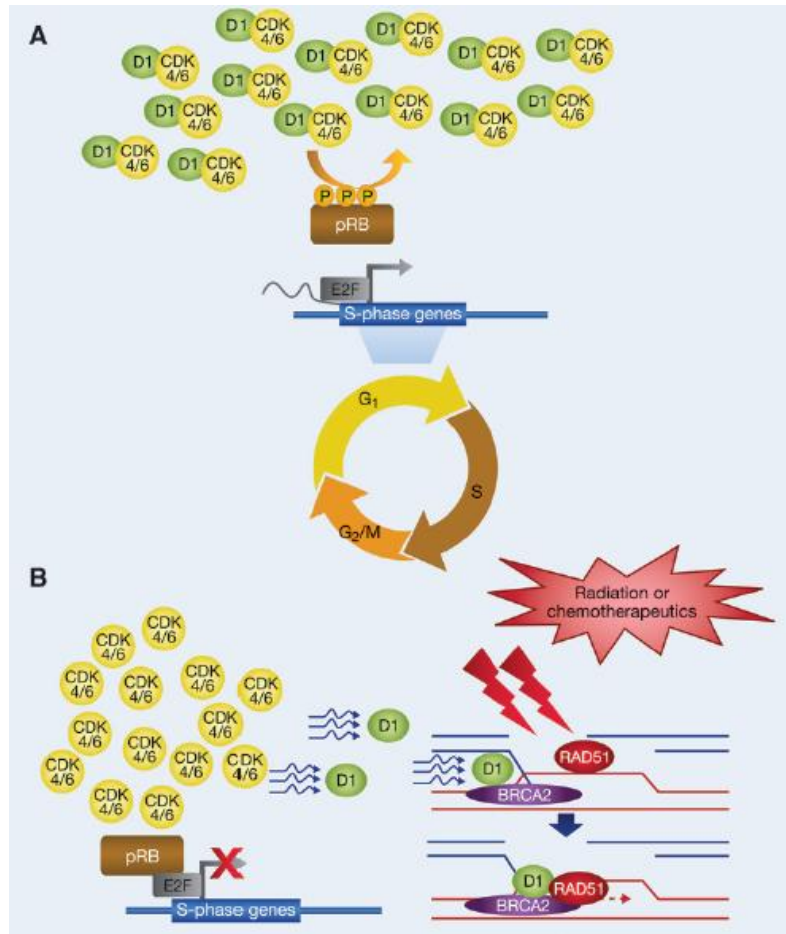
Figure 1.8: *Cyclin D1 functions in cell cycle regulation (A) and DNA repair (B).*
Figure from Jirawatnotai, S *Cancer Res.* (2012)[51]

The RB-E2F complex can also repress transcription by a different mechanism: RB may also inhibit E2F by recruiting chromatin remodeling enzymes, including histone deacetylases (HDACs). HDACs are a family of at least seven different enzymes that remove acetyl groups from the tails of histone octamers, facilitating nucleosomal compaction and negatively affecting accessibility of transcription factors to promoters. In addition, it is possible that RB-mediated recruitment of HDAC to E2F also acts by a repression of the activity of histone acetyltransferases (HATs) that are complexed to E2F.[52]

Furthermore, association of D-type cyclins to CDK4/CDK6 is influenced by important negative regulators such as the INK4 family of CDK inhibitors (p15, p16, p18, p19) and a second family of molecules, CIP/KIP inhibitors, containing p21, p27 and p57. In general, these proteins inhibit CDK association with its cyclin, preventing complex formation.[53]

1.2.2 Cyclin D1 in DNA damage repair

As already explained before, cyclin D1 protein has been recently shown to have an important role in DNA damage repair: after DNA damage by radiation or chemotherapeutics, cyclin D1 protein levels are significantly reduced and the cell cycle is arrested. Part of the remaining pool of cyclin D1 is recruited into the nucleus, to DNA damage sites, in a BRCA2-dependent manner, to facilitate and stabilize RAD51 localization, thereby assisting the homologous recombination (HR)-mediated DNA repair pathway (*Figure 1.8*).[51,54]

One of the first who elucidated this new function of cyclin D1 were Siwanon Jirawatnotai et al. in 2011: they performed a proteomic screen for cyclin D1 partners in order to elucidate the molecular functions of this protein. They analysed four types of human tumors, all overexpressing cyclin D1 gene *CCND1*: mantle cell lymphoma (Granta 519 cells), breast cancer (MCF7 and ZR-75-1), squamous cell carcinoma (UMSCC-2), and colorectal cancer (HT-29). Cyclin D1-containing complexes were purified using double immunoaffinity purification, and the identity of cyclin D1 interactors was determined by rounds of liquid chromatography and high-throughput mass spectrometry (LC-MS/MS). Finally, with the total 132 proteins identified with high confidence, they constructed a biological process/molecular function enrichment heatmap of cyclin D1 interactors. Apart from cell cycle control proteins, unexpectedly, they observed DNA repair category amongst the most enriched functions. A cluster of DNA repair proteins centered on RAD51, the DNA recombinase mediating DNA repair via homologous recombination, was identified. These observations first suggested that cyclin D1 may play a key role in DNA damage repair (*Figure 1.9*). They also observed that if you silence *CCND1*, there is a significant increase in the sensitivity of cancer cells to ionizing radiation (IR) and to DNA damaging drugs as topoisomerase inhibitors. Re-expression of cyclin D1 in these cells restored radiation sensitivity. Furthermore, treatment with a specific inhibitor of CDK4/6 kinase had no effect on sensitivity of cancer cells to radiations; for this reason, cyclin D1 might play a kinase-independent function in DNA repair. They found that radiation induced comparable levels of DNA damage in control and in cyclin D1-depleted cells but that, at 16 hours post-radiation, more unrepaired DNA persisted in cyclin D1-depleted cells.[55]
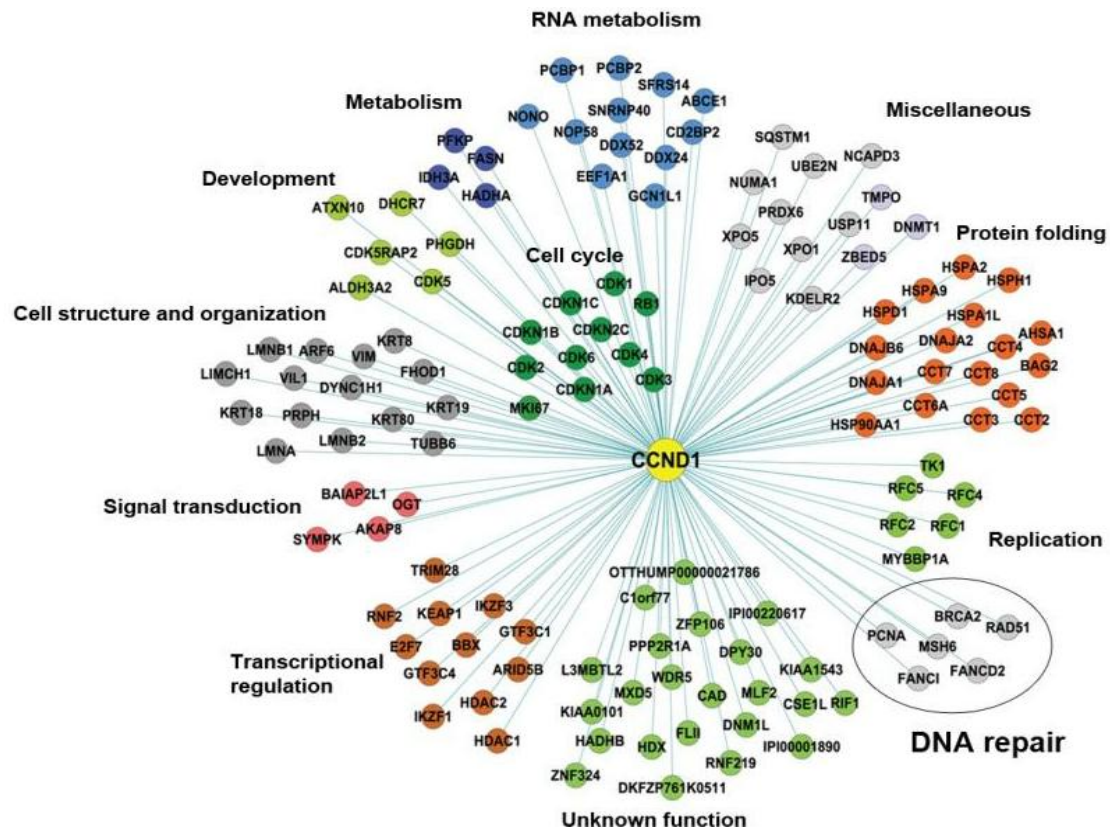
Figure 1.9: *Interactome map of cyclin D1 according to biological process.*
Figure from Jirawatnotai, S *Nature* (2011)[55]

They showed how, in some cells, depletion of cyclin D1 significantly reduced homologous recombination and re-expression of cyclin D1 rescued this effect. To investigate the function of cyclin D1 in HR, they analyzed the interaction of cyclin D1 with RAD51. They established that the amino-terminus of cyclin D1 directly binds to the carboxy-terminus of RAD51 and that this interaction is induced by radiation. RAD51 and cyclin D1 are recruited and colocalize at the sites of double-stranded DNA breaks (DSBs), characterized by histone H2AX phosphorylated on serine 139 (γH2AX). They reported that knock-down of *CCND1* resulted in reduced recruitment of RAD51 to DNA damage foci. With these results, they demonstrated how cyclin D1 helps to recruit RAD51 through a direct cyclin D1-RAD51 physical interaction. Then, in this paper they verified the direct interaction of cyclin D1 with BRCA2 and reported that BRCA2 is essential for recruitment of cyclin D1, consistent with the notion that BRCA2 acts upstream. Collectively, these results are consistent with the DNA damage repair model of cyclin D1: cyclin D1 is recruited to DNA damage sites through BRCA2 and then it helps to recruit RAD51 through a direct cyclin D1-RAD51 interaction. In fact, depletion

of cyclin D1 reduces RAD51 recruitment and reduces RAD51-BRCA2 colocalization at DNA damage sites, leading to impaired homologous recombination. Moreover, cyclin D1 is not required for recruitment of FANCD2, FANCI, PCNA, MSH6, BRCA1 and MRE11. Jirawatnotai et al. also observed that, upon irradiation, cyclin D1-depleted tumors displayed *in vivo* retarded growth as compared to control tumors, revealing increased sensitivity to IR. By all these findings, there is great evidence about cyclin D1 as a possible target to sensitize human cancers to radiation, by limiting DNA repair. Thus, targeting cyclin D1 in combination with radiation treatment may have potential therapeutic value in a large pool of cancers.[55]

Zhiping Li at al. in 2010 already assessed the importance of full-length cyclin D1 protein for a correct DNA damage response. The canonical cyclin D1 isoform (cyclin D1a), but not cyclin D1b, contributes at the recruitment of DNA repair factors at γH2AX foci. They also suggested a possible implication of cyclin D1 in the induction of expression of DNA repair proteins, such as RAD51.[56] Afterwards, the same group verified that cyclin D1 is required for both basal and estrogen-induced expression of RAD51 gene and they hypothesized a model (*Figure 1.10*).[57]
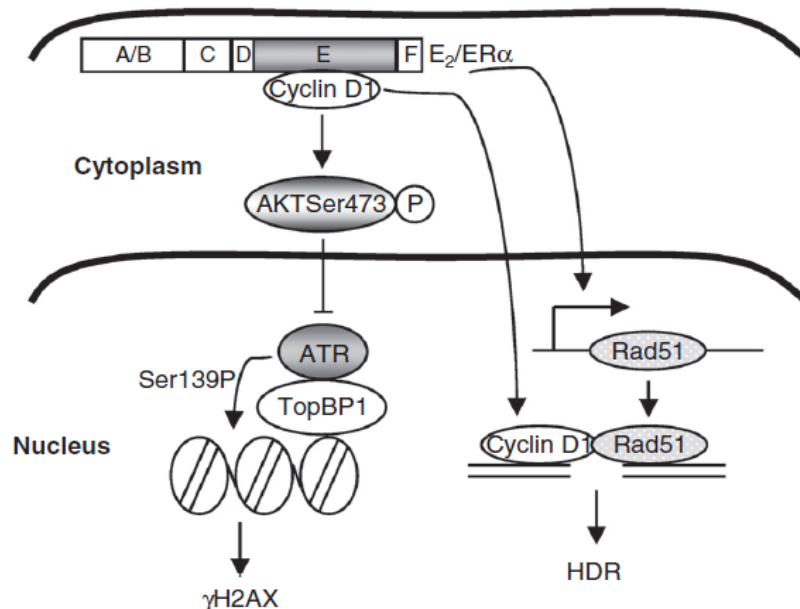
Figure 1.10: *Model for cyclin D1-dependent induction of homology-directed repair.*
Figure from Li, Z *Cancer Res.* (2014)[57]

In this model cyclin D1, associated with ERα in the cytoplasm, augments AKT signaling and is essential for γH2AX foci formation. Cyclin D1 increases homologous

recombination-mediated repair (HDR), in part through binding to DNA at γH2AX foci and through inducing RAD51 recombinase transcription and abundance.[57]

In addition, cyclin D1 binds RAD51 but it does not directly recruit it: cyclin D1 just enhances RAD51 binding to BRCA2 because it prevents the inhibitory BRCA2 serine 3291 phosphorylation. BRCA2 accumulates RAD51 molecules on its RAD51-binding motifs: the BRC repeat domain is in the middle portion of the protein, while the other conserved motif is at the carboxy-terminal domain of BRCA2. BRCA2 carboxy-terminal mutants, such as *BRCA2 6174delT* and *6158insT*, lack the functional RAD51-binding domain and exhibit reduced capacity to recruit RAD51 to DNA damage foci; in such manner these mutants present limited DNA repair and these mutations are characteristic of various human cancers, like pancreatic, breast or ovarian cancer. Normally, HR pathway factors, including CtIP/SAE2, NBS1 and BRCA2, are substrates for CDKs, underlining the direct role of cell cycle proteins in the DNA repair process. Cyclin A-CDK2 and cyclin B-CDK1 can phosphorylate BRCA2 on serine 3291, on the carboxy-terminal RAD51-binding domain. Under DNA damage conditions, BRCA2 is dramatically hypophosphorylated because of the degradation of CDC25A and the rapid decline of CDKs activity; thereby BRCA2 can recruit RAD51 and DNA is repaired. Aminoacids 90-155 of cyclin D1 directly interact with RAD51, but cyclin D1 is not necessary for BRCA2 recuitment at damaged foci. Altogether, these findings suggest that cyclin D1 facilitates RAD51 recruitment to BRCA2-bound DNA damage foci. It is reported that cyclin D1 (aminoacids 20-90) interacts directly with the carboxy-terminus (aminoacids 3189-3418) of BRCA2, and it impedes the inhibitory cyclin A/B-CDK2/1-dependent BRCA2 phosphorylation. In this way, cyclin D1 indirectly facilitates RAD51 recruitment and HDR-mediated DNA repair. Cyclin D1, which preferably interacts with the hypophosphorylated form of BRCA2, accumulates at the carboxy-terminal domain and precludes kinase from this site. These statements underline how in wild-type BRCA2 cancers, targeting cyclin D1 in combination with DNA damaging agents may be beneficial for the cancer treatment.[58]

In the last two years, some papers showed the importance of targeting cyclin D1 in prostate cancer cells, multiple myeloma tumours and mantle cell lymphoma cell lines.[59,60] Prostate cancer cells are frequently characterized by an elevated DNA repair capacity that leads to radiation resistance. Cancer cells escape from radiation therapy by

repairing the DNA lesions through the activation of highly conserved enzymatic pathways: only the accumulation of unrepaired breaks may generate chromosomal aberrations that, after a variable number of cell cycles, induce cell death. Silencing *CCND1* affects the tumorigenic potential of prostate cancer cell lines *in vitro* and *in vivo*; in addition migration and invasion abilities are drastically reduced in the absence of cyclin D1. The radiosensitization induced by silencing cyclin D1 is dependent on the increased accumulation of double-stranded breaks (DSBs).[61] In mantle cell lymphoma cells, *CCND1* depletion results in DSBs and genomic instability during DNA replication. The genome protective function of cyclin D1 is thus relevant to the resistance of mantle cell lymphoma to chemotherapeutic agents.[62]

Activation of DSBs repair genes is one of the reasons for chemo- and radio-resistance, therefore, targeting DNA repair pathways is an attractive strategy to eliminate cancer. Currently, there are no small-molecule inhibitors of *CCND1* under clinical development, but pharmacologic agents that indirectly reduce *CCND1* levels have been reported.[61]

1.2.3 Cyclin D1 in chromosomal instability

As cyclin D1 expression is increased in the early phases of tumorigenesis, it may be an important inducer of chromosomal instability (CIN) in tumors. Cyclin D1 induces CIN in different types of cells: cyclin D1 overexpression correlates with aneuploidy, polyploidy, supernumerary centrosomes, and spindle defects. ChIP-seq analysis have shown how cyclin D1 is bound and enriched on genes that govern CIN. For this reason, cyclin D1 contributes to chromosomal instability and tumorigenesis by directly regulating a transcriptional program that governs CIN.[63]

Some speculations were drawn on the indirect DNA damaging effect of overexpressed cyclin D1. Cyclin D1 or cyclin D1b variant overexpressions are a consequence of *CCND1* gene mutations or genetic variations. Overexpression of cyclin D1 might force a premature S phase entry, accumulating DNA lesions, might antagonize cell cycle arrest signal, promote hyperactive homologous recombination repair, and facilitate transcriptional activation of genes that interfere with genome stability. Overexpression of cyclin D1 also drives cancer cells bearing DNA lesions to undergo clonal expansion (*Figure 1.11*).[64]
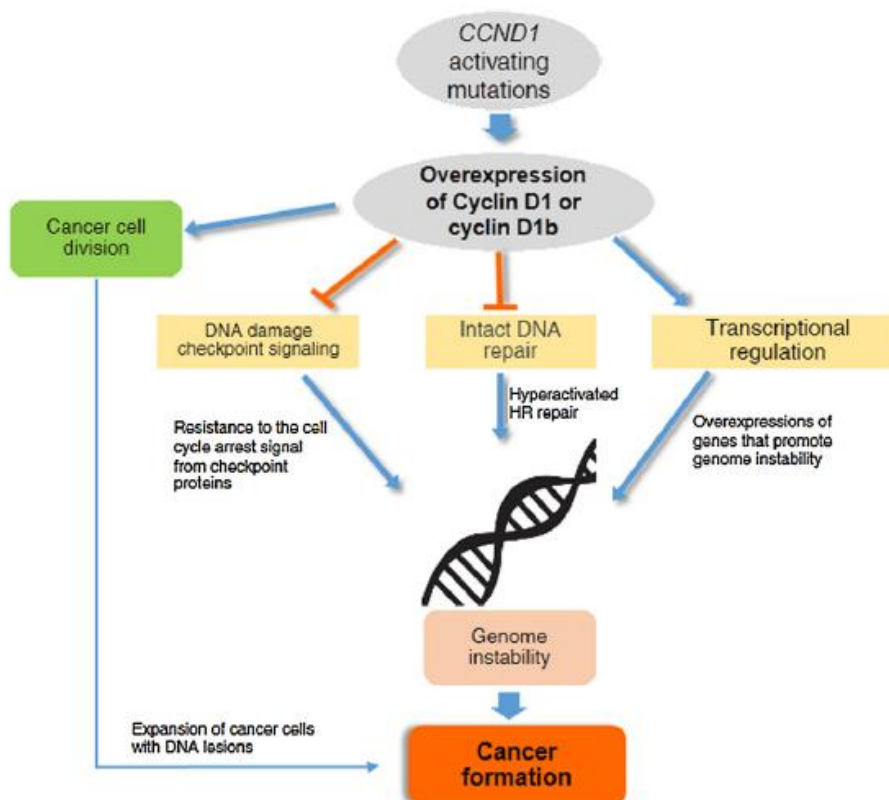
Figure 1.11: *Overexpression of cyclin D1 induces genome instabiliy and cancer formation via different indirect mechanisms.*

Figure from Jirawatnotai, S *DNA Repair (Amst).* (2016)[64]

1.2.4 Cyclin D1 in cell migration

Metastasis is the major cause of death in cancer patients and cellular migration is essential for tumor metastasis. Cyclin D1 induces cell migration in a CDK-dependent manner as some CDK4/CDK6 substrates have roles in cell adhesion, cell migration, and cytoskeletal remodeling. Phosphorylation of these substrates such as filamin A and Ral GEF Rgl2 contributes to enhanced cell detachment and motility. Cyclin D1 induces cell migration also in a CDK-independent manner: it binds p27 and it inhibits RhoA GTPase activity. In addition, cyclin D1 promotes cellular migration by transcriptional upregulation of ROCKII and thrombospondin (TSP-1). The frequent amplification and overexpression of cyclin D1 in cancer cells suggest that cyclin D1 may have a central role in mediating the invasion and metastasis by controlling Rho/ROCK signaling and expression of TSP-1. In fact, if cyclin D1 is depleted, macrophages, fibroblasts, and epithelial cells have enhanced adhesion and decreased motility.[65,66]

CHAPTER 2
AIMS OF THE RESEARCH

Ovarian cancer is the most common cause of gynecological cancer-associated death. Epithelial ovarian cancer can be subdivided into different histological subtypes, but high-grade serous carcinoma (HGSC) is the most commonly diagnosed. Globally, 225,500 new cases of ovarian cancer are diagnosed each year. In the United States, approximately 22,280 new cases occur annually and the projected number of deaths for 2016 is 14,240. Survival varies greatly based on stage at initial diagnosis: 5-year overall survival in patients with stage I cancer is 92.1%, but it is 25% for patients with stage III and stage IV cancers. Effective screening strategies for the early detection of ovarian cancer do not exist, but individuals at high risk of developing ovarian cancer, such as those with germline mutations in *BRCA1* or *BRCA2* genes, can be identified. The most active therapeutic agents against ovarian cancer are platinum analogues (either cisplatin or carboplatin), with the addition of a taxane (either paclitaxel or docetaxel). Treatment paradigms for first-line management of newly diagnosed ovarian cancer include either primary surgical cytoreduction followed by platinum-based chemotherapy or neoadjuvant chemotherapy followed by interval surgical reduction and additional chemotherapy.[67]

The most difficult issue in the treatment of ovarian cancer is the eventual development of platinum resistance. A small population of platinum-resistant cancer cells exists in ovarian tumours before treatment and flourishes once treatment has killed their platinum-sensitive counterparts. This results in regrowth of the tumour, and a low probability that it will respond to further treatment with platinum-based drugs. Advances in new therapeutics for recurrent ovarian cancer treatment include angiogenesis inhibitors, immunotherapy agents, selective estrogen receptor modulators (SERMs), and finally inhibitors of DNA damage repair mechanisms, such as poly(ADP-ribose) polymerase (PARP) inhibitors. Strategies using PARP inhibitors as part of the first-line treatment, as well as combinations of these therapies for the treatment of both newly diagnosed and recurrent ovarian cancer, are underway.[68]

Most subtypes of epithelial ovarian cancer are associated with germline *BRCA* mutations. Survival is improved for women with ovarian cancer carrying germline *BRCA* mutations compared with wild type *BRCA1* and *BRCA2*, probably because *BRCA2* mutation results in enhanced platinum sensitivity. Besides *BRCA1* and *BRCA2*, other germline mutations in genes involved in DNA repair can increase the risk of

developing ovarian cancer, including *RAD51* and *PALB2*. Inherited mutations in other genes involved in DNA repair, such as *CHEK2*, *MRE11A*, *RAD50*, *ATM* and *TP53*, might also increase the risk of developing ovarian cancer.[67]

Scope of this thesis is to find a new possible approach for the treatment of ovarian cancer.

The model in this study is IGROV1, a human ovarian tumor-derived cell line with epithelial morphology, endometrioid histology for the major part of the tumor, with some serous clear and undifferentiated cells. IGROV1 cells are at grade 2 and stage III, with a doubling time of 27 hours. *TP53*, *BRCA1* and *BRCA2* genes are mutated, but *BRCA2* mutation is silent; in total there are three mutated genes in the homologous recombination repair pathway.[69,70]

This study tries to set a combined treatment to increase sensitivity of IGROV1 cells to irradiation.

3l is an E-3-(2-chloro-3-indolylmethylene)1,3-dihydroindol-2one (***Figure 2.1***) that has been synthesized by Professors Rambaldi and Locatelli's research group at Pharmacy and Biotechnology (FaBiT) Department of the University of Bologna.[71]
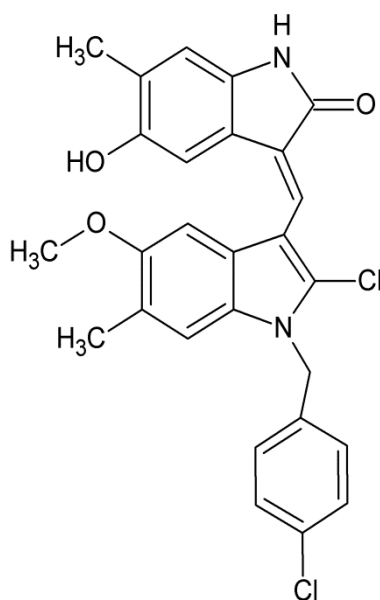
Figure 2.1: *Structural formula of molecule 3l.*

It has been published that 3l has a cytostatic, but not cytotoxic, effect on leukemia, central nervous system, ovarian, renal, prostate and breast cancer cell lines. In ovarian

cancer cell lines, 3l has a pGI$_{50}$ of 5.45 that corresponds to 3.5 μM treatment concentration. 3l 5 μM treatment of IGROV1 cells induces a retained block in cell proliferation with cell cycle arrest in G0/G1 phases.[71]

Furthermore, Professor Calonghi's group has showed how 3l induces a strong irreversible growth arrest characterized by progressive accumulation of IGROV1 cells in G0/G1 phases, and such cells reach nearly synchronization after 72 hours of treatment. With an excitation and an emission wavelengths of 488 nm and 530 nm, respectively, 3l can be visualized by fluorescence-based methods. Confocal microscopy experiments revealed that 3l is already localized in the nucleus after 6 hours of treatment and that the 3l fluorescent signal colocalizes with the estrogen receptor β (ERβ), but not with the estrogen receptor α (ERα). Interestingly, the 3l-ERβ complex is bound to chromatin. Transcription analysis by quantitative Real-Time PCR (qRT-PCR) reported no changes in ERα target genes. Additional chromatin immunoprecipitation (ChIP) experiments of ERα binding to *pS2* promoter, a well known ERα target gene, showed that this event is not modified by 3l treatment, confirming that this nuclear receptor is not involved in 3l mechanism of action. After 6 hours of treatment with 3l, transcription analysis showed a decrease in *CCND1* gene expression, an increase in *p16*, whereas *ERβ* and *p21* gene expressions did not change. After 24 hours of treatment, analysis showed a further decrease in *CCND1* gene expression; *ERβ* gene expression was up-regulated, but not that of *p16*. The analysis of ERβ isoforms showed a transcriptional increase of *ERβ1*, that is the active isoform, whereas *ERβ2* and *ERβ5* truncated isoforms decreased. p16 increase and cyclin D1 decrease had also been confirmed at protein level, by western blot. Finally, the adhesion analysis reported a differentiation phenotype characterized by stretched-shaped cells induced by 3l treatment.[72]

This project focuses on the potential role of molecule 3l in depleting cyclin D1 protein level.

Cyclin D1 has been recently studied as an important protein in DNA damage repair mechanisms, especially in homologous recombination-directed repair (HDR). Cyclin D1 is recruited to damaged foci by BRCA2 and it enhances RAD51 binding to BRCA2 because cyclin D1 prevents BRCA2 inhibitory phosphorylation on serine 3291.

Furthermore, cyclin D1 is essential for *RAD51* gene upregulation in case of double-stranded break (DSB).

3l has been showed to reduce cyclin D1 transcript and protein level at 24 hours of treatment of about 60% (***Figure 2.2***).[72]
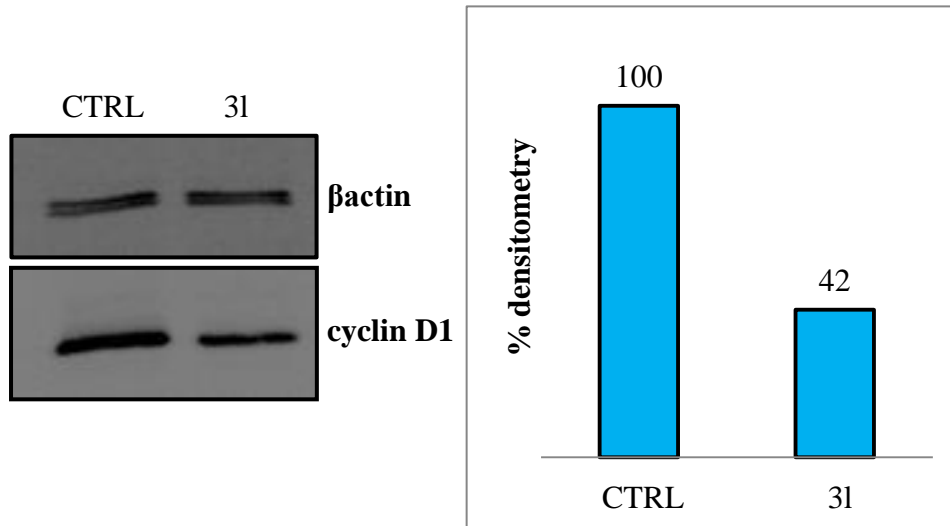
Figure 2.2: Cyclin D1 protein quantification by western blot 24 hours after 5 μM 3l treatment of IGROV1 cells.[72]

For this reason, 3l treatment could be used to study cyclin D1 role in DNA damage repair, especially in an hormone-dependent cancer as ovarian cancer, that has not been well addressed yet.

The experimental model of the project consists of:

- 3l 5 μM treatment for 24 hours to deplete cyclin D1 expression
- UV irradiation to induce DSB damages.

In this way, the consequences of induced DSBs could be analyzed in IGROV1 cells: formation of the repair complex on damaged sites is the crucial event to prevent propagation of the damage.

First of all, it has been essential to set up time and duration of UV treatment, using the well studied breast cancer cell line MCF7 as a template. Then, phosphorylation of histone H2AX on serine 139 has been detected and quantified to prove that UV irradiation induces DNA damage. *RAD51* gene upregulation has been analysed by qRT-PCR to check whether cyclin D1 is really important for *RAD51* expression. By confocal microscopy, colocalization of the repair complex BRCA2-cyclin D1-RAD51 has been

analysed on the γH2AX foci. Finally, siRNA silencing of *CCND1* gene has been assessed to confirm the effect on repair pathway caused by 3l-dependent cyclin D1 depletion.

The combined treatment of a drug leading to a depletion of cyclin D1 and a DNA damage inducer, such as irradiation, could be a potent potential therapy to target cancers with an elevated rate of DNA repair pathways, especially in case of chemo- and radio-resistant tumours.

CHAPTER 3
MATERIAL AND METHODS

3.1 Cell culture

IGROV1, a human epithelial ovarian cancer cell line, and MCF7, a human breast cancer cell line, were used in these experiments. Cells were seeded in flasks or plates (*Sarstedt*) at a density of 20,000 cells/cm^2 and incubated at 37°C in a 5% CO_2 atmosphere. The composition of the complete medium is given in ***Table 3.1***.

Table 3.1: *Composition of cell complete medium.*

RPMI 1640 (*Lonza*)	89%
Fetal bovine serum (FBS) (*EuroClone*)	10%
L-glutamine 200 mM (*Sigma-Aldrich*) in phosphate buffered saline (PBS)	1%

After two washes with PBS, trypsin 0.115% (*Seromed*) in a solution of PBS-ethylenediaminetetraacetic acid (EDTA) (*Sigma-Aldrich*) 0.02% was used to split cells; it was incubated with cells for 5 minutes at 37°C and neutralized with complete medium. Cells were finally counted using a Burker chamber. The composition of PBS is described in ***Table 3.2***.

Table 3.2: *Composition of phosphate buffered saline.*

NaCl (*Sigma-Aldrich*)	8 g/L
Na_2HPO_4 (*Sigma-Aldrich*)	1.15 g/L
KCl (*Sigma-Aldrich*)	0.2 g/L
KH_2PO_4 (*Sigma-Aldrich*)	0.2 g/L

3.2 Treatments and siRNA silencing

3l (***Figure 2.1***) was dissolved in dimethyl sulfoxide (DMSO) (*Sigma-Aldrich*) at 20 mM concentration and cells were treated at the final concentration of 5 μM for 24 hours.

UV irradiation was set up: cells were put for 15 minutes under a nominal power 30 W UV-C lamp (*Philips*) at a distance of 55 cm.

siRNA silencing was applied after 72 hours of adhesion, when cells were 70% confluent. The specific siRNA against *CCND1* gene and the scramble siRNA used in this thesis are described in ***Table 3.3***.

Table 3.3: *Custom validated siRNA used for the experiments.*

Validated Silencer Select siRNA (*Thermo Fisher Scientific*)	s229
Silencer Select Negative Control siRNA (*Thermo Fisher Scientific*)	#1

siRNAs were dissolved in RNase-free water up to a 10 µM stock. A first 1:100 dilution siRNA stock was assessed in OptiMEM (*Thermo Fisher Scientific*). The RNAiMAX (*Thermo Fisher Scientific*) solution was 1:50 diluted in OptiMEM, too. The diluted solution of siRNA was added to an equal volume of the diluted RNAiMAX, everything was gently resuspended and incubated at room temperature for 20 minutes. Finally, the siRNA-RNAiMAX solution was 1:5 diluted in OptiMEM medium and added drop by drop to cells. In this manner, the final siRNA treatment optimized concentration was 10 nM. After 24 hours of siRNA treatment, the medium was changed in complete RPMI 1640 medium and cells were analyzed 24 hours after medium change.

Cells were treated like described in **Table 3.4**.

Table 3.4: *Samples description.*

CTRL	Control cells (no treatment nor irradiation)
UV	Cells UV-irradiated 72 hours after seeding and analyzed 4 hours after irradiation
3l	Cells 3l-treated 72 hours after seeding and analyzed 28 hours after treatment
3l/UV	Cells 3l-treated 72 hours after seeding, UV-irradiated 24 hours after treatment and analyzed 4 hours after irradiation
siRNA	Cells specific siRNA-treated 72 hours after seeding and analyzed 52 hours after treatment
siRNA/UV	Cells specific siRNA-treated 72 hours after seeding, UV-irradiated 48 hours after treatment and analyzed 4 hours after irradiation
scramble	Cells scramble siRNA-treated 72 hours after seeding and analyzed 52 hours after treatment
scramble/UV	Cells scramble siRNA-treated 72 hours after seeding, UV-irradiated 48 hours after treatment and analyzed 4 hours after irradiation

3.3 RNA extraction

IGROV1 cells were seeded and treated as described in ***Paragraph 3.2***. Then, cells were trypsinized and counted. 5 millions cells were centrifuged for 10 minutes at 250 g and washed twice with 1 mL of PBS by centrifugation at 3,000 g for 3 minutes. For the RNA extraction, the RNeasy Mini Kit (*Qiagen*) was used. Pelleted cells were lysed with 350 µL of RLT buffer prepared by adding 10 µL of β-mercaptoethanol (*Sigma-Aldrich*) to 1 mL of buffer, according to the manufacturer's protocol. To homogenize the solution, a syringe with a 20-gauge needle was employed. After the addition of 350 µL of 70% ethanol (*Sigma-Aldrich*), the solution was transferred into a spin column placed in a collection tube and centrifuged for 15 seconds at 8,000 g. After the discard of the flow-through, 700 µL of the RW1 buffer were added to the column and centrifuged as before. Two washes with 500 µL of the RPE buffer were performed by centrifugation at 8,000 g for 15 seconds (first wash) and for 2 minutes (second wash). Then, to eliminate any carry-over of the buffer, the column was centrifuged for 1 minute at full speed with a clean collection tube. Finally, RNA was eluted by adding 30 µL of RNase-free water directly on the membrane of the column. The membrane was hydrated for 3 minutes at room temperature and then centrifuged at 8,000 g for 1 minute. RNA was quantified by NanoDrop spectrophotometer (*Thermo Scientific*) and integrity checked on a 2% agarose gel (*Sigma-Aldrich*).

3.4 Reverse transcription

RNA was employed to generate cDNA using the Transcriptor High Fidelity cDNA Synthesis Kit (*Roche*). The samples were firstly prepared in a PCR tube, as described in ***Table 3.5***.

Table 3.5: *Reagents for RNA reverse transcription (1).*

RNA	1 µg
Random examer primers	2 µL
RNase-free water	up to 11.4 µL

After 10 minutes pre-incubation at 65°C in a thermal cycler (annealing of the primers), at each sample mixture the reagents listed in *Table 3.6* were added.

Table 3.6: Reagents for RNA reverse transcription (2).

Reaction buffer 5x	4 μL
RNase inhibitors	0.5 μL
Deoxynucleotides	2 μL
Dithiothreitol (DTT)	1 μL
Reverse transcriptase	1.1 μL

cDNA synthesis was accomplished using the temperature program detailed in *Table 3.7*.

Table 3.7: Temperature program for RNA reverse transcription.

Activation of the enzyme	10 minutes	29°C
Transcription	60 minutes	48°C
Inactivation of the enzyme	5 minutes	85°C

3.5 Quantitative Real-Time PCR

cDNA was used to analyze the levels of transcripts by quantitative Real-Time PCR (qRT-PCR). The LightCycler FastStart DNA Master SYBR Green I kit (*Roche*) and the LightCycler 2.0 Instrument (*Roche*) were employed. qRT-PCR mixture composition is reported in *Table 3.8*.

Table 3.8: Description of reaction mixture for quantitative Real-Time PCR.

Master mix (containing Sybr Green I, FastStart Taq DNA Polymerase, dNTPs, MgCl$_2$ 1 mM) diluted 1:10
Primer forward (FW) 0.3 μM
Primer reverse (REV) 0.3 μM
MgCl$_2$ at the final concentration of 2.7 mM
2 μL of 1:10 diluted cDNA (nuclease-free water for blank control)
Nuclease-free water up to 12 μL

The first gene analyzed was the house-keeping gene *glyceraldehyde 3-phosphate dehydrogenase* (*G3PDH*) and its C_T values were used as standards in the $\Delta\Delta C_T$ method of results analysis. cDNA samples from IGROV1 treated/irradiated cells were compared to control cells. As blank control, a reaction mixture without the sample was always used. Samples were analyzed at least in triplicate and Student's t-test was used to verify the significance of results (a p-value less than 0.05 was considered significant). Primers (*Sigma-Aldrich*) employed and qRT-PCR conditions are listed in **Table 3.9**.

Table 3.9: *List of primers and conditions for quantitative Real-Time PCR.*

PRIMER	SEQUENCE	$T_{annealing}$	$T_{fluorescence}$	AMPLICON
G3PDH **FW**	atttggtcgtattgggcgcc	60°C	81°C	150 bp
G3PDH **REV**	acggtgccatggaatttgcc			
CCND1 **FW**	gccaactggtgtttgaaagta	60°C	77°C	88 bp
CCND1 **REV**	tccggtgtgaaacatctaaga			
RAD51 FW	cgagcgttcaacacagacca	60°C	80°C	98 bp
RAD51 REV	gtggcactgtctacaataagca			

After the qRT-PCR analysis, the presence of a single amplicon at the expected size was verified on a 1.8% agarose gel.

3.6 Total protein extraction

Cells were seeded and treated as described in **Paragraph 3.2**. They were then washed twice with PBS and incubated with 500 µL of the lysis buffer radio immunoprecipitation assay (RIPA) and 500 µL of the buffer HNTG at 4°C for 15 minutes with agitation. After the cell lysis, the solution was centrifuged for 20 minutes at 8,000 g and the supernatant containing the proteins was quantified using the Bio-Rad protein assay (*Bio-Rad*) based on the method of Bradford. The compositions of the RIPA lysis buffer and the HNTG buffer are given in **Table 3.10**.

Table 3.10: *Compositions of RIPA lysis buffer and HNTG buffer for protein extraction.*

RIPA Buffer	
Trizma Base - HCl, pH 7.4 (*Sigma-Aldrich*)	50 mM
NaCl	150 mM
EDTA	1 mM
NaF (*Sigma-Aldrich*)	1 mM
Sodium deoxycholate (*Sigma-Aldrich*)	1%
Triton X-100 (*Sigma-Aldrich*)	1%
Sodium dodecyl sulfate (SDS) (*Sigma-Aldrich*)	0.1%
Sodium orthovanadate (*Sigma-Aldrich*)	1 mM
Leupeptin, aprotinin, antipain, pepstatin A (*Calbiochem*), phenylmethylsulfonyl fluoride (PMSF) (*Sigma-Aldrich*)	10 μg/mL
HNTG Buffer	
4-(2-Hydroxyethyl)piperazine-1-ethanesulfonic acid (HEPES), pH 7.4 (*Sigma-Aldrich*)	50 mM
NaCl	150 mM
Triton X-100	0.1%
Glycerol (*Sigma-Aldrich*)	10%

3.7 Histone proteins isolation

Cells were seeded and treated as described in ***Paragraph 3.2***. They were trypsinized and counted, then centrifuged for 10 minutes at 250 g and washed three times with 1 mL of PBS by centrifugation at 3,000 g for 3 minutes at 4°C. To extract histones, 750 μL of lysis buffer were added to pelleted cells and the solution was incubated on ice for 15 minutes. The composition of the lysis buffer for histone extraction is reported in ***Table 3.11***.

Table 3.11: Composition of lysis buffer for histone extraction.

Buffer Na-PO$_4$, pH 7.4 (*Sigma-Aldrich*)	0.01 M
NaCl	10 mM
MgCl$_2$ (*Sigma-Aldrich*)	5 mM
(Octylphenoxy)polyethoxyethanol (NONIDET P-40) (*Sigma-Aldrich*)	0.1%
Sodium orthovanadate	0.5 mM
Leupeptin, aprotinin, antipain, pepstatin A, PMSF	10 µg/mL

After 15 minutes of incubation, 250 µL of paraformaldehyde 3% in PBS (*Sigma-Aldrich*) were added to the solution that was incubated on ice for 30 minutes. It was then centrifuged at 3,000 g for 3 minutes at 4°C and the pellet was washed twice with 1 mL of PBS. The pellet was suspended in 200 µL of H$_2$SO$_4$ 0.2 M and incubated for 1 hour at 4°C. Then, the solution was centrifuged for 5 minutes at full speed and the supernatant was mixed with 1 mL of acetone and left overnight at -20°C. The following day, the solution was centrifuged for 5 minutes at 8,000 g, the pellet composed by histones was dried, resuspended in 30 µL of water and quantified using the Bio-Rad protein assay (*Bio-Rad*) based on the method of Bradford.

3.8 Western blot

Proteins were analysed by sodium dodecyl sulfate-polyacrylamide gel electrophoresis (SDS-PAGE) and western blot on nitrocellulose membrane. To detect cyclin D1 from total protein lysate, 30 µg of this were resolved on a 12.5% density gel in running buffer at 200 V for 1 hour. 10 µg of isolated histones were detected resolving samples on a 15% gel in running buffer at 150 V for 90 minutes. The compositions of the running buffer is described in *Table 3.12*.

Table 3.12: Composition of running buffer for SDS-PAGE.

Trizma Base	25 mM
Glycine (*Sigma-Aldrich*)	192 mM
SDS	0.1%

Western blot was performed in transfer buffer at 100 V for 1 hour. The composition of the transfer buffer is given in **Table 3.13**.

Table 3.13: *Composition of transfer buffer for western blot.*

Trizma Base	25 mM
Glycine	192 mM
Methanol (*Sigma-Aldrich*)	20%

After electrophoresis and western blot, the polyacrylamide gel was visualized by Coomassie brilliant blue R-250 (*Sigma-Aldrich*). The nitrocellulose membrane was initially blocked by incubation with PBS-polyoxyethylene sorbitan monolaurate (TWEEN 20) 0.1% (*Sigma-Aldrich*) in agitation for 1 hour, then it was incubated as before with specific primary antibody diluted in PBS-TWEEN 20 0.1%. In **Table 3.14** the specific primary antibodies utilized with their related dilutions are listed.

Table 3.14: *Primary antibodies used in western blot and their dilutions.*

Mouse anti-cyclin D1 (*Millipore*)	1:500
Rabbit anti-γH2AX (*Santa Cruz Biotechnology*)	1:500
Mouse anti-βactin (*Sigma-Aldrich*)	1:5,000

After five washes with PBS-TWEEN 20 0.1%, the membrane was incubated as before with secondary horseradish peroxidase-conjugated antibody (*GE Healthcare*) diluted 1:20,000 in PBS-TWEEN 20 0.1%. After more five washes with PBS-TWEEN 20 0.1%, antibody binding was detected by WESTAR EtaC 2.0 (*Cyanagen*) and quantification was done by Fluor-S Max MultiImager (*Bio-Rad*) using βactin signal or total histone signal as control. Mean of at least three independent analysis and Student's t-test were used to verify the significance of results (a p-value less than 0.05 was considered significant).

3.9 Immunofluorescence

IGROV1/MCF7 cells were seeded on glass slides and after 72 hours they were treated, as described in **Paragraph 3.2**. Cells were after washed twice with 1 mL of PBS and

fixed with 500 µL of paraformaldehyde 3% for 10 minutes. Glass slides were washed twice with 1 mL of PBS-glycine 0.1 M and washed twice again with 1 mL of PBS-bovine serum albumin (BSA) 1% (*Sigma-Aldrich*). Cells were permeabilized by incubation for 3 minutes at -20°C with some drops of 70% ethanol and washed twice with 1 mL of PBS-BSA 1%. At this point, samples were incubated for 1 hour in agitation with specific primary antibody diluted in PBS-BSA 1%. The specific primary antibodies used and their related dilutions are listed in *Table 3.15*.

Table 3.15: Primary antibodies used for immunofluorescence and their dilutions.

Mouse anti-cyclin D1 (*Millipore*)	1:250
Rabbit anti-γH2AX (*Santa Cruz Biotechnology*)	1:250
Rabbit anti-RAD51 (*Santa Cruz Biotechnology*)	1:250
Rabbit anti-BRCA2 (*Santa Cruz Biotechnology*)	1:400

Glass slides were washed again twice with 1 mL of PBS-BSA 1% and incubated as before with secondary fluorescent antibody 1:1,000 diluted in PBS-BSA 1%: Alexa Fluor 568 or fluorescein isothiocyanate (FITC)-conjugated antibodies (*Life Technologies*). Finally, two washes with 1 mL of PBS-BSA 1% were performed and cells were incubated with 4',6-diamidino-2-phenylindole (DAPI) 5 µg/mL in PBS for 5 minutes at 37°C. Samples were mounted in Mowiol solution (*Calbiochem*), before being observed by a fluorescent confocal microscope (*Nikon C1s*). Quantification was managed using Adobe Photoshop CS3 by selecting at least seven cells in three different acquisitions for each sample. Student's t-test was used to verify the significance of results (a p-value less than 0.05 was considered significant).

CHAPTER 4
RESULTS

4.1 Set up of UV exposure and repair time point

The first experiments focused on the set up of UV exposure and time point for the repair analysis: breast cancer MCF7 cells have been taken as a model because they are normally used to study homologous recombination-directed repair pathway in literature. Different time of exposure were used to irradiate MCF7 cells and analysis was assessed at different time points after UV irradiation. The optimal UV irradiation should induce DNA damage and repair, but not cell death; the optimal time point for DNA repair analysis should immortalize the repair complex BRCA2-cyclin D1-RAD51 on repair foci, characterized by the phosphorylation of histone H2AX on serine 139 (γH2AX). Later, after the set up, the experiments focused on ovarian cancer, such as IGROV1 cells, the cellular model of this project.

At the beginning, different UV exposure (5 minutes, 15 minutes, 30 minutes) were analyzed on MCF7 cells: 30 minutes of UV exposure killed nearly all the cells after 24 hours of treatment; while 5 minutes of UV exposure did not show damaged foci (data not showed). For this reason, 15 minutes of UV exposure were decided as the optimal exposure for DNA damage induction.

The quantification of the double-stranded break (DSB) marker γH2AX was analyzed in MCF7 cells at different time points after UV irradiation for 15 minutes. Histone proteins were isolated and separated by SDS-PAGE; γH2AX was identified by western blot and quantified by normalization on the amount of total histones in the same gel lane (*Figure 4.1*).

The time point analysis showed that UV irradiation for 15 minutes induced an hyperphosphorylation of histone H2AX that was present already after 2 hours, that increased at 4 hours and doubled at 6 hours after irradiation. Time point of 4 hours after irradiation was selected as an optimal time point of analysis.
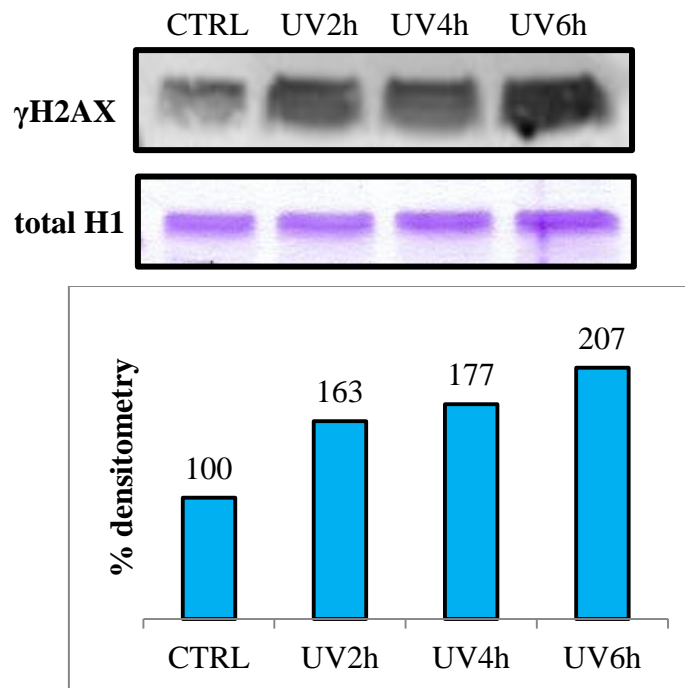
Figure 4.1: Quantification of γH2AX marker in MCF7 cells by western blot. CTRL control sample, UV2h-UV6h histones extracted 2-6 hours after UV irradiation for 15 minutes.

Then, BRCA2-cyclin D1 complex was identified in MCF7 cells by immunoflurescence after 4 hours and 24 hours from UV irradiation (***Figure 4.2***).
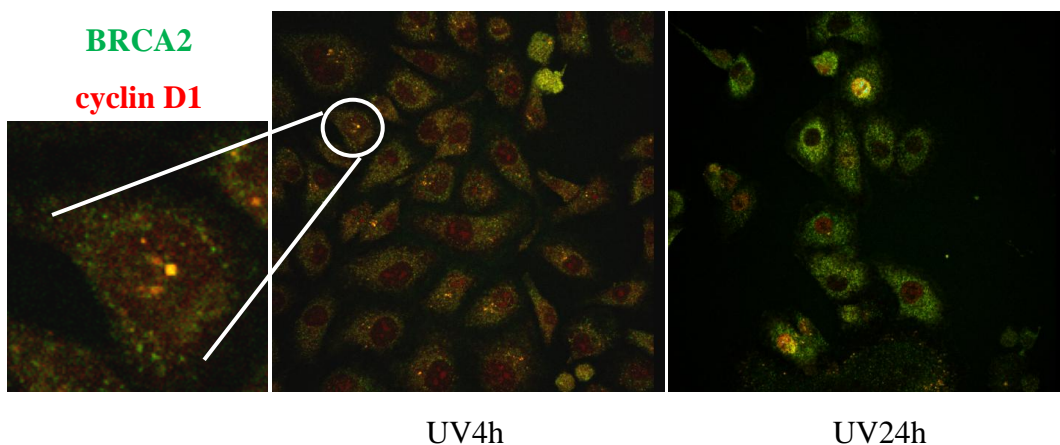
UV4h   UV24h

Figure 4.2: Immunofluorescence of BRCA2 (green) and cyclin D1 (red) proteins in MCF7 cells. UV4h-UV24h cells fixed 4-24 hours after UV irradiation for 15 minutes.

BRCA2-cyclin D1 complex was present in MCF7 cells nucleus after 4 hours from UV irradiation: clear colocalization yellow dots were present in some cells, like the zoomed one. 24 hours after UV irradiation the immunofluorescence analysis showed the

resolution of damage with no colocalization of cyclin D1 and BRCA2. Here again, time point of 4 hours after irradiation was selected as the optimal one.

4.2 Repair proteins colocalization in MCF7 cells

Once established the UV exposure (15 minutes) and the time point for colocalization analysis of repair proteins (4 hours after irradiation), immunofluorescence analysis of control MCF7 cells and irradiated cells was performed. In *Figure 4.3* γH2AX and cyclin D1 immunofluorescences are reported.
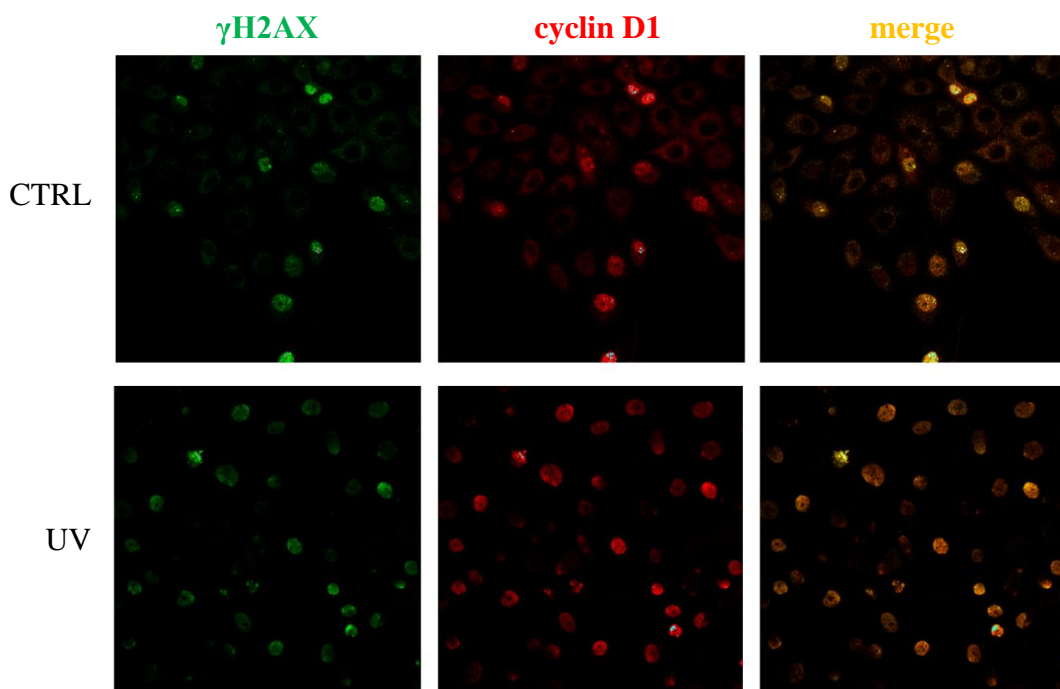
Figure 4.3: Immunofluorescence of γH2AX (green) and cyclin D1 (red) proteins in MCF7 cells. CTRL control sample, UV cells fixed 4 hours after UV irradiation for 15 minutes.

The results showed an increase in γH2AX-positive cells when irradiated with UV. Furthermore, γH2AX-cyclin D1 colocalization signal was more present in the nucleus of these damaged cells, compared to control cells.

In *Figure 4.4* BRCA2 and cyclin D1 immunofluorescences are reported.

In this images, the decrease of cyclin D1 in UV-irradiated cells compared to control MCF7 cells was underlined. Despite this decrease, BRCA2-cyclin D1 colocalization was present in damaged cells.
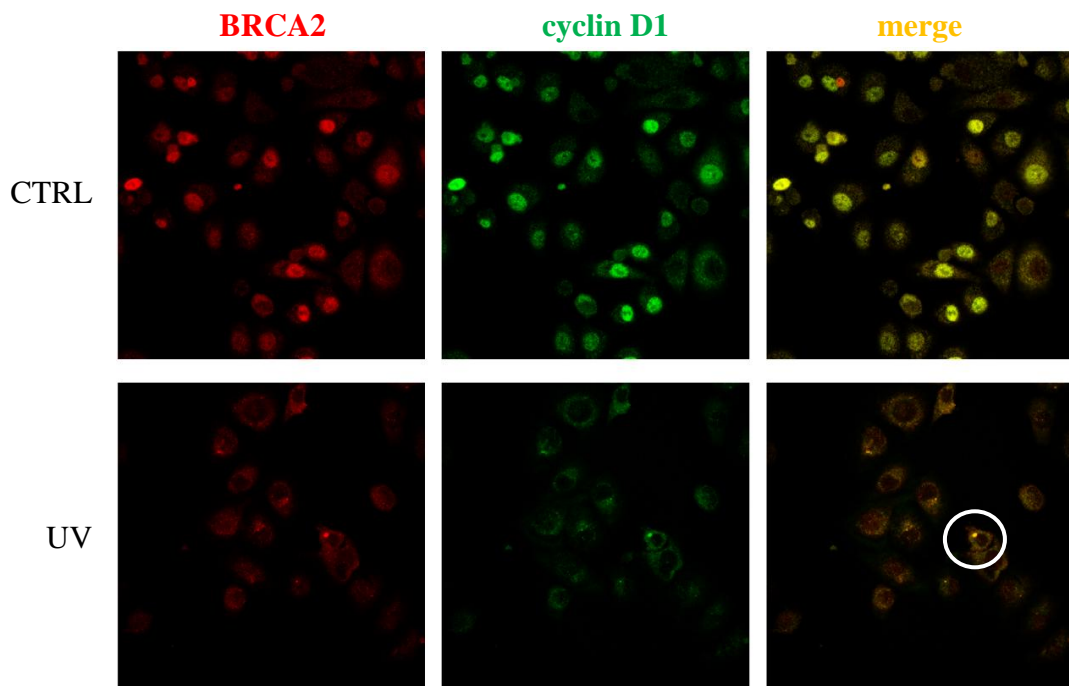
Figure 4.4: *Immunofluorescence of BRCA2 (red) and cyclin D1 (green) proteins in MCF7 cells. CTRL control sample, UV cells fixed 4 hours after UV irradiation for 15 minutes.*
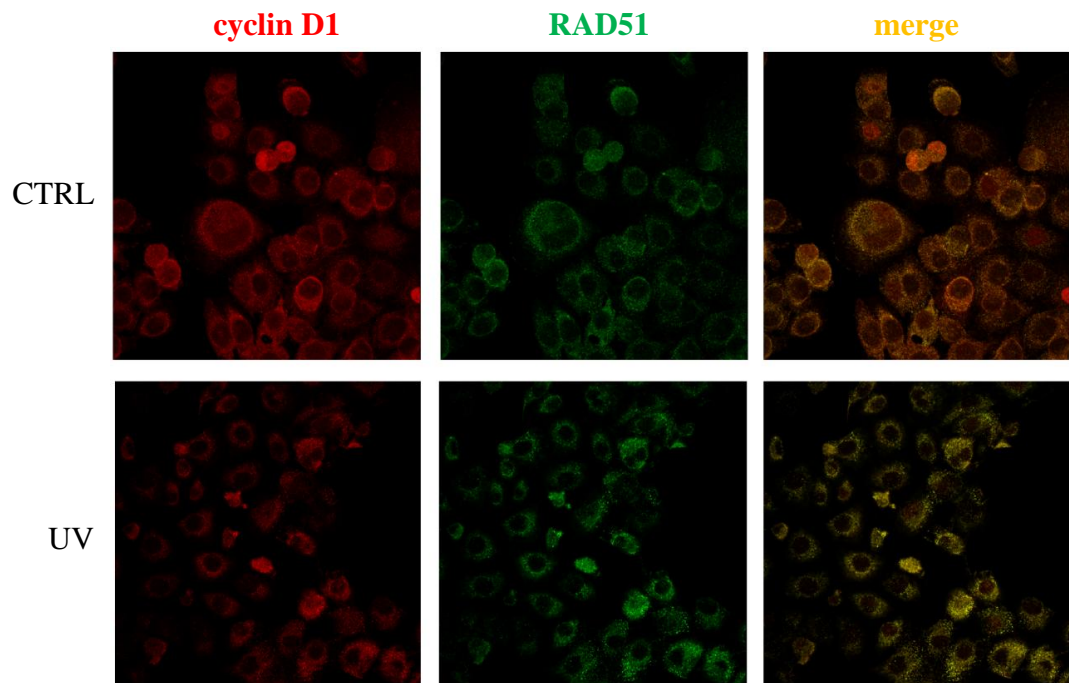
Figure 4.5: *Immunofluorescence of cyclin D1 (red) and RAD51 (green) proteins in MCF7 cells. CTRL control sample, UV cells fixed 4 hours after UV irradiation for 15 minutes.*

In *Figure 4.5* cyclin D1 and RAD51 are identified by immunofluorescence in control MCF7 cells and UV-irradiated cells.

These results showed an increase in the amount of RAD51 protein in cells irradiated with UV and cyclin D1-RAD51 yellow colocalization signal only in damaged cells.

In *Figure 4.6* γH2AX and RAD51 immunofluorescences are reported.
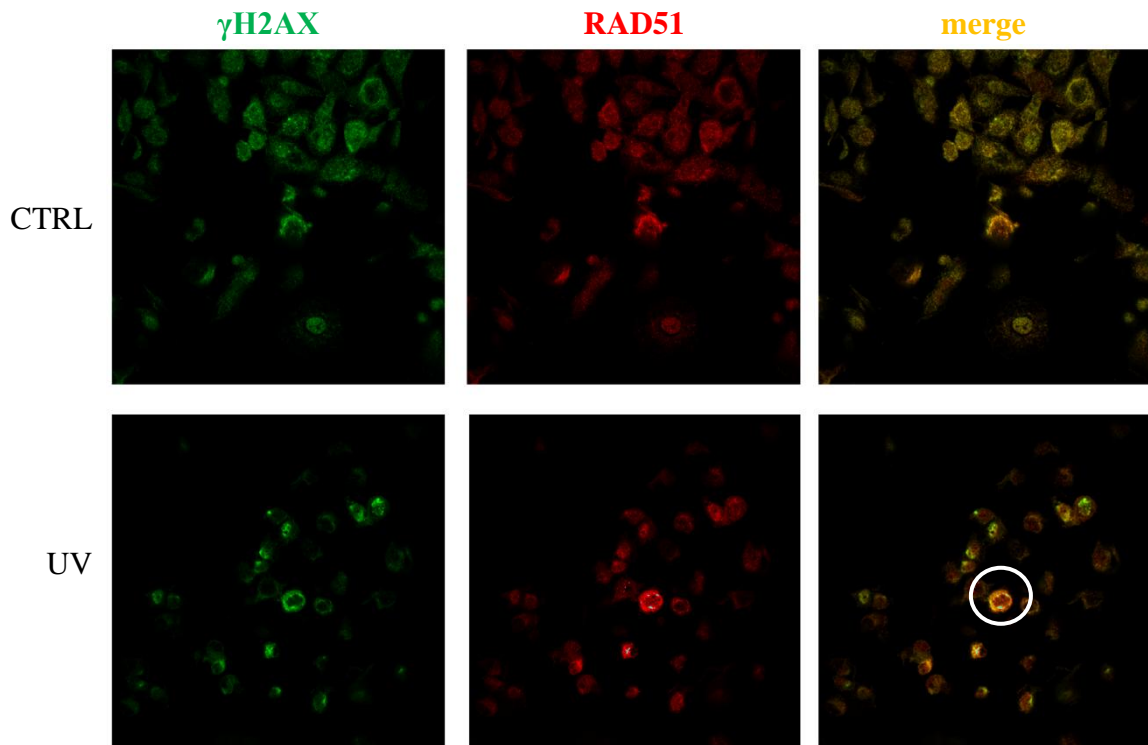
Figure 4.6: *Immunofluorescence of γH2AX (green) and RAD51 (red) proteins in MCF7 cells. CTRL control sample, UV cells fixed 4 hours after UV irradiation for 15 minutes.*

UV irradiation for 15 minutes induced colocalization of γH2AX and RAD51 in MCF7 cells.

4.3 Induction of DNA damage in IGROV1 cells

After the repair mechanisms analysis in MCF7 cells, the research focused on ovarian cancer IGROV1 cells. The quantification of the DSB marker γH2AX was analyzed in IGROV1 cells at different time points after UV irradiation for 15 minutes. Histone proteins were isolated and separated by SDS-PAGE; γH2AX was identified by western blot and quantified by normalization on the amount of total histones in the same gel

lane. Quantification of three independent analysis was done and Student's t-test was used to check the significance of the results (***Figure 4.7***).
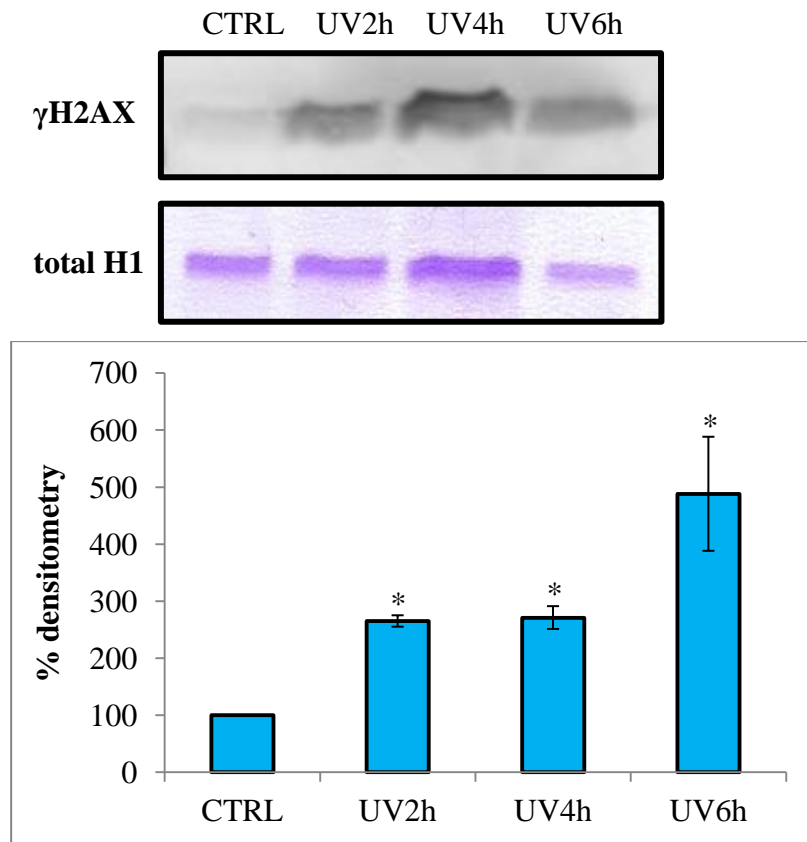
Figure 4.7: *Quantification of γH2AX marker in IGROV1 cells by western blot. CTRL control sample, UV2h-UV6h histones extracted 2-6 hours after UV irradiation for 15 minutes. (* p ≤ 0.05 vs CTRL)*

The time point analysis showed that UV irradiation for 15 minutes induced an hyperphosphorylation on serine 139 of histone H2AX that was present already after 2 hours, that persisted at 4 hours and increased 6 hours after irradiation. Given these results, time point of 4 hours after irradiation was considered optimal also in IGROV1 cells.

After 4 hours from irradiation, γH2AX and RAD51 protein amounts were quantified by immunofluorescence (***Figure 4.8***). At least seven cells in three different acquisitions were selected for quantification and Student's t-test was used to verify the significance of results.

UV irradiation caused an increased amount of the marker γH2AX, signal of induced DNA damage; the recombinase RAD51 was also increased in response to DSBs.
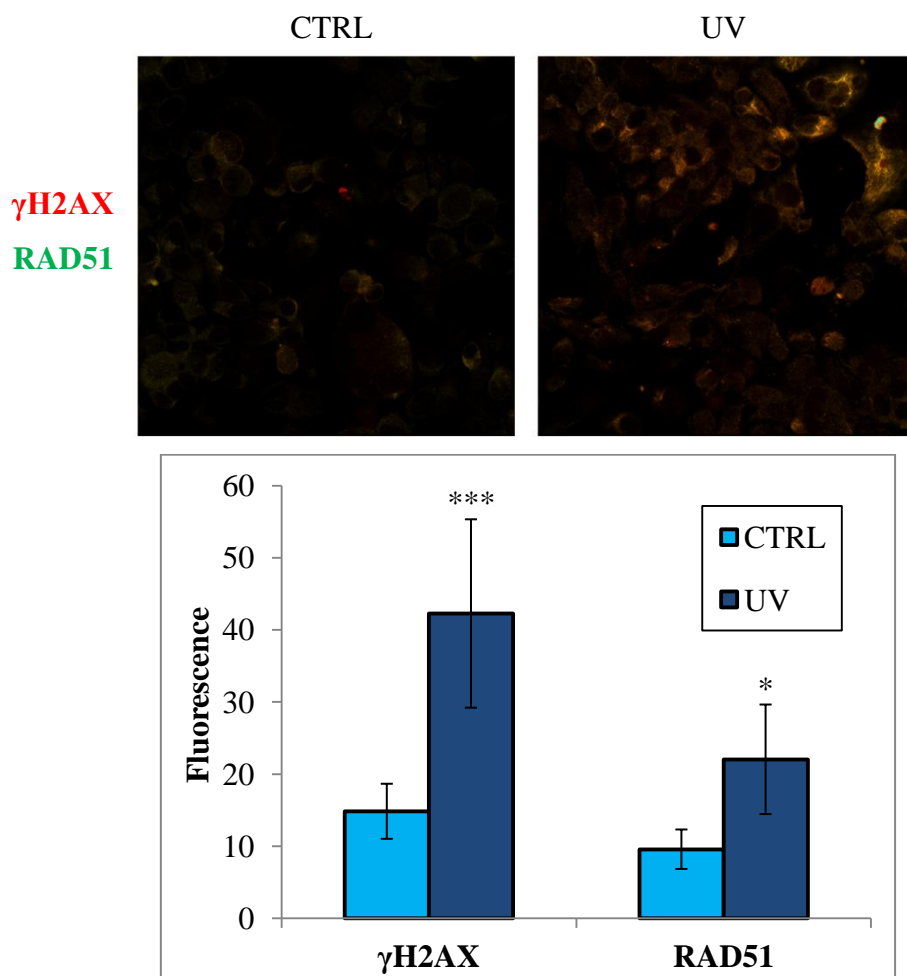
Figure 4.8: Quantification of γH2AX (red) and RAD51 (green) proteins by immunofluorescence in IGROV1 cells. CTRL control sample, UV cells fixed 4 hours after UV irradiation for 15 minutes. (* p ≤ 0.05, *** p ≤ 0.005 vs CTRL)

4.4 3l treatment inhibits DNA repair complex

At this point, IGROV1 cells treated with 3l were introduced in the analysis. The quantification of γH2AX marker was assessed after 5 μM 3l treatment for 28 hours and after 4 hours from UV irradiation of 3l-treated cells. Histone proteins were isolated and separated by SDS-PAGE; γH2AX was identified by western blot and quantified by normalization on the amount of total histones in the same gel lane. Quantification of three independent analysis was done and Student's t-test was used to check the significance of the results (***Figure 4.9***).
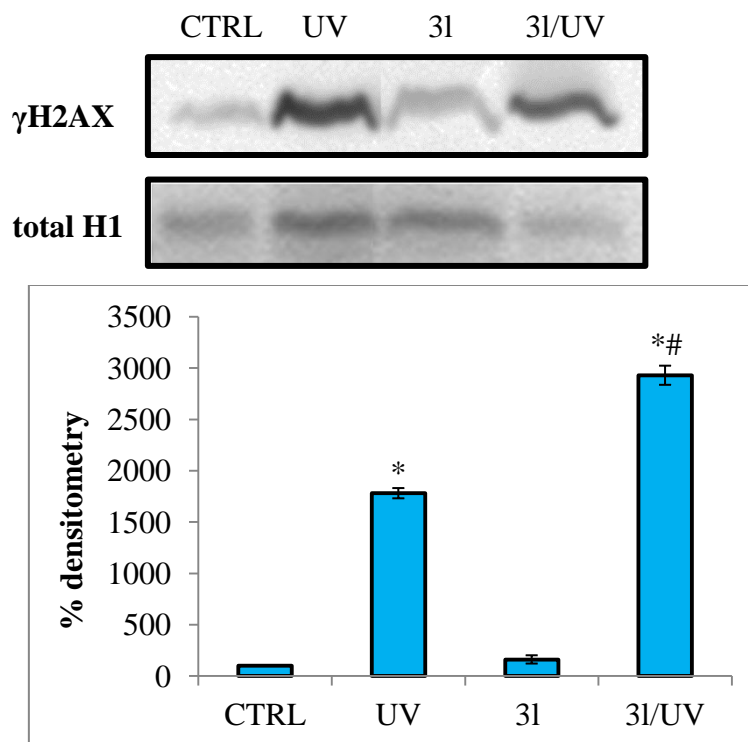
Figure 4.9: *Quantification of γH2AX marker in IGROV1 cells by western blot. CTRL control sample, UV histones extracted 4 hours after UV irradiation for 15 minutes, 3l histones extracted 28 hours after 5 μM 3l treatment, 3l/UV histones extracted 28 hours after 5 μM 3l treatment and 4 hours after UV irradiation for 15 minutes. (* p ≤ 0.05 vs CTRL, # p ≤ 0.05 vs 3l)*

The analysis showed a huge increase of DSBs marker in irradiated cells compared to control cells. Furthermore, UV irradiation significantly increased H2AX phosphorylation in 3l-treated cells for 28 hours compared to control cells and to 3l-treated cells.

In ***Figure 4.10*** and ***Figure 4.11*** BRCA2 and cyclin D1 immunofluorescences in control, UV-irradiated and 3l-treated cells are reported and quantified by selecting at least seven cells in three different acquisitions for each sample. Student's t-test was used to verify the significance of results.

These results showed that 3l treatment reduced significantly cyclin D1 protein amount and that BRCA2-cyclin D1 point colocalization was present only in IGROV1 cells irradiated with UV.
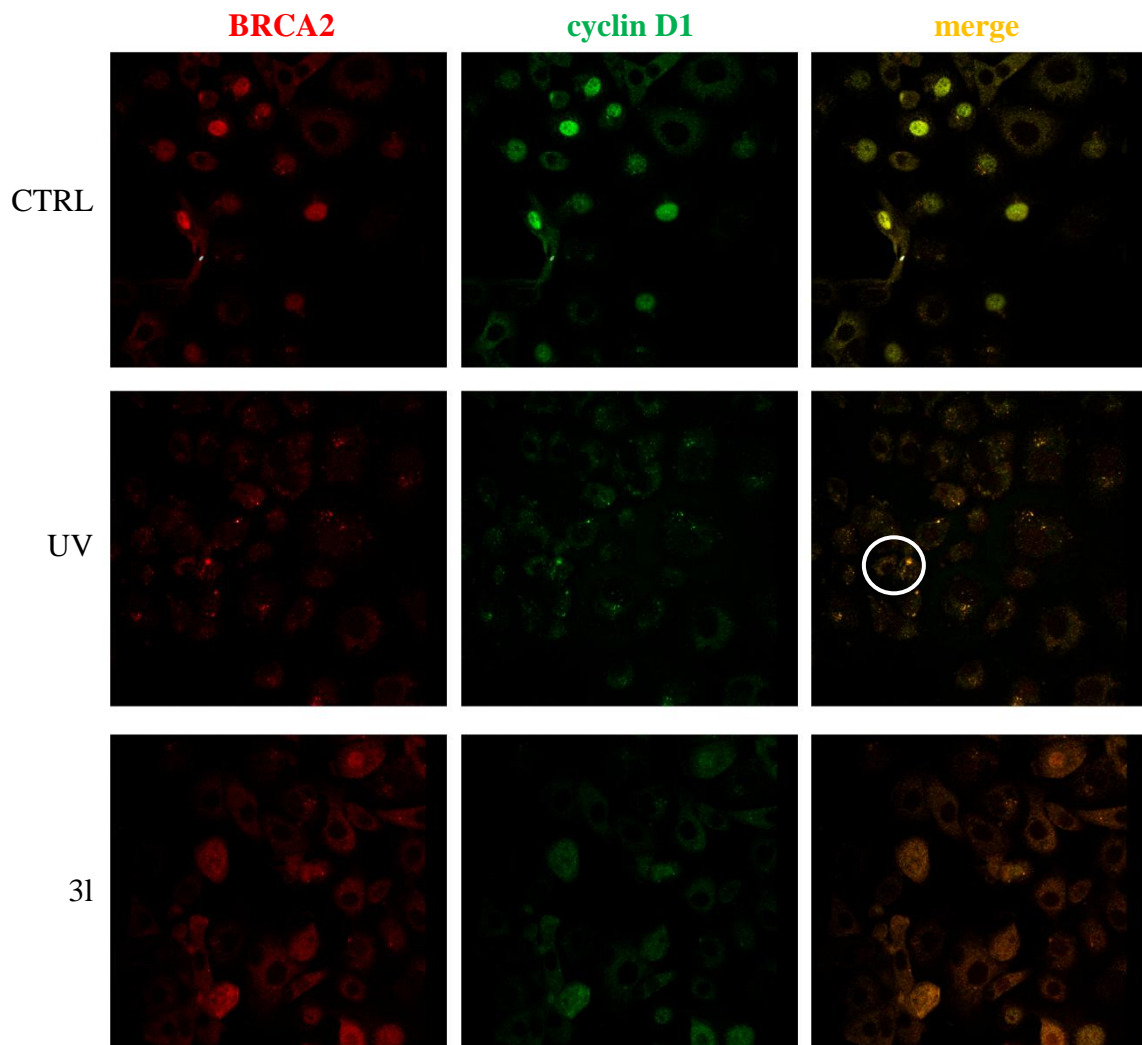
Figure 4.10: *Immunofluorescence of BRCA2 (red) and cyclin D1 (green) proteins in IGROV1 cells. CTRL control sample, UV cells fixed 4 hours after UV irradiation for 15 minutes, 3l cells fixed 28 hours after 5 µM 3l treatment.*
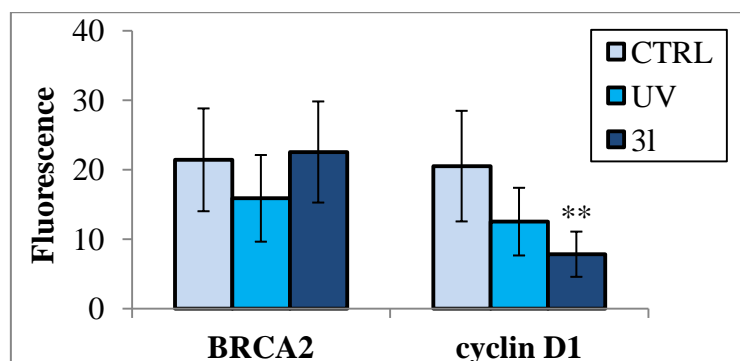
Figure 4.11: *Quantification of BRCA2 and cyclin D1 proteins by immunofluorescence in IGROV1 cells. CTRL control sample, UV cells fixed 4 hours after UV irradiation for 15 minutes, 3l cells fixed 28 hours after 5 µM 3l treatment. (** p ≤ 0.01 vs CTRL)*

Then, qRT-PCR analysis of *CCND1* and *RAD51* genes was used to study cyclin D1 protein-dependent RAD51 expression (***Figure 4.12***). qRT-PCR analysis was managed as described in ***Paragraph 3.5***.
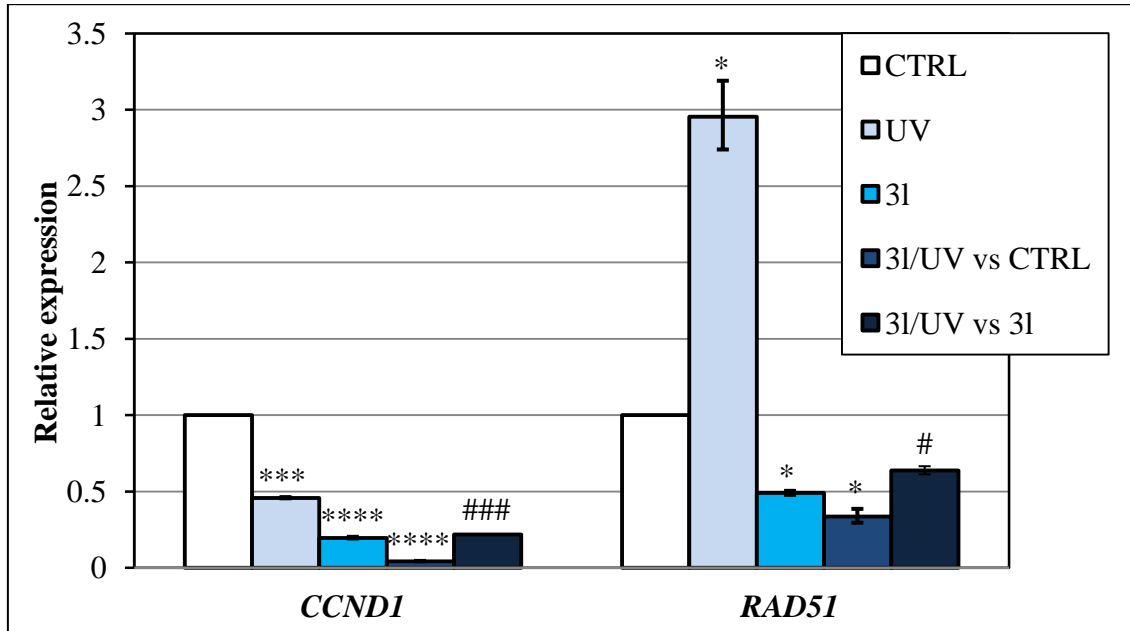
Figure 4.12: *$2^{-\Delta\Delta CT}$ values of CCND1 and RAD51 gene expressions in IGROV1 cells. CTRL control sample, UV RNA extracted 4 hours after UV irradiation for 15 minutes, 3l RNA extracted 28 hours after 5 µM 3l treatment, 3l/UV RNA extracted 28 hours after 5 µM 3l treatment and 4 hours after UV irradiation for 15 minutes. (* p ≤ 0.05, *** p ≤ 0.005, **** p ≤ 0.001 vs CTRL, # p ≤ 0.05, ### p ≤ 0.005 vs 3l)*

These results underlined the down-regulation of *CCND1* both in UV-irradiated and 3l-treated cells. 3l/UV sample presented a decrease in cyclin D1 expression compared to control. Analysis of *RAD51* mRNA showed its up-regulation induced by irradiation, that was not present in cells treated with 3l and then irradiated.

Subsequently, cyclin D1 and RAD51 immunofluorescences in control, UV-irradiated, 3l-treated and irradiated cells after 3l treatment were analyzed and quantified (***Figure 4.13*** and ***Figure 4.14***). At least seven cells in three different acquisitions for each sample were selected and Student's t-test was used to verify the significance of results.
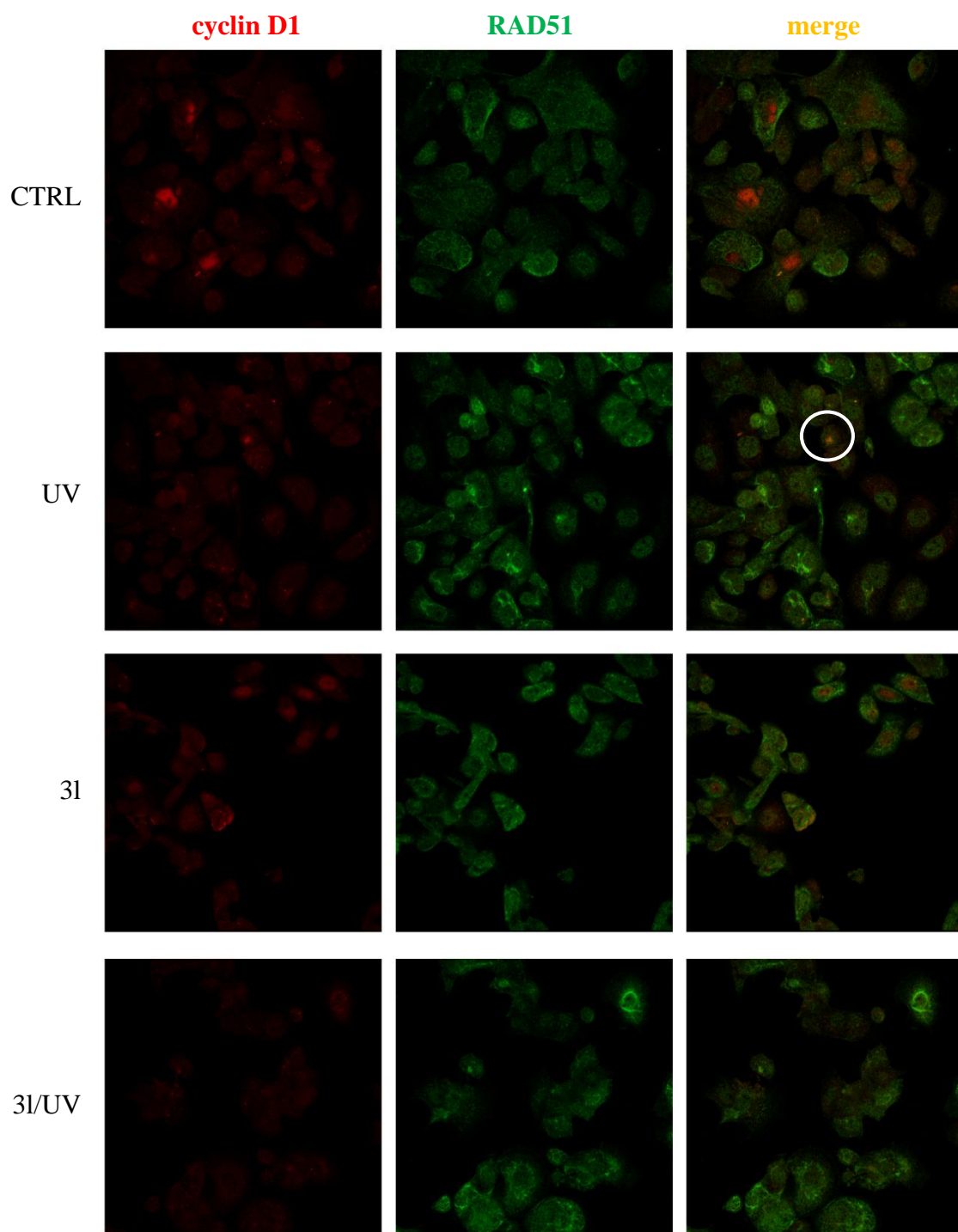
Figure 4.13: *Immunofluorescence of cyclin D1 (red) and RAD51 (green) proteins in IGROV1 cells. CTRL control sample, UV cells fixed 4 hours after UV irradiation for 15 minutes, 3l cells fixed 28 hours after 5 µM 3l treatment, 3l/UV cells fixed 28 hours after 5 µM 3l treatment and 4 hours after UV irradiation for 15 minutes.*
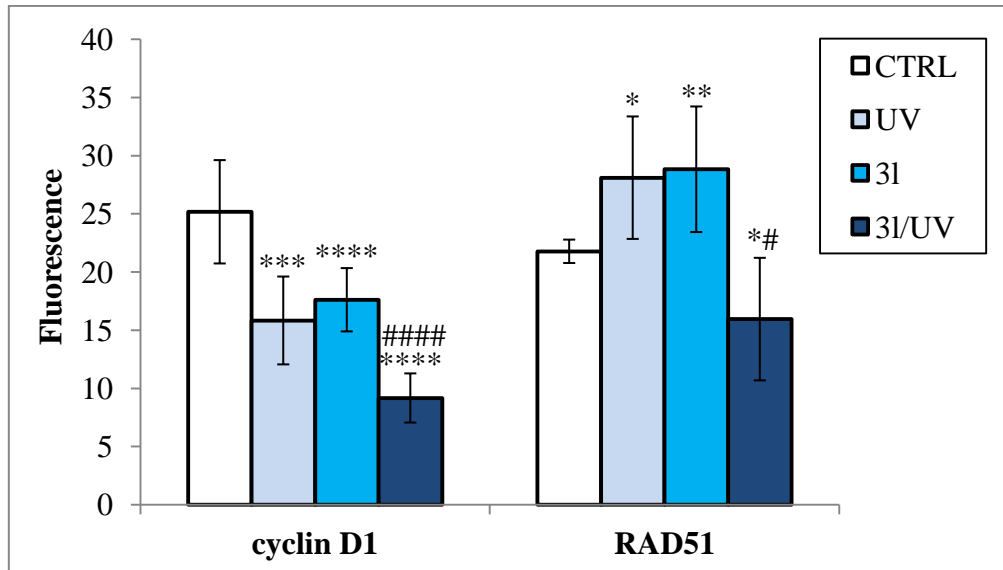
Figure 4.14: *Quantification of cyclin D1 and RAD51 proteins by immunofluorescence in IGROV1 cells. CTRL control sample, UV cells fixed 4 hours after UV irradiation for 15 minutes, 3l cells fixed 28 hours after 5 μM 3l treatment, 3l/UV cells fixed 28 hours after 5 μM 3l treatment and 4 hours after UV irradiation for 15 minutes. (* p ≤ 0.05, ** p ≤ 0.01, *** p ≤ 0.005, **** p ≤ 0.001 vs CTRL, # p ≤ 0.05, #### p ≤ 0.001 vs 3l)*

Here, only in UV sample cyclin D1-RAD51 colocalization was present. Furthermore, the cyclin D1 amount decreased in all the treated cells, and RAD51 increased in UV-irradiated and 3l-treated cells, but not in cells treated with 3l for 24 hours and then irradiated.

4.5 Set up of *CCND1* siRNA silencing

siRNA silencing of *CCND1* gene codifying cyclin D1 protein was set up to have a comparable sample for 3l treatment. Custom and validated siRNAs were used for the analysis: a specific anti-*CCND1* and a correspondent negative siRNA were chosen. First, the silencing concentration was set up by quantification of cyclin D1 protein 48 hours after treatment with the siRNA. Total protein lysates were resolved in SDS-PAGE and cyclin D1 protein was identified by specific antibody in western blot. By normalization on the amount of βactin, quantification of cyclin D1 in the specific anti-*CCND1* siRNA sample was compared with the relative negative sample (***Figure 4.15***).
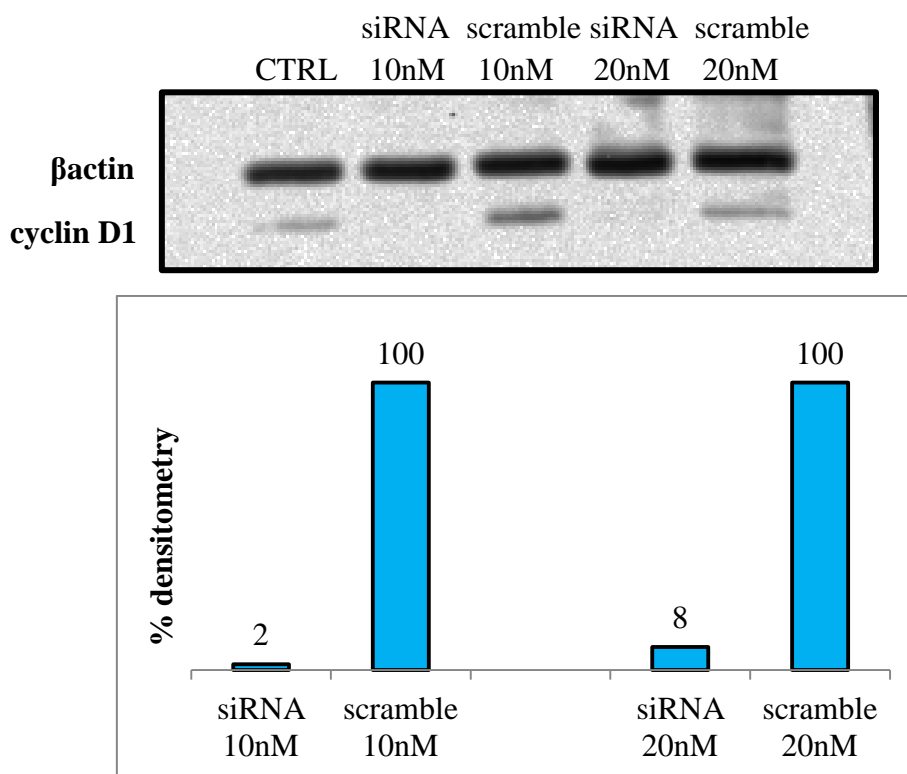
Figure 4.15: *Quantification of cyclin D1 in IGROV1 cells by western blot. CTRL control sample, siRNA 10nM-20nM proteins extracted 48 hours after treatment with anti-CCND1 siRNA 10 nM-20 nM, scramble 10nM-20nM proteins extracted 48 hours after treatment with scramble siRNA 10 nM-20 nM.*

The results showed a nearly total silencing with both concentrations: 10 nM siRNA was chosen as the optimal concentration for further analysis.

Secondly, a silencing time course was assessed by quantification of cyclin D1 protein 48-72-96 hours after treatment with siRNA 10 nM. Total protein lysates were resolved in SDS-PAGE and cyclin D1 protein was identified by specific antibody in western blot. By normalization on the amount of βactin, quantification of cyclin D1 in the specific siRNA sample was compared with the relative scramble sample (***Figure 4.16***). These results showed the best silencing after 48 hours and this time point was chosen as optimal.
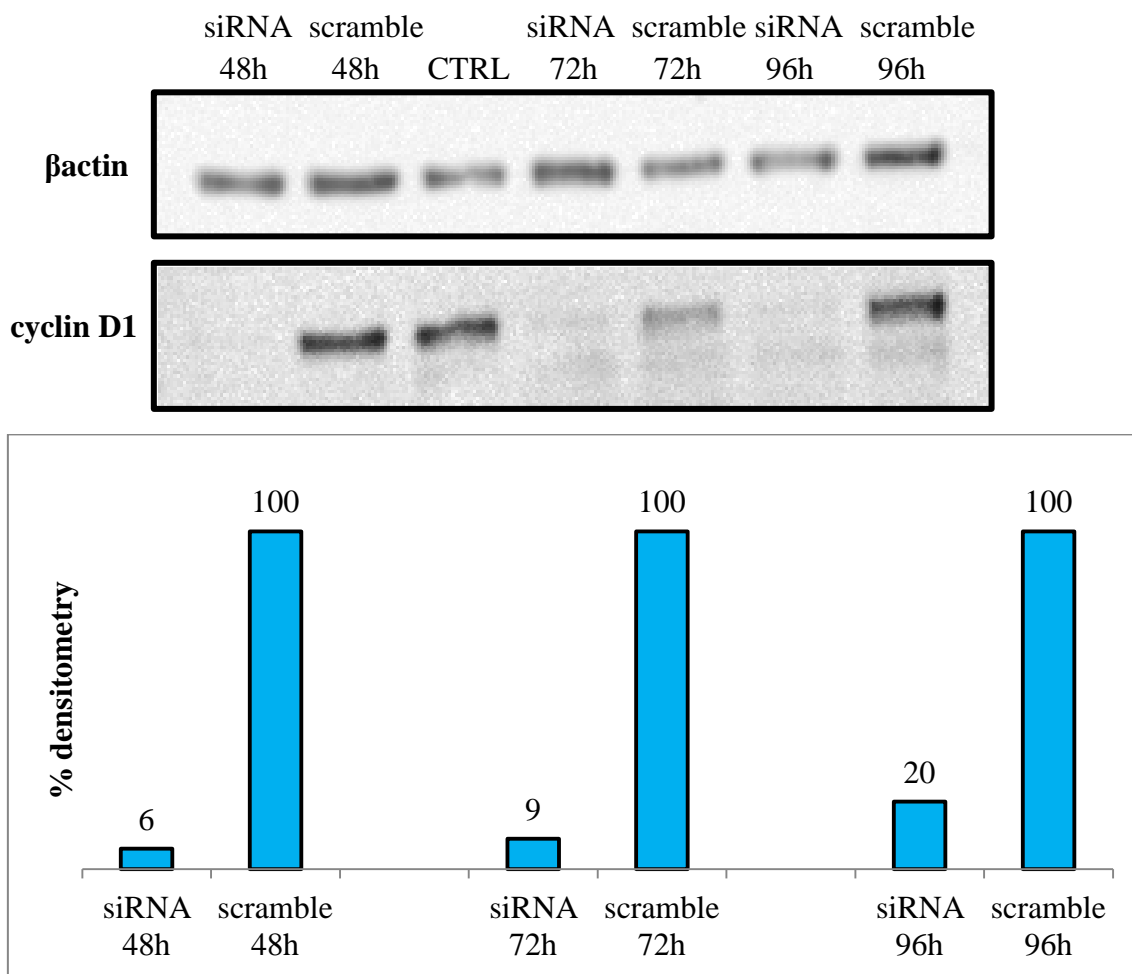
Figure 4.16: *Quantification of cyclin D1 in IGROV1 cells by western blot. CTRL control sample, siRNA 48h-96h proteins extracted 48-96 hours after treatment with anti-CCND1 siRNA 10 nM, scramble 48h-96h proteins extracted 48-96 hours after treatment with scramble siRNA 10 nM.*

4.6 Comparison between 3l treatment and *CCND1* silencing

4.6.1 γH2AX and cyclin D1 quantification

In the last part of the project, IGROV1 cells silenced for *CCND1* were introduced in the samples list to compare them with cells treated with 3l. The γH2AX marker was again analyzed: histones were isolated and separated by SDS-PAGE, γH2AX was identified by western blot and quantified by normalization on the amount of total histones in the same gel lane. Quantification of three independent analyses was done and Student's t-test was used to check the significance of the results (***Figure 4.17***).
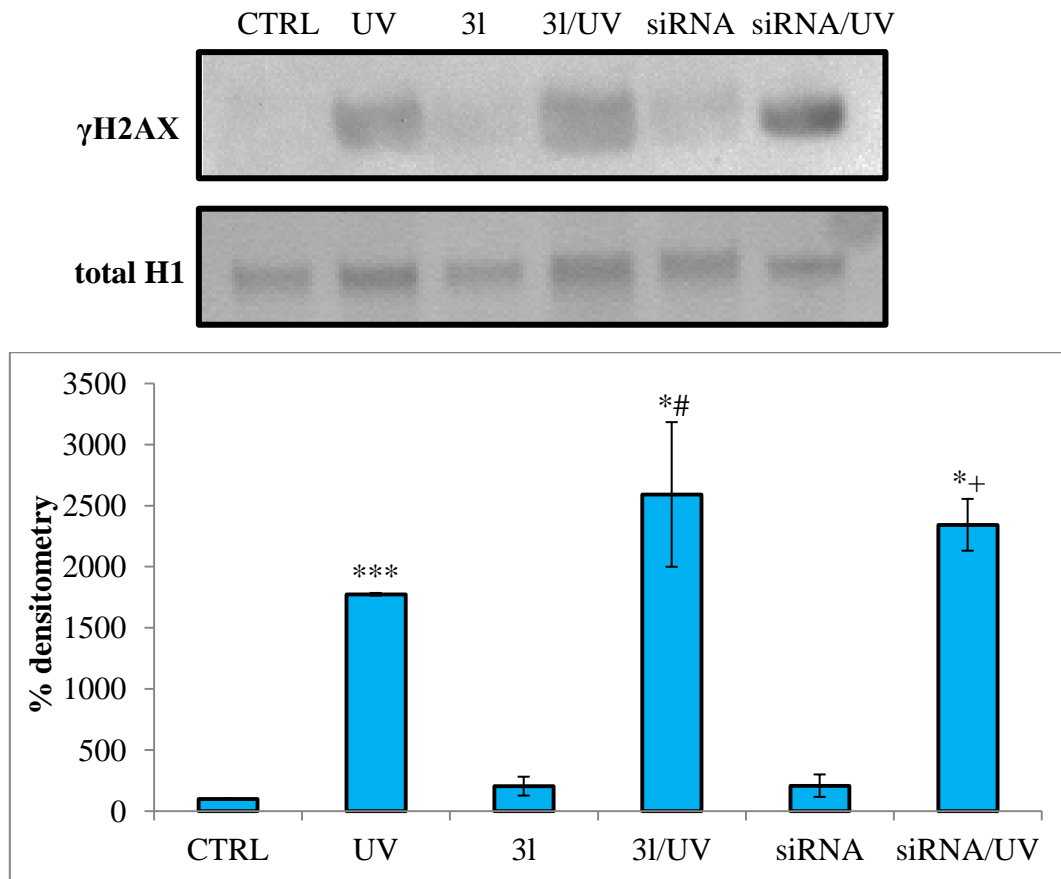
Figure 4.17: Quantification of γH2AX marker in IGROV1 cells by western blot. CTRL control sample, UV histones extracted 4 hours after UV irradiation for 15 minutes, 3l histones extracted 28 hours after 5 μM 3l treatment, 3l/UV histones extracted 28 hours after 5 μM 3l treatment and 4 hours after UV irradiation for 15 minutes, siRNA histones extracted 52 hours after treatment with anti-CCND1 siRNA 10 nM, siRNA/UV histones extracted 52 hours after treatment with anti-CCND1 siRNA 10 nM and 4 hours after UV irradiation for 15 minutes. (* p ≤ 0.05, *** p ≤ 0.005 vs CTRL, # p ≤ 0.05 vs 3l, + p ≤ 0.05 vs siRNA)

The quantification analysis presented a hyperphosphorylation of histone H2AX twenty-fold higher in all samples irradiated with UV for 15 minutes, indicating induced DNA damage.

In *Figure 4.18* cyclin D1 protein was then quantified by western blot in all the samples. Results showed a decrease in cyclin D1 amount in all the cells irradiated with UV, even if this decrease was evident also in cells treated only with 3l as well as cells treated only with selected siRNA against *CCND1*.
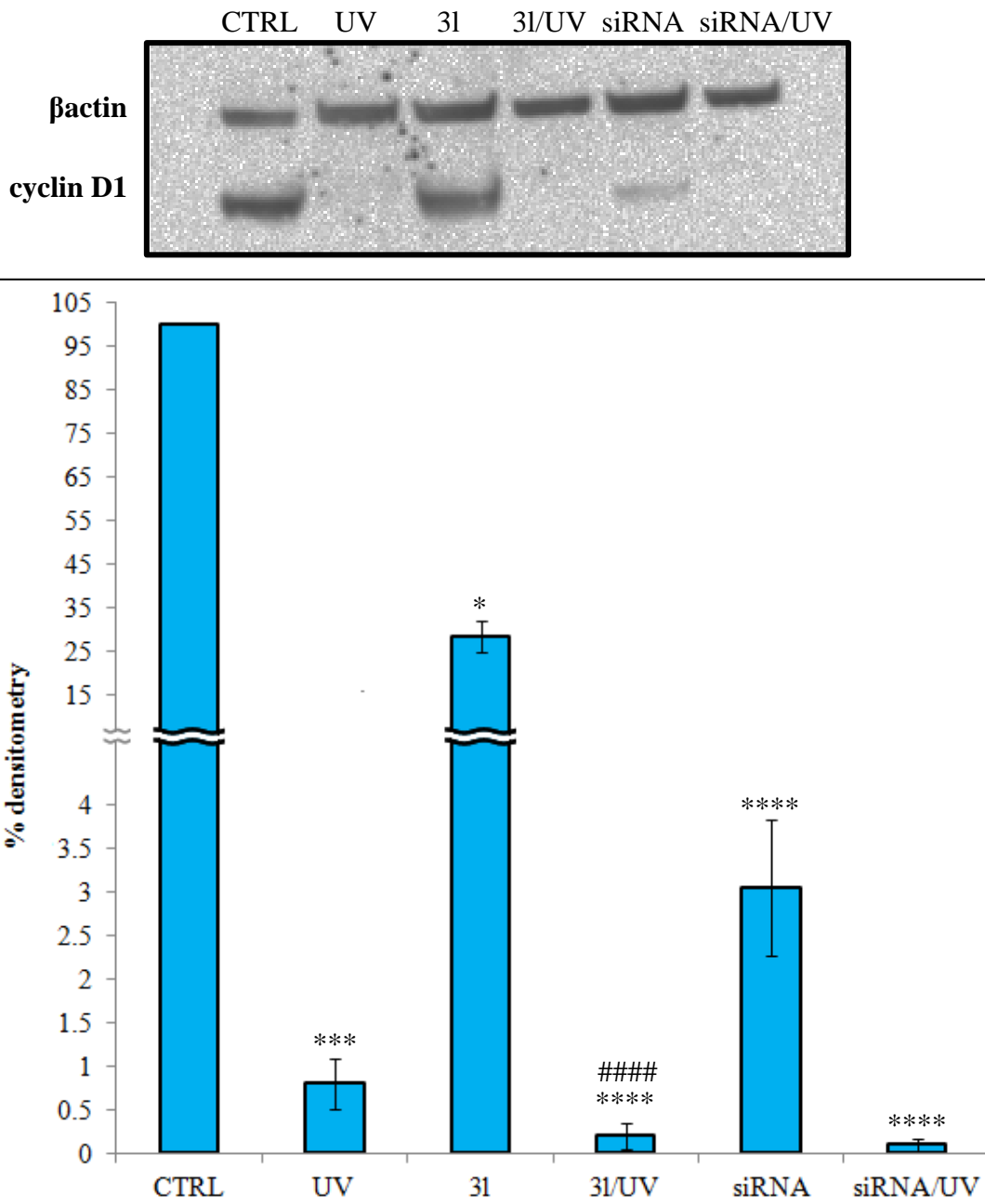
Figure 4.18: *Quantification of cyclin D1 in IGROV1 cells by western blot. CTRL control sample, UV proteins extracted 4 hours after UV irradiation for 15 minutes, 3l proteins extracted 28 hours after 5 μM 3l treatment, 3l/UV proteins extracted 28 hours after 5 μM 3l treatment and 4 hours after UV irradiation for 15 minutes, siRNA proteins extracted 52 hours after treatment with anti-CCND1 siRNA 10 nM, siRNA/UV proteins extracted 52 hours after treatment with anti-CCND1 siRNA 10 nM and 4 hours after UV irradiation for 15 minutes. (* $p \leq 0.05$, *** $p \leq 0.005$, **** $p \leq 0.001$ vs CTRL, #### $p \leq 0.05$ vs 3l)*

4.6.2 *CCND1* and *RAD51* genes expression

qRT-PCR analysis of *CCND1* (***Figure 4.19***) and *RAD51* (***Figure 4.20***) genes was applied to study cyclin D1 protein-dependent RAD51 expression in all the samples set. qRT-PCR analysis was performed as described in ***Paragraph 3.5***.
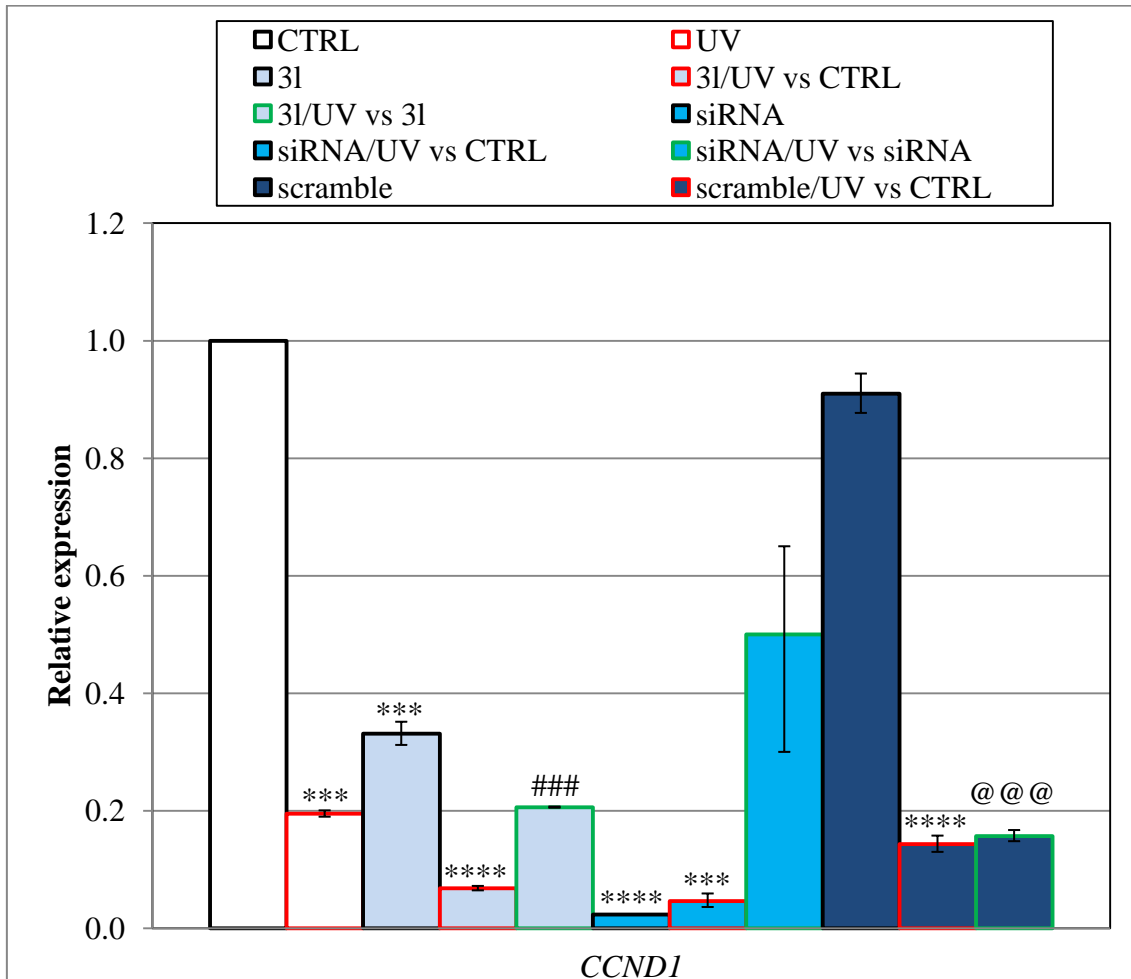
Figure 4.19: *$2^{-\Delta\Delta CT}$ values of CCND1 gene expression in IGROV1 cells. CTRL control sample, UV RNA extracted 4 hours after UV irradiation for 15 minutes, 3l RNA extracted 28 hours after 5 μM 3l treatment, 3l/UV RNA extracted 28 hours after 5 μM 3l treatment and 4 hours after UV irradiation for 15 minutes, siRNA RNA extracted 52 hours after treatment with anti-CCND1 siRNA 10 nM, siRNA/UV RNA extracted 52 hours after treatment with anti-CCND1 siRNA 10 nM and 4 hours after UV irradiation for 15 minutes, scramble RNA extracted 52 hours after treatment with scramble siRNA 10 nM, scramble/UV RNA extracted 52 hours after treatment with scramble siRNA 10 nM and 4 hours after UV irradiation for 15 minutes. (*** p ≤ 0.005, **** p ≤ 0.001 vs CTRL, ### p ≤ 0.005 vs 3l, @@@ p ≤ 0.005 vs scramble)*
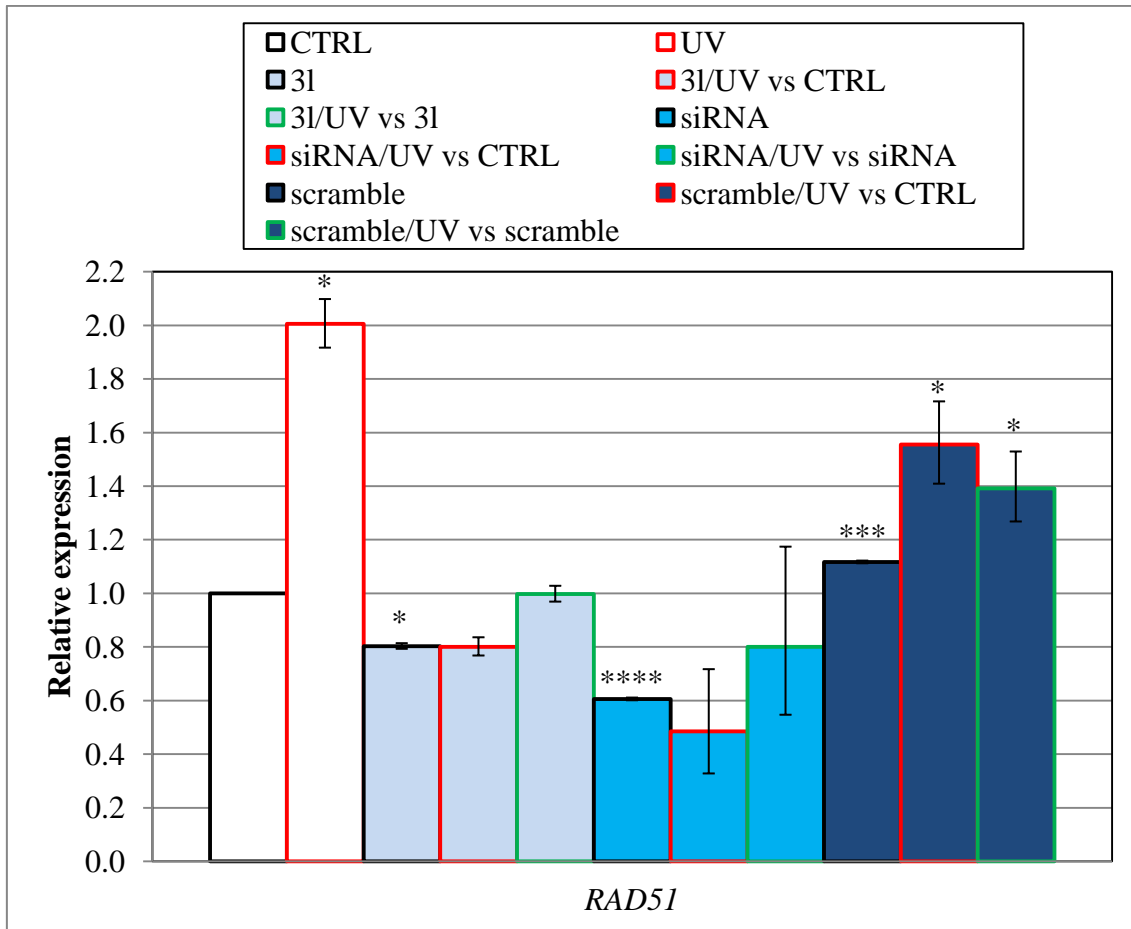
Figure 4.20: *2^{-ΔΔCT} values of RAD51 gene expression in IGROV1 cells. CTRL control sample, UV RNA extracted 4 hours after UV irradiation for 15 minutes, 3l RNA extracted 28 hours after 5 μM 3l treatment, 3l/UV RNA extracted 28 hours after 5 μM 3l treatment and 4 hours after UV irradiation for 15 minutes, siRNA RNA extracted 52 hours after treatment with anti-CCND1 siRNA 10 nM, siRNA/UV RNA extracted 52 hours after treatment with anti-CCND1 siRNA 10 nM and 4 hours after UV irradiation for 15 minutes, scramble RNA extracted 52 hours after treatment with scramble siRNA 10 nM, scramble/UV RNA extracted 52 hours after treatment with scramble siRNA 10 nM and 4 hours after UV irradiation for 15 minutes. (* p ≤ 0.05, *** p ≤ 0.005 vs CTRL)*

Irradiation induced down-regulation of *CCND1* and up-regulation of *RAD51* genes. Surprisingly, 3l-treated and silenced cells presented *CCND1* down-regulation but not present *RAD51* up-regulation in response to UV irradiation. Scramble sample behaved like control cells.

4.6.3 Immunofluorescence of repair proteins

Last experiments' scope was to detect the repair complex by immunofluorescence. The first analysis was the detection (*Figure 4.21*) and the quantification (*Figure 4.22*) of marker γH2AX. At least seven cells in three different acquisitions for each sample were selected and Student's t-test was used to verify the significance of the results.
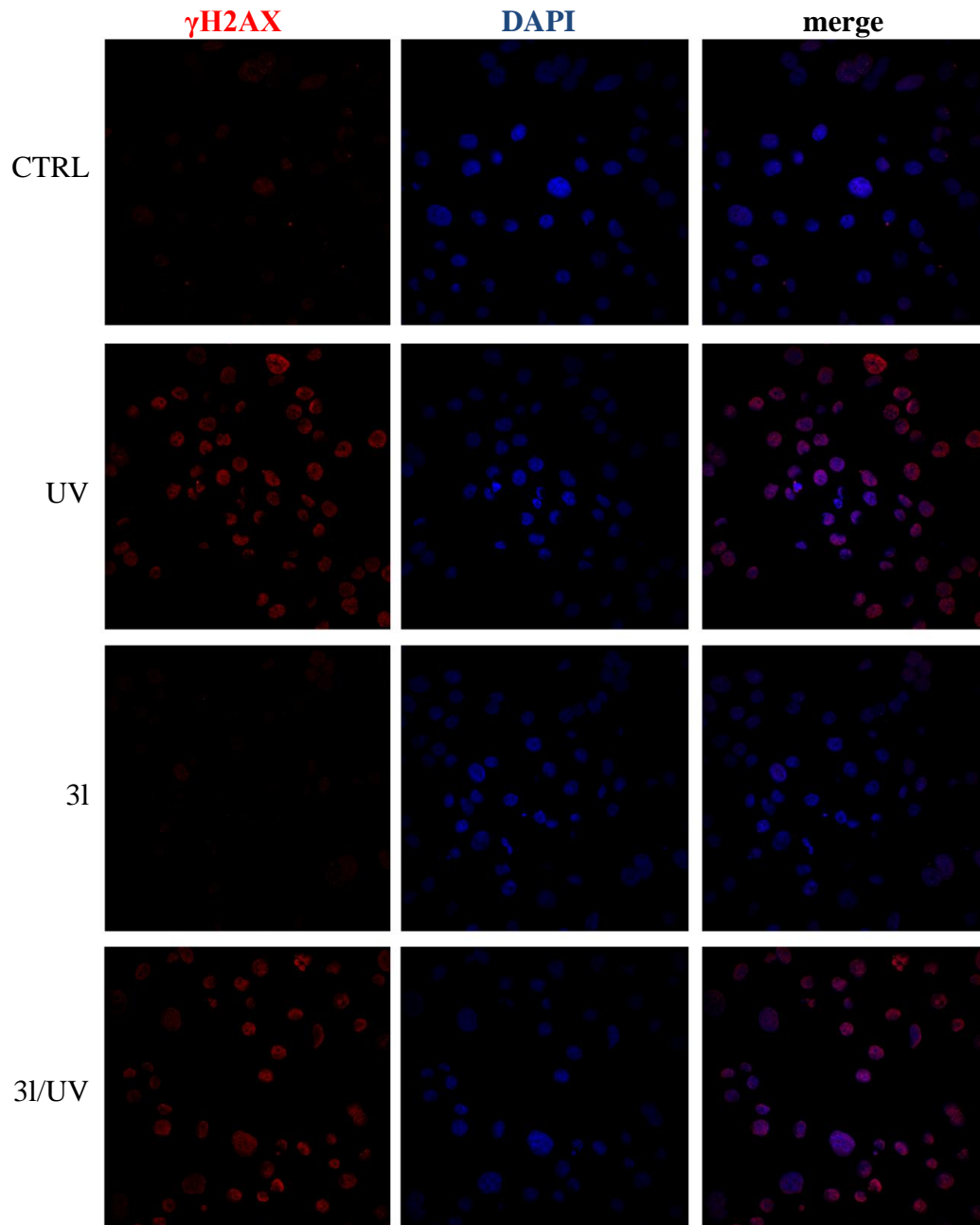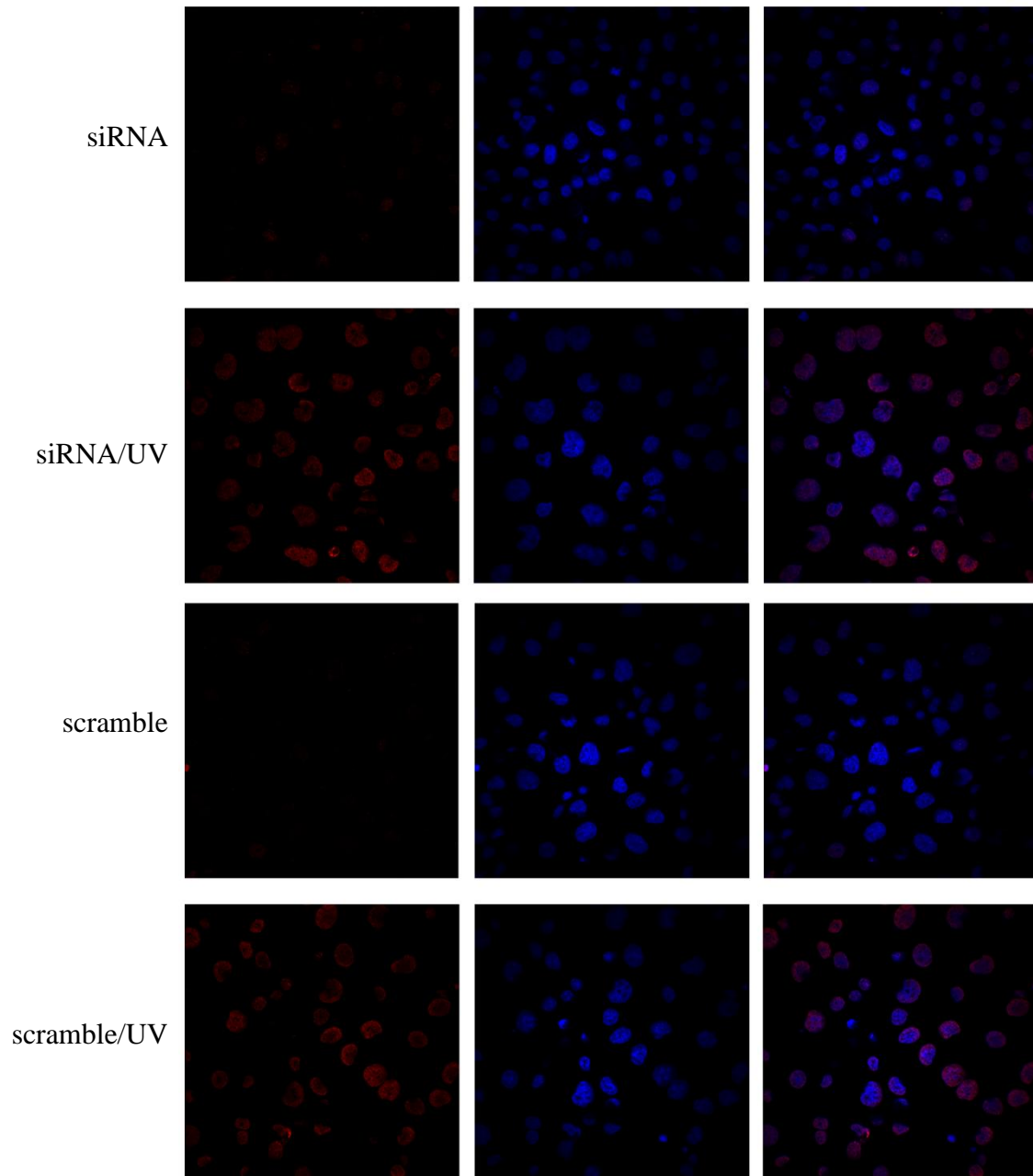
Figure 4.21: *Immunofluorescence of γH2AX (red) protein in IGROV1 cells. DAPI (blue). CTRL control sample, UV cells fixed 4 hours after UV irradiation for 15 minutes, 3l cells fixed 28 hours after 5 μM 3l treatment, 3l/UV cells fixed 28 hours after 5 μM 3l treatment and 4 hours after UV irradiation for 15 minutes, siRNA cells fixed 52 hours after treatment with anti-CCND1 siRNA 10 nM, siRNA/UV cells fixed 52 hours after treatment with anti-CCND1 siRNA 10 nM and 4 hours after UV irradiation for 15 minutes, scramble RNA extracted 52 hours after treatment with scramble siRNA 10 nM, scramble/UV RNA extracted 52 hours after treatment with scramble siRNA 10 nM and 4 hours after UV irradiation for 15 minutes.*
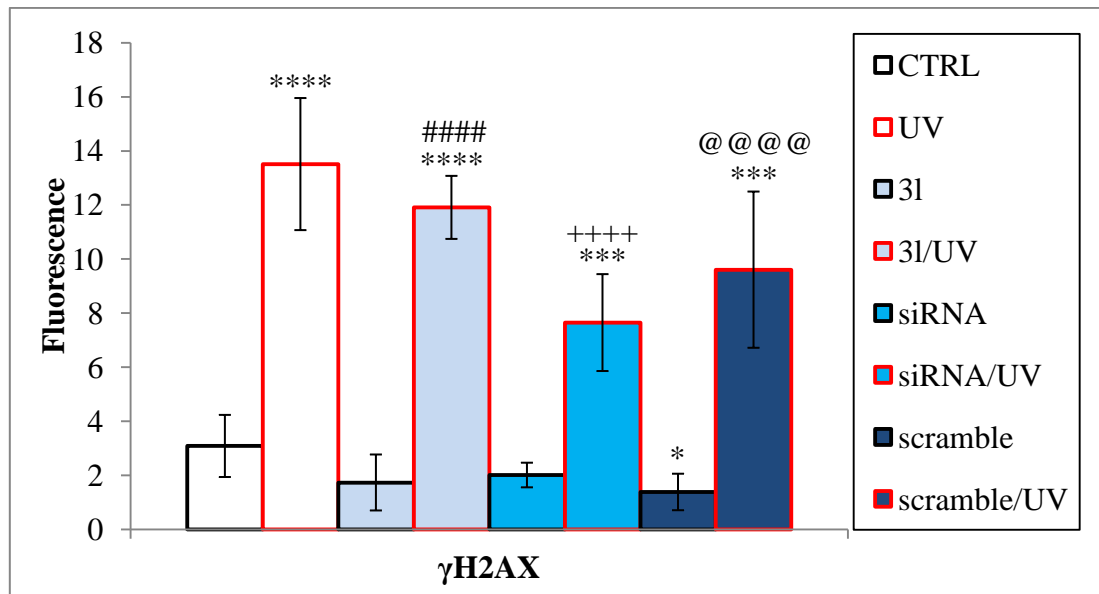
Figure 4.22: Quantification of γH2AX protein by immunofluorescence in IGROV1 cells. CTRL control sample, UV cells fixed 4 hours after UV irradiation for 15 minutes, 3l cells fixed 28 hours after 5 μM 3l treatment, 3l/UV cells fixed 28 hours after 5 μM 3l treatment and 4 hours after UV irradiation for 15 minutes, siRNA cells fixed 52 hours after treatment with anti-CCND1 siRNA 10 nM, siRNA/UV cells fixed 52 hours after treatment with anti-CCND1 siRNA 10 nM and 4 hours after UV irradiation for 15 minutes, scramble RNA extracted 52 hours after treatment with scramble siRNA 10 nM, scramble/UV RNA extracted 52 hours after treatment with scramble siRNA 10 nM and 4 hours after UV irradiation for 15 minutes. (* p ≤ 0.05, *** p ≤ 0.005, **** p ≤ 0.001 vs CTRL, #### p ≤ 0.001 vs 3l, ++++ p ≤ 0.001 vs siRNA, @@@@ p ≤ 0.001 vs scramble)

These results showed the increase in hyperphosphorylation of histone H2AX in all the samples irradiated with UV rays.

The second analysis was the detection (**Figure 4.23**) and the quantification (**Figure 4.24**) of BRCA2 and cyclin D1 proteins by immunofluorescence. At least seven cells in three different acquisitions for each sample were selected and Student's t-test was used to verify the significance of the results.
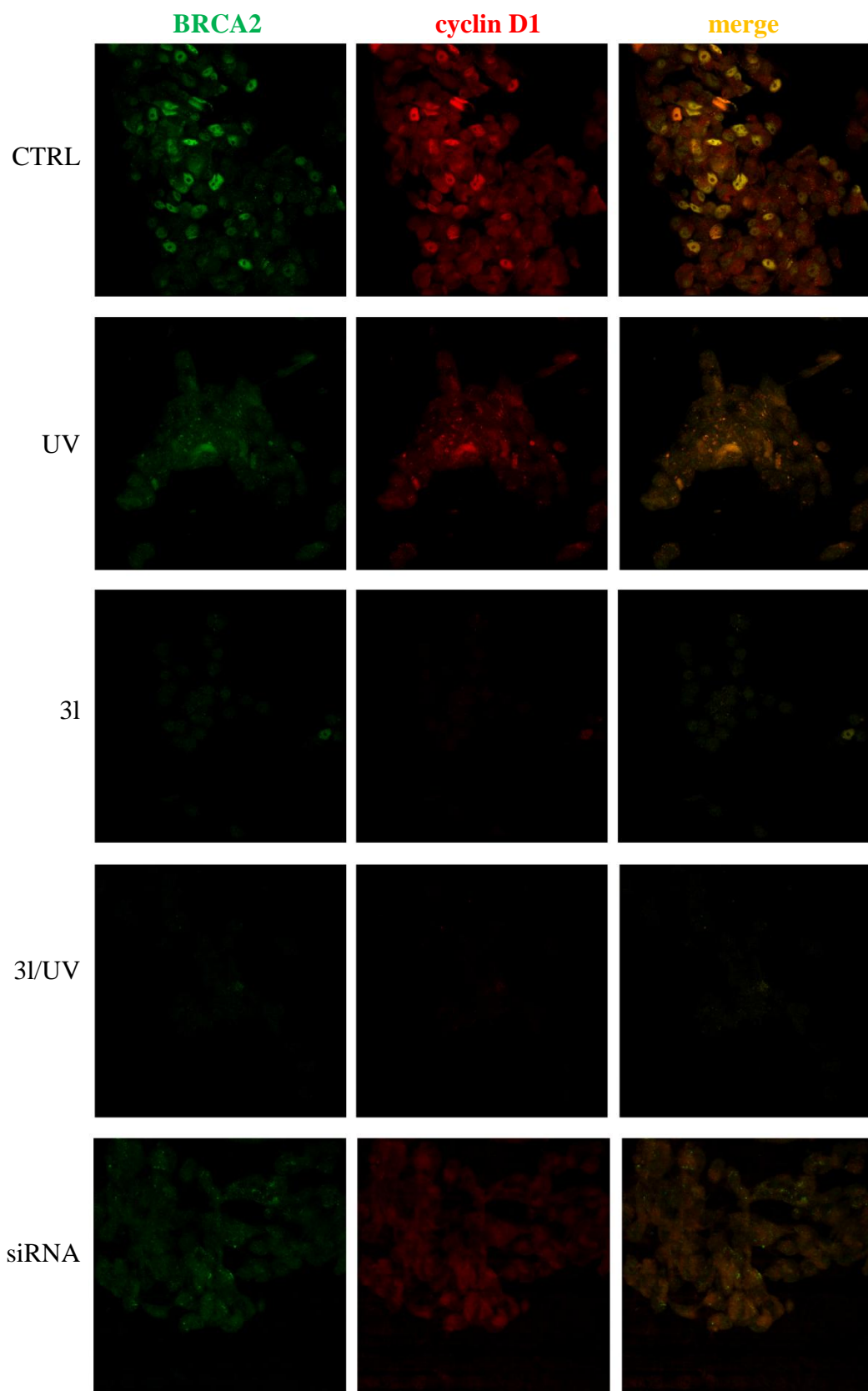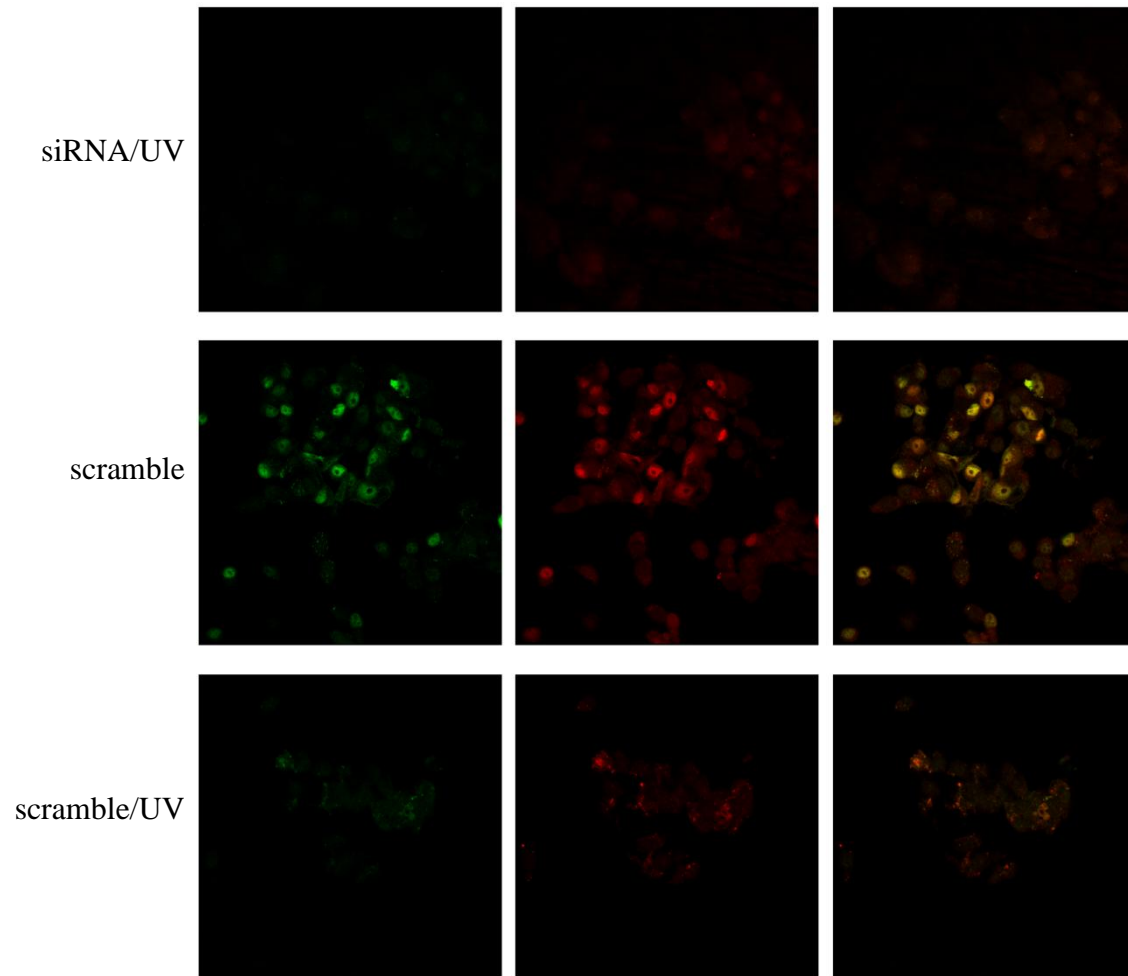
Figure 4.23: Immunofluorescence of BRCA2 (green) and cyclin D1 (red) proteins in IGROV1 cells. CTRL control sample, UV cells fixed 4 hours after UV irradiation for 15 minutes, 3l cells fixed 28 hours after 5 µM 3l treatment, 3l/UV cells fixed 28 hours after 5 µM 3l treatment and 4 hours after UV irradiation for 15 minutes, siRNA cells fixed 52 hours after treatment with anti-CCND1 siRNA 10 nM, siRNA/UV cells fixed 52 hours after treatment with anti-CCND1 siRNA 10 nM and 4 hours after UV irradiation for 15 minutes, scramble RNA extracted 52 hours after treatment with scramble siRNA 10 nM, scramble/UV RNA extracted 52 hours after treatment with scramble siRNA 10 nM and 4 hours after UV irradiation for 15 minutes.

Figure 4.24: *Quantification of BRCA2 and cyclin D1 proteins by immunofluorescence in IGROV1 cells. CTRL control sample, UV cells fixed 4 hours after UV irradiation for 15 minutes, 3l cells fixed 28 hours after 5 µM 3l treatment, 3l/UV cells fixed 28 hours after 5 µM 3l treatment and 4 hours after UV irradiation for 15 minutes, siRNA cells fixed 52 hours after treatment with anti-CCND1 siRNA 10 nM, siRNA/UV cells fixed 52 hours after treatment with anti-CCND1 siRNA 10 nM and 4 hours after UV irradiation for 15 minutes, scramble RNA extracted 52 hours after treatment with scramble siRNA 10 nM, scramble/UV RNA extracted 52 hours after treatment with scramble siRNA 10 nM and 4 hours after UV irradiation for 15 minutes. (* p ≤ 0.05, ** p ≤ 0.01, *** p ≤ 0.005, **** p ≤ 0.001 vs CTRL, # p ≤ 0.05, ### p ≤ 0.005 vs 3l, ++++ p ≤ 0.001 vs siRNA, @ p ≤ 0.05, @@@@ p ≤ 0.001 vs scramble)*

UV irradiation induced BRCA2-cyclin D1 colocalization, but only in CTRL and scramble samples. 3l treatment and siRNA silencing induced same effects in IGROV1 cells: down-regulation of both BRCA2 and cyclin D1.

Detection (***Figure 4.25***) and quantification (***Figure 4.26***) of BRCA2 and RAD51 by immunofluorescence were the next steps. At least seven cells in three different acquisitions for each sample were selected and Student's t-test was used to verify the significance of the results.

	BRCA2	RAD51	merge
CTRL			
UV			
3l			
3l/UV			
siRNA			
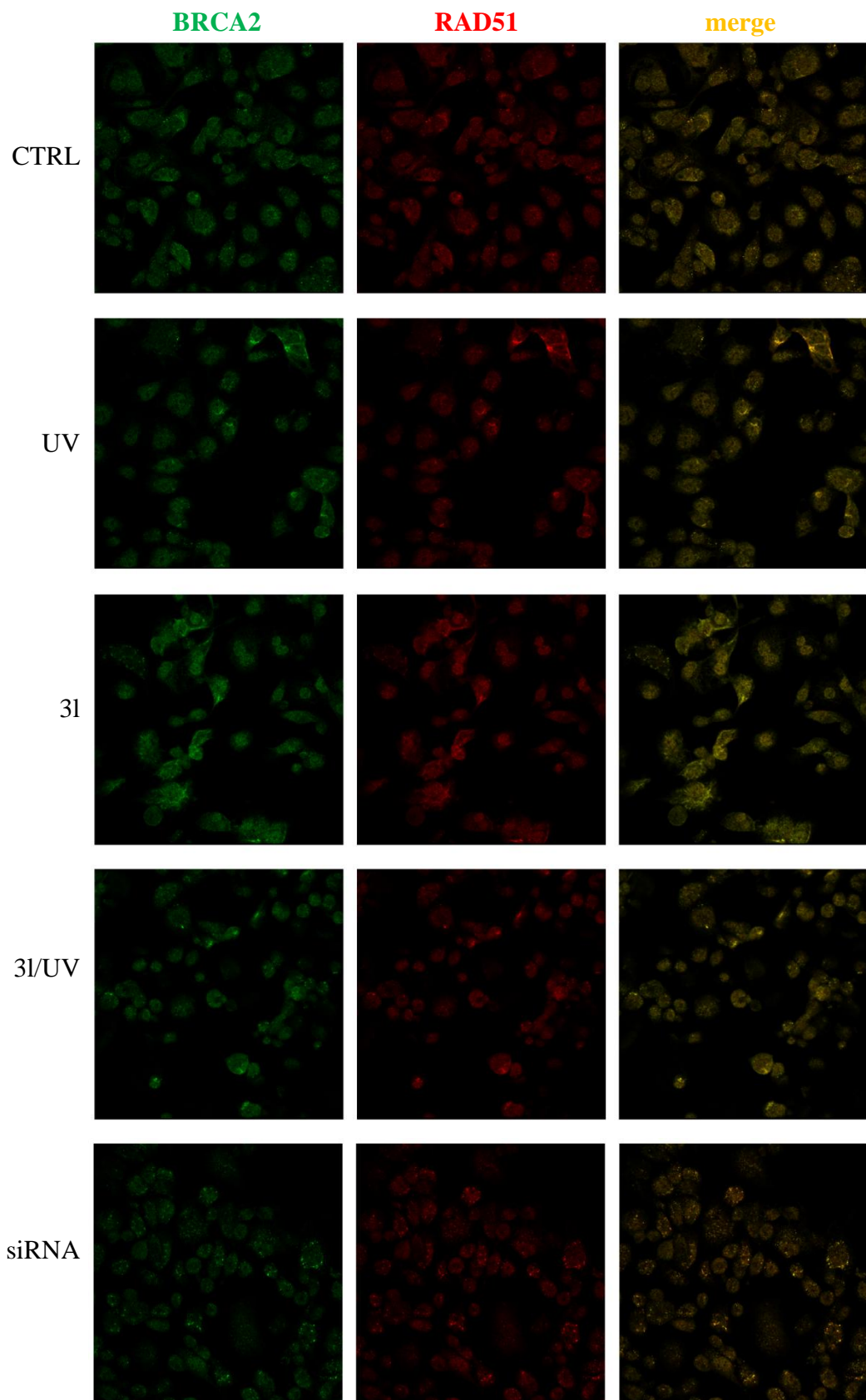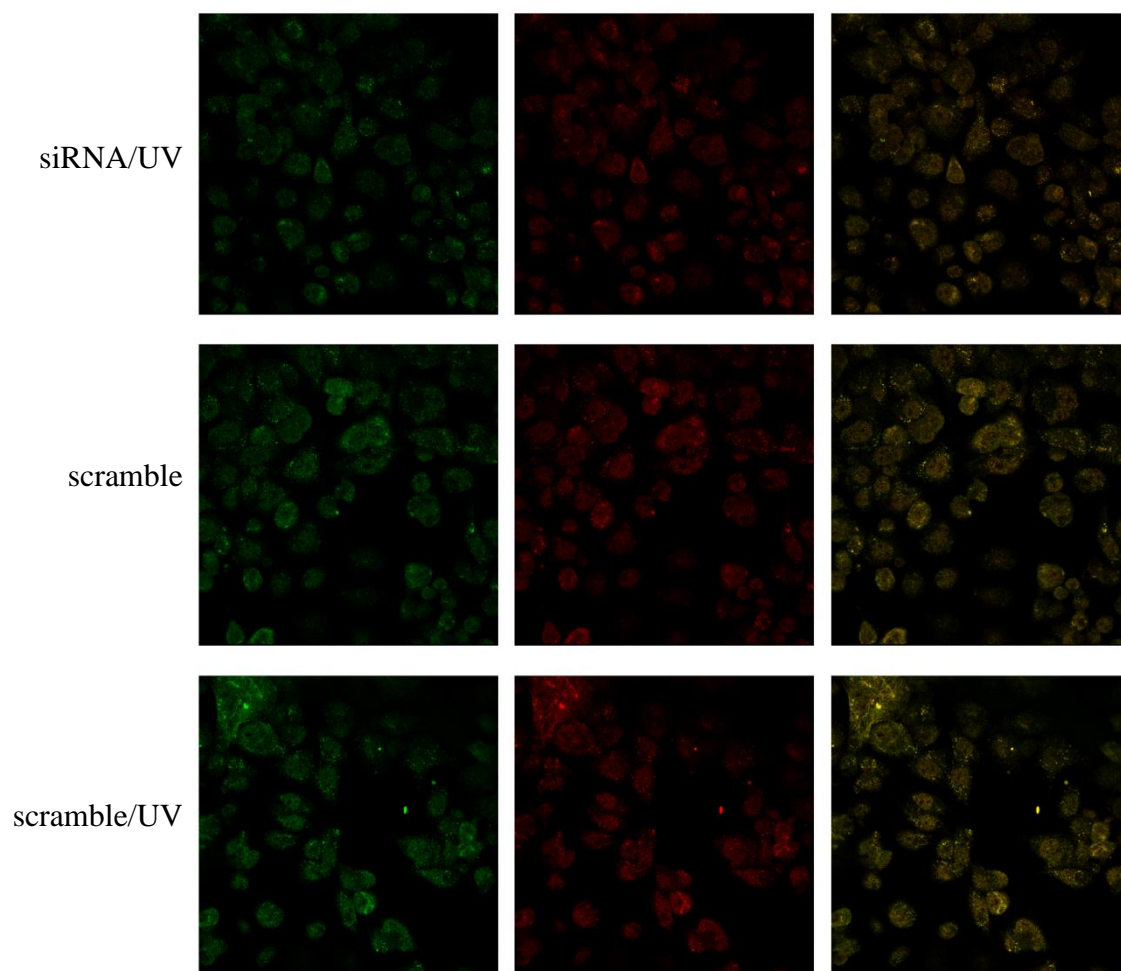
Figure 4.25: *Immunofluorescence of BRCA2 (green) and RAD51 (red) proteins in IGROV1 cells. CTRL control sample, UV cells fixed 4 hours after UV irradiation for 15 minutes, 3l cells fixed 28 hours after 5 μM 3l treatment, 3l/UV cells fixed 28 hours after 5 μM 3l treatment and 4 hours after UV irradiation for 15 minutes, siRNA cells fixed 52 hours after treatment with anti-CCND1 siRNA 10 nM, siRNA/UV cells fixed 52 hours after treatment with anti-CCND1 siRNA 10 nM and 4 hours after UV irradiation for 15 minutes, scramble RNA extracted 52 hours after treatment with scramble siRNA 10 nM, scramble/UV RNA extracted 52 hours after treatment with scramble siRNA 10 nM and 4 hours after UV irradiation for 15 minutes.*
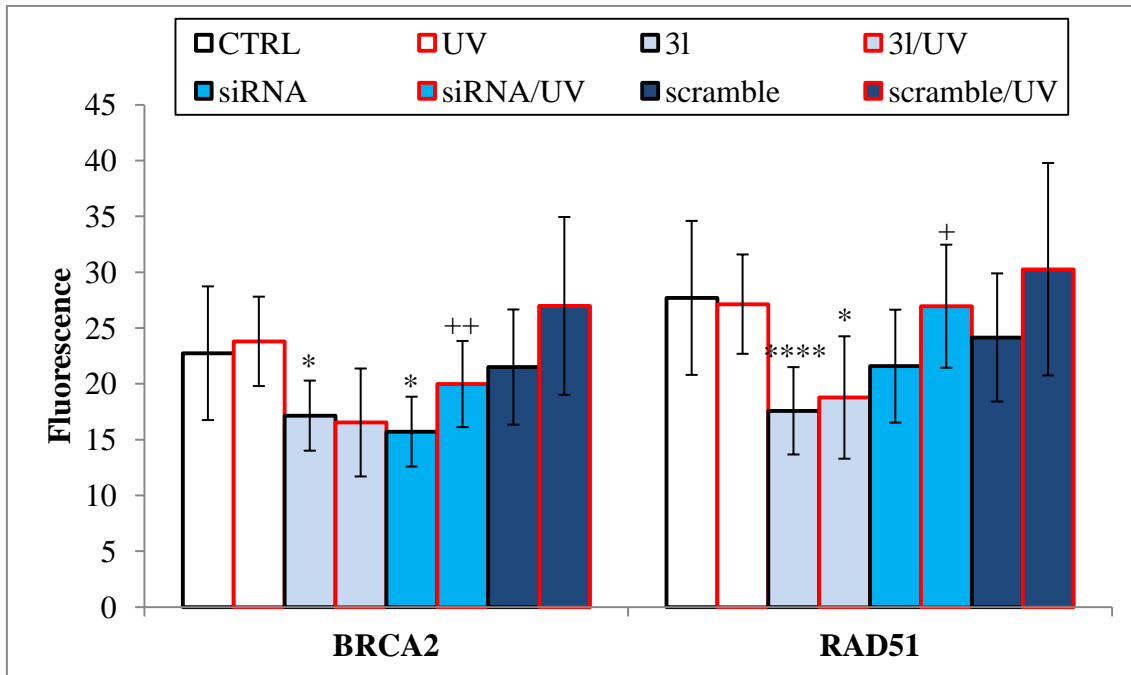
Figure 4.26: *Quantification of BRCA2 and RAD51 proteins by immunofluorescence in IGROV1 cells. CTRL control sample, UV cells fixed 4 hours after UV irradiation for 15 minutes, 3l cells fixed 28 hours after 5 μM 3l treatment, 3l/UV cells fixed 28 hours after 5 μM 3l treatment and 4 hours after UV irradiation for 15 minutes, siRNA cells fixed 52 hours after treatment with anti-CCND1 siRNA 10 nM, siRNA/UV cells fixed 52 hours after treatment with anti-CCND1 siRNA 10 nM and 4 hours after UV irradiation for 15 minutes, scramble RNA extracted 52 hours after treatment with scramble siRNA 10 nM, scramble/UV RNA extracted 52 hours after treatment with scramble siRNA 10 nM and 4 hours after UV irradiation for 15 minutes. (* p ≤ 0.05, **** p ≤ 0.001 vs CTRL, + p ≤ 0.05, ++ p ≤ 0.01 vs siRNA)*

These results showed no important differences between the samples: BRCA2 colocalized with RAD51 and only IGROV1 cells treated with 3l presented a significant decrease in the amount of recombinase RAD51.

Finally, detection (***Figure 4.27***) and the quantification (***Figure 4.28***) of cyclin D1 and RAD51 were carried on. At least seven cells in three different acquisitions for each sample were selected and Student's t-test was used to verify the significance of the results.

	cyclin D1	RAD51	merge
CTRL			
UV			
3l			
3l/UV			
siRNA			
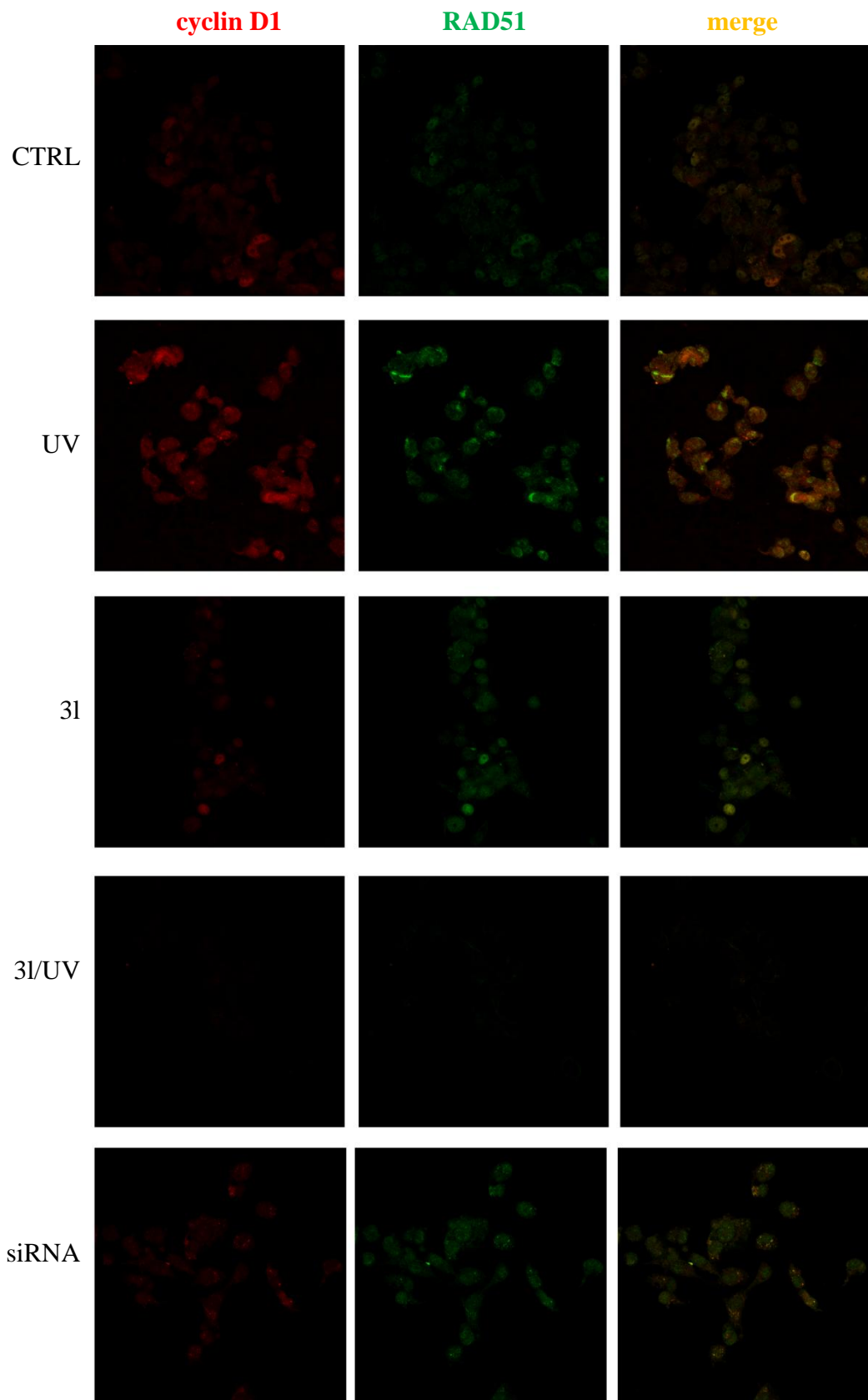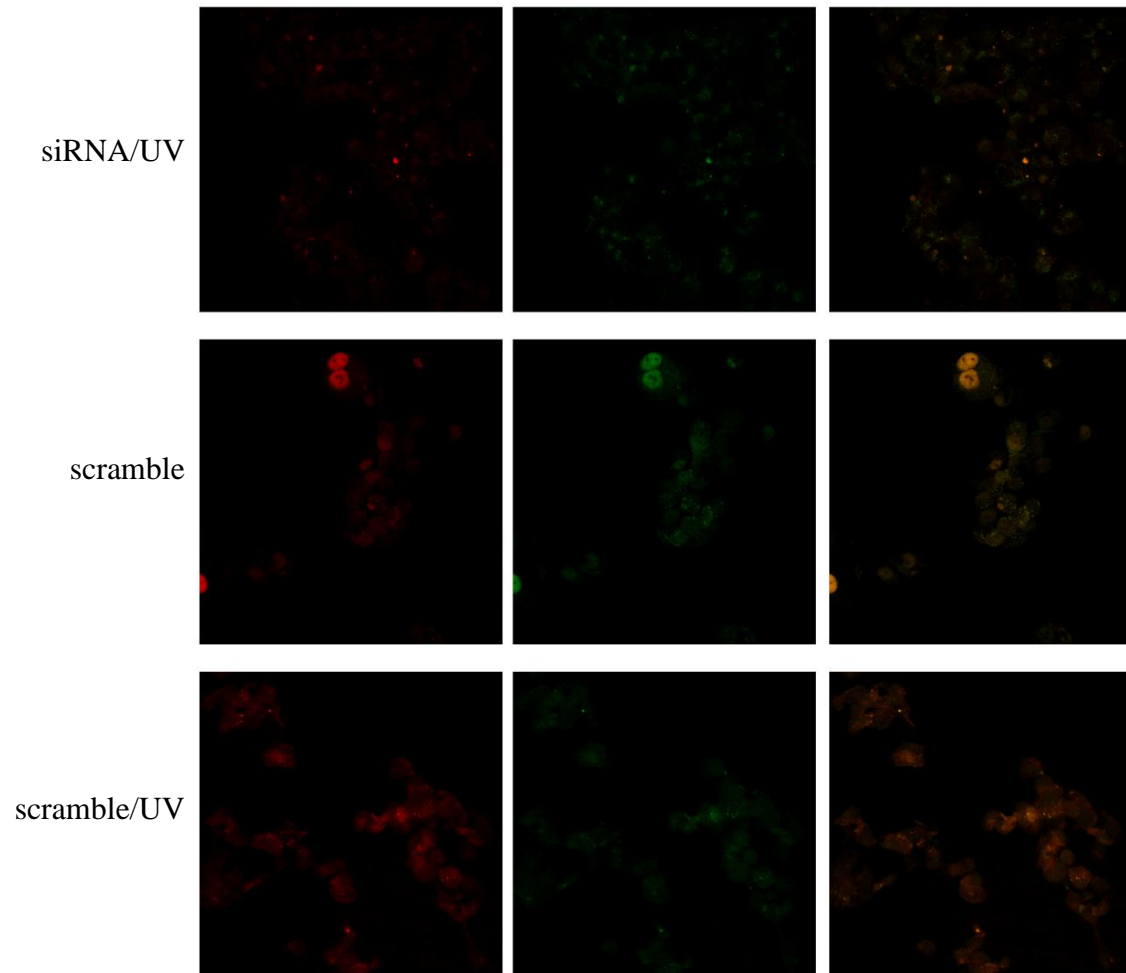
Figure 4.27: *Immunofluorescence of cyclin D1 (red) and RAD51 (green) proteins in IGROV1 cells. CTRL control sample, UV cells fixed 4 hours after UV irradiation for 15 minutes, 3l cells fixed 28 hours after 5 µM 3l treatment, 3l/UV cells fixed 28 hours after 5 µM 3l treatment and 4 hours after UV irradiation for 15 minutes, siRNA cells fixed 52 hours after treatment with anti-CCND1 siRNA 10 nM, siRNA/UV cells fixed 52 hours after treatment with anti-CCND1 siRNA 10 nM and 4 hours after UV irradiation for 15 minutes, scramble RNA extracted 52 hours after treatment with scramble siRNA 10 nM, scramble/UV RNA extracted 52 hours after treatment with scramble siRNA 10 nM and 4 hours after UV irradiation for 15 minutes.*

Figure 4.28: *Quantification of cyclin D1 and RAD51 proteins by immunofluorescence in IGROV1 cells. CTRL control sample, UV cells fixed 4 hours after UV irradiation for 15 minutes, 3l cells fixed 28 hours after 5 μM 3l treatment, 3l/UV cells fixed 28 hours after 5 μM 3l treatment and 4 hours after UV irradiation for 15 minutes, siRNA cells fixed 52 hours after treatment with anti-CCND1 siRNA 10 nM, siRNA/UV cells fixed 52 hours after treatment with anti-CCND1 siRNA 10 nM and 4 hours after UV irradiation for 15 minutes, scramble RNA extracted 52 hours after treatment with scramble siRNA 10 nM, scramble/UV RNA extracted 52 hours after treatment with scramble siRNA 10 nM and 4 hours after UV irradiation for 15 minutes. (* p ≤ 0.05, ** p ≤ 0.01, *** p ≤ 0.005, **** p ≤ 0.001 vs CTRL, ### p ≤ 0.005, #### p ≤ 0.001 vs 3l, + p ≤ 0.05, ++++ p ≤ 0.001 vs siRNA, @@@ p ≤ 0.005, @@@@ p ≤ 0.001 vs scramble)*

Remarkably, only IGROV1 cells treated with 3l and cells treated with selected anti-*CCND1* siRNA presented down-regulation of cyclin D1 amount and RAD51 recombinase. Cyclin D1-RAD51 colocalization was present only in control cells and cells treated with scramble siRNA, later irradiated with UV.

CHAPTER 5

DISCUSSION AND CONCLUSIONS

Scope of this thesis was to find a new possible approach for the treatment of ovarian cancer: using the human ovarian cancer cell line IGROV1 as a model, this study set up a combined treatment to increase sensitivity of these cells to irradiation. This project focused on the potential role of molecule 3l, an E-3-(2-chloro-3-indolylmethylene)1,3-dihydroindol-2one, in depleting cyclin D1 protein level. Cyclin D1 has been recently studied as an important protein in DNA damage repair mechanisms, especially in homologous recombination-directed repair (HDR). Cyclin D1 is recruited to damaged foci by BRCA2 and it enhances RAD51 binding to BRCA2. Furthermore, cyclin D1 is essential for *RAD51* gene up-regulation in case of double-stranded break (DSB). 3l has been showed to reduce cyclin D1 transcript and protein levels and, for this reason, 3l treatment was used to study cyclin D1 role in DNA damage repair, especially in an hormone-dependent cancer as ovarian cancer, that has not been well addressed yet.

The experimental model consisted in a first 5 µM 3l treatment for 24 hours in order to deplete cyclin D1 expression, with a further UV irradiation to induce DSB damages. In this case, the repair of induced DSBs were analyzed in IGROV1 cells with a small amount of cyclin D1 protein.

First of all, time and duration of UV treatment were set up using the well studied breast cancer cell line MCF7 as a template: 15 minutes of UV irradiation resulted optimal to induce DNA damage, but not cell death; the time point of 4 hours after irradiation resulted optimal for DNA repair pathway analysis. In MCF7 cells UV irradiation induced DNA damage as histone H2AX was hyperphosphorylated on serine 139 (γH2AX). Down-regulation of cyclin D1 was present, but the remaining pool of this protein was in the nucleus forming BRCA2-cyclin D1-RAD51 repair complex at damaged foci.

Then, UV irradiation set up was confirmed also in IGROV1 cells. *CCND1* siRNA silencing were also assessed: 10 nM siRNA treatment for 48 hours resulted as the maximum silencing pick of cyclin D1 protein.

In IGROV1 cells, UV irradiation induced H2AX hyperphosphorylation, marker of DSBs, in all the samples and a down-regulation of cyclin D1 was also present. UV-irradiated cells resulted in an up-regulation of *RAD51* gene and formation of repair complex BRCA2-cyclin D1-RAD51 on damaged foci. 3l-treated cells presented a

depletion of cyclin D1 protein levels and irradiation of these 3l-treated cells induced DNA damage as normal. However, 3l-treated and then UV-irradiated cells did not present up-regulation of *RAD51* gene and they did not present repair proteins colocalization. Anti-*CCND1* siRNA silenced cells showed comparable results to 3l-treated cells, while scramble siRNA silenced cells presented comparable results to control cells.

This thesis confirmed the important role of protein cyclin D1 in the repair pathway of DSBs:

- **cyclin D1 participates in and it is essential for repair complex formation on damaged foci**
- **cyclin D1 is necessary for *RAD51* gene up-regulation in case of DSB.**

The combined treatment of a drug leading to a depletion of cyclin D1 and a DNA damage inducer, such as irradiation, could be a potent potential therapy to target cancers with an elevated rate of DNA repair pathways, especially in case of chemo- and radio-resistant tumours.

CHAPTER 6
REFERENCES

1. Lord, C. The DNA damage response and cancer therapy. *Nature* **481,** 287–294 (2012).

2. Roos, W. P., Thomas, A. D. & Kaina, B. DNA damage and the balance between survival and death in cancer biology. *Nat. Rev. Cancer* **16,** 20–33 (2015).

3. Gavande, N. S. *et al.* DNA repair targeted therapy: The past or future of cancer treatment? *Pharmacol. Ther.* **160,** 65–83 (2016).

4. Khanna, A. DNA damage in cancer therapeutics: A boon or a curse? *Cancer Res.* **75,** 2133–2138 (2015).

5. Pearl, L. H., Schierz, A. C., Ward, S. E., Al-lazikani, B. & Pearl, F. M. G. Therapeutic opportunities within the DNA damage response. *Nat. Rev. Cancer* **15,** 166–180 (2015).

6. Curtin, N. J. DNA repair dysregulation from cancer driver to therapeutic target. *Nat. Rev. Cancer* **12,** 801–817 (2012).

7. Yi, C. & He, C. DNA repair by reversal of DNA damage. *Cold Spring Harb. Perspect. Biol.* **5,** 1–18 (2013).

8. Eker, A. P. M., Quayle, C., Chaves, I. & Van Der Horst, G. T. J. Direct DNA damage reversal: Elegant solutions for nasty problems. *Cell. Mol. Life Sci.* **66,** 968–980 (2009).

9. Sancar, A. Structure and Function of DNA Photolyase and Cryptochrome Blue-Light Photoreceptors. *Chem. Rev.* **103,** 2203–2237 (2003).

10. Lindahl, T. An N-glycosidase from Escherichia coli that releases free uracil from DNA containing deaminated cytosine residues. *Proc. Natl. Acad. Sci. U. S. A.* **71,** 3649–3653 (1974).

11. Carter, R. J. & Parsons, J. L. Base Excision Repair, a Pathway Regulated by Posttranslational Modifications. *Mol. Cell. Biol.* **36,** 1426–1437 (2016).

12. Krokan, H. E. & Bjørås, M. Base Excision Repair. *Cold Spring Harb. Perspect. Biol.* **5,** 1–22 (2013).

13. Kim, Y.-J. & Wilson, D. M. Overview of base excision repair biochemistry. *Curr. Mol. Pharmacol.* **5,** 3–13 (2012).

14. Jacobs, A. L. & Schär, P. DNA glycosylases: In DNA repair and beyond. *Chromosoma* **121,** 1–20 (2012).

15. Wallace, S. S. Base excision repair: A critical player in many games. *DNA Repair (Amst).* **19,** 14–26 (2014).

16. Schärer, O. D. Nucleotide Excision Repair in Eukaryotes. *Cold Spring Harb Perspect Biol.* **5,** 1–19 (2013).

17. Spivak, G. Nucleotide excision repair in humans. *DNA Repair (Amst).* **36,** 13–18 (2015).

18. Marteijn, J. A., Lans, H., Vermeulen, W. & Hoeijmakers, J. H. J. Understanding nucleotide excision repair and its roles in cancer and ageing. *Nat. Rev. Mol. Cell Biol.* **15,** 465–481 (2014).

19. Modrich, P. Mechanisms in eukariotic mismatch repair. *J. Biol. Chem.* **281,** 30305–30309 (2006).

20. Li, G.-M. Mechanisms and functions of DNA mismatch repair. *Cell Res.* **18115,** 85–98 (2008).

21. Li, Z., Pearlman, A. H. & Hsieh, P. DNA mismatch repair and the DNA damage response. *DNA Repair (Amst).* **38,** 94–101 (2016).

22. Larrea, A. A., Lujan, S. A. & Kunkel, T. A. SnapShot: DNA Mismatch Repair. *Cell* **141,** 730 (2010).

23. Kunz, C., Saito, Y. & Schär, P. DNA Repair in mammalian cells: Mismatched repair: variations on a theme. *Cell. Mol. Life Sci.* **66,** 1021–1038 (2009).

24. Srivastava, M. & Raghavan, S. C. DNA Double-Strand Break Repair Inhibitors as Cancer Therapeutics. *Chem. Biol.* **22,** 17–29 (2015).

25. Aparicio, T., Baer, R. & Gautier, J. DNA double-strand break repair pathway choice and cancer. *DNA Repair (Amst).* **19,** 169–175 (2014).

26. Rastogi, R. P., Richa, Kumar, A., Tyagi, M. B. & Sinha, R. P. Molecular mechanisms of ultraviolet radiation-induced DNA damage and repair. *J Nucleic Acids* **6551,** 1–32 (2010).

27. Ceccaldi, R., Rondinelli, B. & D'Andrea, A. D. Repair Pathway Choices and Consequences at the Double-Strand Break. *Trends Cell Biol.* **26,** 52–64 (2016).

28. Hustedt, N. & Durocher, D. The control of DNA repair by the cell cycle. *Nat Cell Biol* **19,** 1–9 (2017).

29. Pardo, B., Gómez-González, B. & Aguilera, A. DNA double-strand break repair: How to fix a broken relationship. *Cell. Mol. Life Sci.* **66,** 1039–1056 (2009).

30. Lazzerini-Denchi, E. & Sfeir, A. Stop pulling my strings - what telomeres taught us about the DNA damage response. *Nat Rev Mol Cell Biol* **17,** 364–378 (2016).

31. Waters, C. A., Strande, N. T., Wyatt, D. W., Pryor, J. M. & Ramsden, D. A. Nonhomologous end joining: A good solution for bad ends. *DNA Repair (Amst).* **17,** 39–51 (2014).

32. Radhakrishnan, S. K., Jette, N. & Lees-Miller, S. P. Non-homologous end joining: Emerging themes and unanswered questions. *DNA Repair (Amst).* **17,** 2–8 (2014).

33. Mladenov, E., Magin, S., Soni, A. & Iliakis, G. DNA double-strand-break repair in higher eukaryotes and its role in genomic instability and cancer: Cell cycle and proliferation-dependent regulation. *Semin. Cancer Biol.* **37–38,** 51–64 (2016).

34. Scully, R. & Xie, A. Double strand break repair functions of histone H2AX. *Mutat. Res. Mol. Mech. Mutagen.* **750,** 5–14 (2013).

35. Xu, Y. & Price, B. D. Chromatin dynamics and the repair of DNA double strand breaks. *Cell Cycle* **10,** 261–267 (2011).

36. Pellegrini, L. *et al.* Insights into DNA recombination from the structure of a RAD51-BRCA2 complex. *Nature* **420,** 287–293 (2002).

37. Chen, Z., Yang, H. & Pavletich, N. P. Mechanism of homologous recombination from the RecA-ssDNA/dsDNA structures. *Nature* **453,** 489–494 (2008).

38. Mazón, G., Mimitou, E. P. & Symington, L. S. SnapShot: Homologous recombination in DNA double-strand break repair. *Cell* **142,** 646 (2010).

39. Chapman, J. R., Taylor, M. R. G. & Boulton, S. J. Playing the End Game: DNA Double-Strand Break Repair Pathway Choice. *Mol. Cell* **47,** 497–510 (2012).

40. Verma, P. & Greenberg, R. A. Noncanonical views of homology-directed DNA repair. *Genes Dev.* **30,** 1138–1154 (2016).

41. Li, X. & Heyer, W.-D. D. Homologous recombination in DNA repair and DNA damage tolerance. *Cell Res.* **18,** 99–113 (2008).

42. Jasin, M. & Rothstein, R. Repair of strand breaks by homologous recombination. *Cold Spring Harb. Perspect. Biol.* **5,** 1–18 (2013).

43. Lopez-Martinez, D., Liang, C.-C. & Cohn, M. A. Cellular response to DNA interstrand crosslinks: the Fanconi anemia pathway. *Cell. Mol. Life Sci.* **73,** 3097–3114 (2016).

44. Michl, J., Zimmer, J. & Tarsounas, M. Interplay between Fanconi anemia and homologous recombination pathways in genome integrity. *EMBO J.* **35,** 909–923 (2016).

45. Kottemann, M. C. & Smogorzewska, A. Fanconi anaemia and the repair of Watson and Crick DNA crosslinks. *Nature* **493,** 356–363 (2013).

46. Zhang, J. & Walter, J. C. Mechanism and regulation of incisions during DNA interstrand cross-link repair. *DNA Repair (Amst).* **19,** 135–142 (2014).

47. Musgrove, E., Caldon, C., Barraclough, J., Stone, A. & Sutherland, R. Cyclin D as a therapeutic target in cancer. *Nat. Rev. Cancer* **11,** 558–72 (2011).

48. Casimiro, M. C., Crosariol, M., Loro, E., Li, Z. & Pestell, R. G. Cyclins and cell cycle control in cancer and disease. *Genes Cancer* **3,** 649–657 (2012).

49. Pestell, R. G. New Roles of Cyclin D1. *Am. J. Pathol.* **183,** 3–9 (2013).

50. Satyanarayana, A. & Kaldis, P. Mammalian cell-cycle regulation: several Cdks, numerous cyclins and diverse compensatory mechanisms. *Oncogene* **28,** 2925–2939 (2009).

51. Jirawatnotai, S., Hu, Y., Livingston, D. M. & Sicinski, P. Proteomic identification of a direct role for cyclin D1 in DNA damage repair. *Cancer Res.* **72,** 4289–4293 (2012).

52. Harbour, J. W. & Dean, D. C. The Rb/E2F pathway: Expanding roles and emerging paradigms. *Genes Dev.* **14,** 2393–2409 (2000).

53. Lim, S. & Kaldis, P. Cdks, cyclins and CDKIs: roles beyond cell cycle regulation. *Development* **140,** 3079–3093 (2013).

54. Bartek, J. & Lukas, J. Cyclin D1 multitasks. *Nature* **474,** 171–172 (2011).

55. Jirawatnotai, S., Hu, Y., Michowski, W., Elias, J. E. & Becks, L. A function for cyclin D1 in DNA repair uncovered by interactome analyses in human cancers. *Nature* **474,** 230–234 (2011).

56. Li, Z. *et al.* Alternative cyclin D1 splice forms differentially regulate the DNA damage response. *Cancer Res.* **70,** 8802–8811 (2010).

57. Li, Z. *et al.* Cyclin D1 integrates estrogen-mediated DNA damage repair signaling. *Cancer Res.* **74,** 3959–3970 (2014).

58. Chalermrujinanant, C., Michowski, W., Sittithumcharee, G., Esashi, F. & Jirawatnotai, S. Cyclin D1 promotes BRCA2-Rad51 interaction by restricting cyclin A/B-dependent BRCA2 phosphorylation. *Oncogene* **35,** 2815–2823 (2016).

59. Casimiro, M. C. *et al.* Cyclin D1 promotes androgen-dependent DNA damage repair in prostate cancer cells. *Cancer Res.* **76,** 329–338 (2016).

60. Smith, D., Mann, D. & Yong, K. Cyclin D type does not influence cell cycle response to DNA damage caused by ionizing radiation in multiple myeloma tumours. *Br. J. Haematol.* **173,** 693–704 (2016).

61. Marampon, F. *et al.* Cyclin D1 silencing suppresses tumorigenicity, impairs DNA double strand break repair and thus radiosensitizes androgen- independent prostate cancer cells to DNA damage. *Oncotarget* **7,** 5383–5400 (2015).

62. Mohanty, S. *et al.* Cyclin D1 depletion induces DNA damage in mantle cell lymphoma lines. *Leuk. Lymphoma* **58,** 676–688 (2017).

63. Casimiro, M. C. *et al.* ChIP sequencing of cyclin D1 reveals a transcriptional role in chromosomal instability in mice. *J. Clin. Invest.* **122,** 833–843 (2012).

64. Jirawatnotai, S. & Sittithumcharee, G. Paradoxical roles of cyclin D1 in DNA stability. *DNA Repair (Amst).* **42,** 56–62 (2016).

65. Li, Z. *et al.* Cyclin D1 regulates cellular migration through the inhibition of thrombospondin 1 and ROCK signaling. *Mol. Cell. Biol.* **26,** 4240–4256 (2006).

66. Li, Z., Wang, C., Prendergast, G. C. & Pestell, R. G. Cyclin D1 functions in cell migration. *Cell Cycle* **5,** 2440–2442 (2006).

67. Matulonis, U. A. *et al.* Ovarian cancer. *Nat. Rev. Dis. Prim.* **2,** 1–22 (2016).

68. Holmes, D. Ovarian cancer: beyond resistance. *Nature* **527,** S217-219 (2015).

69. Bénard, J. *et al.* Characterization of a Human Ovarian Adenocarcinoma Line, IGROV1, in Tissue Culture and in Nude Mice. *Cancer Res.* **45,** 4970–4979 (1985).

70. Beaufort, C. M. *et al.* Ovarian cancer cell line panel (OCCP): Clinical importance of in vitro morphological subtypes. *PLoS One* **9,** e103988 (2014).

71. Andreani, A. *et al.* Substituted E-3-(2-chloro-3-indolylmethylene)1,3-dihydroindol-2-ones with antitumor activity. Effect on the cell cycle and apoptosis. *J. Med. Chem.* **50,** 3167–3172 (2007).

72. Verardi, L. Role of estrogen receptor beta in ovarian cancer. Master thesis in Pharmaceutical Biotechnology discussed at University of Bologna (2013).

PUBLICATIONS

Scientific Papers

- Calonghi N., Parolin C., Sartor G., <u>Verardi L.</u>, Giordani B., Frisco G., Marangoni A., Vitali B. "Interaction of vaginal Lactobacillus strains with HeLa cells plasma membrane" Beneficial Microbes (2017) Just Accepted

- Abruzzo A., Zuccheri G., Belluti F., Provenzano S., <u>Verardi L.</u>, Bigucci F., Cerchiara T., Luppi B., Calonghi N. "Chitosan nanoparticles for lipophilic anticancer drug delivery: development, characterization and in vitro studies on HT29 cancer cells" Colloids and Surfaces B: Biointerfaces 145 (2016): 362-372

Communications

- <u>Verardi L.</u>, Locatelli A., Rambaldi M., Calonghi N. "The function of cyclin D1 in homologous recombination-mediated DNA repair" Poster presented at 2nd Department of Pharmacy and Biotechnology (FaBiT) retreat, 7th - 8th February 2017, Bologna, Italy

- <u>Verardi L.</u>, Locatelli A., Rambaldi M., Calonghi N. "The function of cyclin D1 in homologous recombination-mediated DNA repair" Poster presented at Mechanisms of Recombination 2016 Conference, 16th - 20th May 2016, Alicante, Spain

- <u>Verardi L.</u>, Locatelli A., Rambaldi M., Calonghi N. "The function of cyclin D1 in DNA repair: a new possible approach to increase sensitivity of ovarian cancer cells to irradiation" Poster presented at Proteins 2016 congress, 30th March - 1st April 2016, Bologna, Italy

- <u>Verardi L.</u>, Calonghi N. "New role of cyclin D1 in DNA damage repair" Poster presented at 58th National Meeting of the Italian Society of Biochemistry and Molecular Biology, 14th -16th September 2015, Urbino, Italy

- <u>Verardi L.</u> "New role of cyclin D1 in DNA damage repair" Oral Presentation at Summer School Chemical and genomics-based strategies in the discovery of novel drug targets, 22nd - 26th June 2015, Bologna, Italy

- <u>Verardi L.</u>, Béneut C., Sommermeyer V., Borde V. "Regulation of meiotic recombination initiation by histone modifications in budding yeast" Poster presented at Labex Retreat of the Institut Curie, 19th - 21st May 2014, Montpellier, France
- <u>Verardi L.</u>, Béneut C., Sommermeyer V., Borde V. "Regulation of meiotic recombination by histone modifications in budding yeast" Poster presented at 10th International Course on Epigenetics, 12th - 19th March 2014, Paris, France
- Locatelli A., Morigi R., Rambaldi M., <u>Verardi L.</u>, Calonghi N. "Identification of a new potential ligand of the estrogen receptor beta, inhibiting human ovarian cancer cell growth" Abstract presented at 22nd National Meeting of Medicinal Chemistry, 10th - 13th September 2013, Rome, Italy